

2013

# Investigating the Relationships Among Peer Athlete Mentor Leadership Behaviours, Mentoring Functions, and Perceptions of Satisfaction

Matt Hoffman  
*University of Windsor*

Follow this and additional works at: <http://scholar.uwindsor.ca/etd>

---

## Recommended Citation

Hoffman, Matt, "Investigating the Relationships Among Peer Athlete Mentor Leadership Behaviours, Mentoring Functions, and Perceptions of Satisfaction" (2013). *Electronic Theses and Dissertations*. Paper 4978.

This online database contains the full-text of PhD dissertations and Masters' theses of University of Windsor students from 1954 forward. These documents are made available for personal study and research purposes only, in accordance with the Canadian Copyright Act and the Creative Commons license—CC BY-NC-ND (Attribution, Non-Commercial, No Derivative Works). Under this license, works must always be attributed to the copyright holder (original author), cannot be used for any commercial purposes, and may not be altered. Any other use would require the permission of the copyright holder. Students may inquire about withdrawing their dissertation and/or thesis from this database. For additional inquiries, please contact the repository administrator via email ([scholarship@uwindsor.ca](mailto:scholarship@uwindsor.ca)) or by telephone at 519-253-3000ext. 3208.

# Simulation of a Wind Energy Conversion System Utilizing a Vector Controlled Doubly Fed Induction Generator

by

Matthew L. Hurajt

A Thesis

Submitted to the Faculty of Graduate Studies  
through Electrical Engineering  
in Partial Fulfillment of the Requirements for  
the Degree of Master of Applied Science at the  
University of Windsor

Windsor, Ontario, Canada

© 2013 Matthew L. Hurajt

# Author's Declaration of Originality

I hereby certify that I am the sole author of this thesis and that no part of this thesis has been published or submitted for publication.

I certify that, to the best of my knowledge, my thesis does not infringe upon anyone's copyright nor violate any proprietary rights and that any ideas, techniques, quotations, or any other material from the work of other people included in my thesis, published or otherwise, are fully acknowledged in accordance with the standard referencing practices. Furthermore, to the extent that I have included copyrighted material that surpasses the bounds of fair dealing within the meaning of the Canada Copyright Act, I certify that I have obtained a written permission from the copyright owner(s) to include such material(s) in my thesis and have included copies of such copyright clearances to my appendix.

I declare that this is a true copy of my thesis, including any final revisions, as approved by my thesis committee and the Graduate Studies office, and that this thesis has not been submitted for a higher degree to any other University or Institution.

# Abstract

This dissertation provides the reader with the theory and mathematical background to understand the working principal of a wound rotor induction machine under double supply to effectively capture the power provided by a wind turbine. The dynamic model proposed by *P. Vas* is presented in equation form and in Matlab scripts and functional Simulink blocks that provide the reader with a working simulation immediately. The control of the system employs the well established stator flux oriented vector control method with improvements proposed by *Tapia et al.* to track the maximum power available from the wind turbine. The model is completely validated through comparison of characteristics to published literature.

# Contents

<b>Author's Declaration of Originality</b>	<b>iii</b>
<b>Abstract</b>	<b>iv</b>
<b>List of Figures</b>	<b>ix</b>
<b>List of Tables</b>	<b>xi</b>
<b>Nomenclature</b>	<b>xii</b>
<b>1 Introduction</b>	<b>1</b>
1.1 Standard Wind Turbine Generator Configurations . . . . .	1
1.1.1 The Doubly-Fed Induction Generator Configuration . . . . .	2
1.1.1.1 The Advantage of a DFIG Configuration . . . . .	3
1.2 Control Strategies for DFIGs . . . . .	6
1.2.1 Vector Control . . . . .	6
1.3 Thesis Overview . . . . .	6
<b>2 Steady State Analysis</b>	<b>8</b>
2.1 The Steady State Equivalent Circuit of a DFIG . . . . .	8
2.1.1 Elementary Two Pole Machine . . . . .	9
2.1.2 Slip and Frequency Relations . . . . .	10
2.1.3 Equivalent Turns Ratio . . . . .	12
2.1.4 Steady State Equations . . . . .	13
2.2 Power Balance Relations . . . . .	14
2.2.1 Active Power Balance . . . . .	14
2.2.2 Reactive Power Balance . . . . .	16
2.3 Modes of Operation . . . . .	17
2.3.1 Power Flow . . . . .	18
2.3.1.1 Subsynchronous Motoring . . . . .	18
2.3.1.2 Supersynchronous Motoring . . . . .	19
2.3.1.3 Supersynchronous Generating . . . . .	19
2.3.1.4 Subsynchronous Generating . . . . .	20
2.4 Steady State Torque . . . . .	20
2.5 Steady State Solution . . . . .	21

<b>3</b>	<b>Dynamic Model of a Wound Rotor Induction Machine</b>	<b>23</b>
3.1	Brief Introduction to the Model . . . . .	23
3.2	Simplifying Assumptions . . . . .	23
3.3	Mathematical Concepts . . . . .	24
3.3.1	The Space Vector . . . . .	24
3.3.1.1	Physical Interpretation of a Space Vector . . . . .	24
3.3.1.2	Definition of Space Vector Notation . . . . .	26
3.3.1.3	Mathematical Description of a Space Vector . . . . .	27
3.3.2	Reference Frames and the Two-Axis Transformation . . . . .	28
3.3.2.1	Clarke Transformation . . . . .	29
3.3.2.2	Rotational Transform . . . . .	31
3.3.2.3	Definition of Reference Frames . . . . .	33
3.3.3	The Relationship Between Time Phasors and Space Vectors . . . . .	34
3.4	Interaction of Electrical Variables . . . . .	35
3.4.1	Electrical Equations in their Natural Reference Frames . . . . .	35
3.4.2	Electrical Equations in the General Synchronously Rotating Reference Frame . . . . .	36
3.4.3	Electrical Equations in Scalar Form . . . . .	38
3.4.4	Electromagnetic Torque Equation . . . . .	39
3.4.5	Dynamic Power Expressions . . . . .	40
3.5	The Mechanical Subsystem . . . . .	40
3.6	The Complete Fifth Order Model . . . . .	41
3.7	Wound Rotor Induction Machine Parameters . . . . .	41
<b>4</b>	<b>Aerodynamic Model of the Wind Turbine</b>	<b>43</b>
4.1	Turbine Construction . . . . .	43
4.2	Turbine Operating Regions . . . . .	44
4.3	Aerodynamic Turbine Model . . . . .	45
4.3.1	Turbine Gearbox . . . . .	47
4.4	Modelling a Wind Turbine From Manufacturer Data . . . . .	47
4.5	Maximum Power Point Tracking (MPPT) . . . . .	49
4.5.1	Turbine Operation and Stability . . . . .	50
<b>5</b>	<b>Vector Control of the DFIG and Wind Turbine System</b>	<b>52</b>
5.1	Vector Control Principals of the Grid Connected DFIG . . . . .	52
5.2	Cascaded Control Methodology . . . . .	53
5.3	Vector Control Equations of the DFIG . . . . .	55
5.3.1	Stator Flux Orientation . . . . .	56
5.3.2	Rotor Voltage Dynamics . . . . .	57
5.3.2.1	Feed-Forward Cancellation . . . . .	57
5.3.2.2	Estimator . . . . .	58
5.3.3	Inner Loop Controller Design . . . . .	60
5.3.3.1	Inner Loop Controller Structure . . . . .	60
5.3.3.2	Calculation of Inner Loop Controller Constants $K_{P1}$ and $K_{I1}$ . . . . .	61
5.3.4	Outer Loop Controller Design . . . . .	62

5.3.4.1	Outer Loop Control Equations . . . . .	62
5.3.4.2	Outer Loop Controller Structure . . . . .	63
5.3.4.3	Calculation of Outer Loop Controller Constants $K_{P2}$ and $K_{I2}$ . . . . .	63
5.3.5	Implementation of MPPT Control . . . . .	64
<b>6</b>	<b>Simulation Model Description</b>	<b>66</b>
6.1	Description of Simulink Model . . . . .	66
6.1.1	System Overview . . . . .	67
6.2	Detailed Description of Simulink Blocks . . . . .	67
6.2.1	Input Stator Voltage Block . . . . .	67
6.2.2	Clarke Transformation Blocks . . . . .	68
6.2.3	Vector Rotation Block . . . . .	69
6.2.4	Wind Turbine Block . . . . .	69
6.2.5	Wound Rotor Induction Machine Block . . . . .	70
6.2.6	Estimator Block . . . . .	71
6.2.7	Feed Forward Cancellation Block . . . . .	72
6.2.8	PI Controller Blocks . . . . .	72
6.2.9	MPPT Block . . . . .	72
6.3	Initialization of the Model . . . . .	72
6.3.1	System Initialization . . . . .	73
6.3.2	Calculation of the Initial Conditions for System Integrators . . . . .	74
6.3.2.1	Wound Rotor Induction Machine Initial Conditions . . . . .	74
6.3.2.2	Estimator Initial Conditions . . . . .	75
6.3.2.3	PI Controller Initial Conditions . . . . .	75
<b>7</b>	<b>Model Validation, Testing and Discussion</b>	<b>77</b>
7.1	Validation of System Components . . . . .	77
7.1.1	Validation of the Wound Rotor Induction Machine Model . . . . .	77
7.1.1.1	Free Acceleration Test . . . . .	78
7.1.1.2	Initialization of the System to a Stable Doubly Fed Operating Point . . . . .	78
7.1.2	Validation of the Wind Turbine Model . . . . .	81
7.1.3	Validation of the Vector Control Subsystem . . . . .	82
7.1.3.1	Validation of the Inner Loop Vector Control . . . . .	82
7.1.3.2	Validation of the Approximation of the Inner Loop Dynamics . . . . .	84
7.1.3.3	Validation of the Outer Loop Vector Control . . . . .	84
7.2	Case Study . . . . .	86
7.2.1	Initialization to a Subsynchronous Operating Point . . . . .	86
7.2.2	Initialization to a Supersynchronous Operating Point . . . . .	88
7.2.3	Modification of the MPPT Reference to Improve Wind Power Capture for DFIG Power Flow . . . . .	89
7.2.4	Dynamic Response Through Synchronous Speed . . . . .	90
7.3	Future Work . . . . .	94
7.3.1	Deficiencies in the Model . . . . .	95
7.3.2	Towards a Practical Implementation . . . . .	95

7.4 Conclusion . . . . .	95
<b>Appendix A Derivations</b>	<b>96</b>
A.1 Equations 2.42 and 2.43: Steady State Torque Equations . . . . .	96
A.2 Equation 3.4: Space Vector from Three Phase Components . . . . .	97
A.3 Equation 3.5: Choosing $c$ . . . . .	98
A.4 Equations 3.21, and 3.22: Solution to Derivatives . . . . .	99
A.5 Equation 3.36: Cross Product of Space Vectors . . . . .	100
A.6 Equations 5.17: Transfer Functions the Modified Inner Loop Control Structure . . .	101
A.7 Ensuring a Negative Feedback Structure in the Presence of a Negative Static Loop Gain . . . . .	101
A.8 Derivation of Equation 5.34: The Outer Loop Transfer Function . . . . .	103
<b>Appendix B Initialization Script</b>	<b>104</b>
<b>Bibliography</b>	<b>110</b>
<b>Vita Auctoris</b>	<b>113</b>



# List of Figures

1.1	General Turbine Characteristics . . . . .	2
1.2	Turbine Configuration Using Full-Scale Converters and Synchronous Generators . . .	2
1.3	DFIG Configuration Using Partial-Scale Converters . . . . .	3
1.4	Suitability of the DFIG for Wind Energy Conversion . . . . .	5
2.1	Caged Rotor Induction Machine Equivalent Circuit . . . . .	8
2.2	Doubly Fed Induction Machine Equivalent Circuit . . . . .	9
2.3	Two Pole Fundamental Machine . . . . .	9
2.4	Reversal of Rotor Phase Sequence as Rotor Crosses Synchronous Speed . . . . .	11
2.5	Active Power Associated with Each Equivalent Circuit Parameter . . . . .	15
2.6	Reactive Power Associated with Each Equivalent Circuit Parameter . . . . .	17
2.7	Four Quadrant Operation Definitions . . . . .	18
2.8	Power Flow in the Subsynchronous Motoring Mode . . . . .	19
2.9	Power Flow in the Supersynchronous Motoring Mode . . . . .	19
2.10	Power Flow in the Supersynchronous Generating Mode . . . . .	20
2.11	Power Flow in the Subsynchronous Generating Mode . . . . .	20
3.1	Physical Definition of a Space Vector . . . . .	24
3.2	Space Vector Representing Instantaneous Field Density from One Winding . . . . .	25
3.3	Three Phase Axis Placement in Electrical Degrees . . . . .	25
3.4	Three Phase Rotating Space Vector . . . . .	26
3.5	Space Vector Notation . . . . .	27
3.6	Graphic Representation of Space Vector in Equation 3.4 . . . . .	28
3.7	Stator and Rotor Reference Frames Overlaid on their Respective Three Phase Axes .	29
3.8	Graphical Representation of Clarke Transformation and its Inverse . . . . .	30
3.9	Changing from Stator to Rotor Reference Frames . . . . .	31
3.10	Different Interpretations of the Rotation Transformation . . . . .	32
3.11	Definition of Reference Frames . . . . .	33
4.1	Main Structural Features of a Wind Turbine . . . . .	44
4.2	Operating Regions of a Wind Turbine . . . . .	45
4.3	Coefficient of Performance Vs Tip Speed Ratio for Several Pitch Angles . . . . .	46
4.4	Coefficient of Performance Vs Tip Speed Ratio for D49 Blades . . . . .	48
4.5	Power Curves for the wt2000df Turbine . . . . .	49

4.6	Torque Curves for wt2000df Turbine . . . . .	49
4.7	Maximum Power Point Tracking Curve . . . . .	50
4.8	Turbine Operation through Wind Speed Change . . . . .	51
5.1	Basic Diagram of Vector Control . . . . .	53
5.2	Standard Cascading Control Structure . . . . .	54
5.3	Cascaded Control Structure of the DFIG . . . . .	55
5.4	Rotor Voltage Dynamics of the Machine (plant) . . . . .	58
5.5	Feed-Forward Cancellation . . . . .	58
5.6	System after Feed-Forward Cancellation . . . . .	59
5.7	PI Controller Structures for the Inner Loop . . . . .	60
5.8	Outer Control Loops . . . . .	64
6.1	Overview of the Simulation . . . . .	67
6.2	Simulink Block Diagram of Wind Turbine . . . . .	69
6.3	Simulink Block Diagram of Two-Axis Wound Rotor Induction Machine . . . . .	70
6.4	Simulink Block Diagram of Estimator . . . . .	71
7.1	Comparison of Model and Calculations from <i>P.C. Krause et al.</i> . . . . .	79
7.2	Comparison of Model and Calculations from <i>G. Abad et al.</i> . . . . .	80
7.3	Dynamic Model after begin Initialized to a Stable Steady State Operating Point . . . . .	81
7.4	Comparison of Wind Turbine Model to Data Sheet Characteristic . . . . .	82
7.5	Acid Test of Inner Loop Vector Control . . . . .	83
7.6	Acid Test of Inner Loop Vector Control Without Feed-Forward Compensation . . . . .	84
7.7	Step Response of Inner Loop Dynamics . . . . .	85
7.8	Acid Test of Outer Loop Vector Control . . . . .	86
7.9	Simulation Result for 5 m/s Steady Wind . . . . .	87
7.10	Simulation Result for 10 m/s Steady Wind . . . . .	88
7.11	Improved Power Reference Tracking Net Power . . . . .	90
7.12	Dynamic Response to a 5 m/s to 10 m/s Gust of Wind . . . . .	91
7.13	Wind Gust: Generator Shaft Speed Trace . . . . .	92
7.14	Wind Gust: System Torque Trace . . . . .	92
7.15	Wind Gust: Power Trace . . . . .	93
7.16	Wind Gust: Stator Current Trace . . . . .	93
7.17	Wind Gust: Rotor Current Trace . . . . .	94
7.18	Wind Gust: Rotor Voltage Trace . . . . .	94
A.1	Standard Feedback Control Structure . . . . .	102
A.2	Modified Feedback Control Structure . . . . .	102

# List of Tables

2.1	Angular Velocity and Frequency Notations . . . . .	10
3.1	Rotational Transforms to Change Between Reference Frames . . . . .	34
3.2	Wound Rotor Induction Generator Parameters . . . . .	42
4.1	Parameters of the wt2000df Turbine . . . . .	48
6.1	Simulation Variables of Stator Voltage Input Block . . . . .	68
6.2	Simulink Parameters for the Voltage Input Block . . . . .	68
6.3	Simulation Variables of Clarke Transformation Block . . . . .	68
6.4	Simulation Variables of Inverse Clarke Transformation Block . . . . .	68
6.5	Simulation Variables of Vector Rotation Block . . . . .	69
6.6	Simulation Variables of the Wind Turbine Block . . . . .	69
6.7	Simulation Variables of the Wound Rotor Induction Machine . . . . .	70
6.8	Simulation Variables of the Estimator Block . . . . .	71
6.9	Simulation Variables of the Feed Forward Cancellation . . . . .	72
6.10	Simulation Variables of the PI Controller Block . . . . .	72
6.11	Simulation Variables of the MPPT Block . . . . .	72
7.1	Krause's Parameters for 2250 hp IM . . . . .	78

# Nomenclature

$\beta$	wind turbine blade pitch angle [deg]
$\lambda$	tip speed ratio [dimensionless]
$\lambda_{rD}, \lambda_{rQ}$	$D$ and $Q$ -axis rotor flux linkage components (referred to stator frame) [wb-turns]
$\lambda_{rd}, \lambda_{rq}$	$d$ and $q$ -axis rotor flux linkage components (referred to synchronous frame) [wb-turns]
$\lambda_{s\alpha}, \lambda_{s\beta}$	$\alpha$ and $\beta$ -axis stator flux linkage components (referred to rotor frame) [wb-turns]
$\lambda_{sD}, \lambda_{sQ}$	$D$ and $Q$ -axis stator flux linkage components (referred to stator frame) [wb-turns]
$\lambda_{sd}, \lambda_{sq}$	$d$ and $q$ -axis stator flux linkage components (referred to synchronous frame) [wb-turns]
$\lambda_{sd}^{est}$	estimated $d$ -axis stator flux linkage component [wb-turns]
$\omega$	miscellaneous angular velocity [elec. rad/sec]
$\omega_B$	target bandwidth frequency [rad/sec]
$\omega_g$	angular velocity of general synchronous reference frame [elec. rad/sec]
$\omega_m$	rotor shaft angular velocity [elec. rad/sec]
$\omega_n$	miscellaneous natural frequency [rad/sec]
$\omega_r$	angular frequency of rotor waveforms [elec. rad/sec]
$\omega_s$	angular frequency of stator waveforms [elec. rad/sec]
$\omega_t$	angular velocity of turbine shaft [mech. rad/sec]
$\omega_{\lambda_s}^{est}$	estimated stator flux linkage angular velocity [elec. rad/sec]
$\omega_{base}$	base angular velocity [elec. rad/sec]
$\omega_{mech,base}$	base mechanical angular velocity [mech. rad/sec]
$\omega_{mech}$	rotor shaft angular velocity [mech. rad/sec]
$\omega_{n1}$	inner loop target natural frequency [rad/sec]
$\omega_{n2}$	outer loop target natural frequency [rad/sec]

$\omega_{rotor}$	angular frequency of rotor waveforms [mech. rad/sec]
$\omega_{stator}$	angular frequency of stator waveforms [mech. rad/sec]
$\omega_{sync}$	synchronous angular velocity [mech. rad/sec]
$\omega_{t, rated}$	rated turbine angular shaft speed [mech. rad/sec]
$\overline{\lambda}_r$	rotor flux linkage phasor [wb-turns (rms)]
$\overline{\lambda}_s$	stator flux linkage phasor [wb-turns (rms)]
$\overline{I}_r$	rotor current phasor [A (rms)]
$\overline{I}_{r, act}$	actual rotor current phasor [A (rms)]
$\overline{I}_s$	stator current phasor [A (rms)]
$\overline{V}_r$	referred rotor voltage phasor [V (rms)]
$\overline{V}_{r, act}$	actual rotor voltage phasor [V (rms)]
$\overline{V}_s$	stator voltage phasor [V (rms)]
$\vec{\lambda}_r$	rotor flux linkage space vector [A]
$\vec{\lambda}_s$	stator flux linkage space vector [A]
$\vec{i}_r$	rotor current space vector [A]
$\vec{i}_s$	stator current space vector [A]
$\vec{v}_a$	<i>a</i> -axis stator voltage space vector [V]
$\vec{v}_b$	<i>b</i> -axis stator voltage space vector [V]
$\vec{v}_c$	<i>c</i> -axis stator voltage space vector [V]
$\vec{v}_r$	rotor voltage space vector [V]
$\vec{v}_s$	stator voltage space vector [V]
$\phi$	miscellaneous phase angle [elec. rad]
$\rho$	air density [kg/m <sup>3</sup> ]
$\sigma$	total leakage factor [dimensionless]
$\frac{d}{dt} \lambda_{sd}^{est}$	estimated <i>d</i> -axis stator flux linkage component derivative [wb-turns/sec]
$\theta$	miscellaneous angular position [elec. rad]
$\theta_g$	angular position of general synchronous reference frame [elec. rad]
$\theta_{\lambda_s}$	stator flux angle [rad]
$\theta_{\lambda_s}^{est}$	estimated stator flux angle [elec. rad]

$\theta_{mech}$	rotor position from reference axis [mech. rad]
$\theta_m$	rotor position from reference axis [elec. rad]
$\zeta$	damping ratio [dimensionless]
$c$	constant used in Clarke Transformation [dimensionless]
$C_p$	wind turbine coefficient of performance [dimensionless]
$EMF_r$	induced electromotive force across rotor winding [V]
$EMF_s$	induced electromotive force across stator winding [V]
$F$	general variable that can represent voltage, current or flux linkage [undefined]
$f_s$	frequency of stator waveforms [Hz]
$f_{grid}$	grid frequency [Hz]
$GR$	gear ratio of gear box [dimensionless]
$i_{rd}, i_{rq}$	$d$ and $q$ -axis rotor current components (referred to synchronous frame) [A]
$i_{rd}^*, i_{rq}^*$	$d$ and $q$ -axis rotor current references [A]
$i_{rd}^{err}, i_{rq}^{err}$	$d$ and $q$ -axis rotor current errors [A]
$i_{rd}^{KI}, i_{rq}^{KI}$	$d$ and $q$ -axis outer loop PI integrator outputs [A]
$I_{s,rated}$	rated stator current [A]
$i_{sd}, i_{sq}$	$d$ and $q$ -axis stator current components (referred to synchronous frame) [A]
$J$	combined inertia of turbine and generator rotor [ $\text{kg}\cdot\text{m}^2$ ]
$K_r$	rotor winding factor [ $K_s/K_r$ dimensionless]
$K_s$	stator winding factor [ $K_s/K_r$ dimensionless]
$K_{I1}$	integral constant for inner loop PI controller [V/A]
$K_{I2}$	integral constant for outer loop PI controller [A/W]
$K_{opt}$	coefficient used to fit the MPPT power curve to a cubic function [ $\text{sec}^3/\text{W}$ ]
$K_{P1}$	proportional constant for inner loop PI controller [V/A]
$K_{P2}$	proportional constant for outer loop PI controller [A/W]
$L_m$	magnetizing inductance of one phase [H]
$L_r$	total rotor inductance of one phase [H]
$L_s$	total stator inductance of one phase [H]
$L_{lr,act}$	actual rotor inductance in one phase [H]

$L_{lr}$	leakage rotor inductance in one phase [H]
$L_{ls}$	leakage stator inductance in one phase [H]
$N_r$	number of turns of rotor winding [dimensionless]
$N_s$	number of turns of stator winding [dimensionless]
$n_m$	rotor shaft speed [rpm]
$P_p$	number of pole pairs [dimensionless]
$P_r$	real power exchanged through rotor (positive injected) [W]
$P_s$	real power exchanged through stator (positive injected) [W]
$P_s^{err}$	three phase stator real power error [W]
$P_s^{ref}$	reference three phase stator real power (positive consuming) [W]
$P_t$	power provided by the wind turbine [W]
$P_{ag}$	air gap power (positive stator to rotor) [W]
$P_{cu,r}$	rotor winding copper loss in one phase [W]
$P_{cu,s}$	stator winding copper loss in one phase [W]
$P_{grid}$	real power injected to grid (positive supplying) [W]
$P_{mech,R_r}$	component of mechanical power modelled by resistance $R_r$ [W]
$P_{mech,V_r}$	component of mechanical power modelled by voltage source $V_r$ [W]
$P_{mech}$	mechanical power (positive motoring) [W]
$P_{MPPT}$	real power on the MPPT curve [W]
$P_{net}$	net power produced from both stator and rotor (positive generating) [W]
$P_{net}^{ref}$	reference net power (positive generating) [W]
$P_{rated}$	rated three phase generator power [W]
$P_{slip}$	power transferred through rotor slip rings (positive supplying) [W]
$P_{wind}$	power provided by the wind [W]
$Q_r$	reactive power exchanged through rotor in one phase (positive injected) [VAR]
$Q_s$	reactive power exchanged through stator in one phase (positive injected) [VAR]
$Q_s^{err}$	three phase stator reactive power error [VAR]
$Q_s^{ref}$	reference three phase stator reactive power (positive consuming) [VAR]
$Q_{L_m}$	reactive power consumed in magnetizing inductance [VAR]

$Q_{Llr}$	reactive power consumed in referred rotor leakage inductance [VAR]
$Q_{Lls}$	reactive power consumed in stator leakage inductance [VAR]
$Q_{vir}$	reactive power associated with the $V_r \frac{1-s}{s}$ element (positive consuming) [VAR]
$R_r$	referred rotor winding resistance [ $\Omega$ ]
$R_s$	stator winding resistance [ $\Omega$ ]
$r_t$	turbine radius [m]
$R_{r,act}$	actual rotor winding resistance [ $\Omega$ ]
$s$	slip and Laplace complex argument (context specifies) [dimensionless]
$S_{base}$	base power [VA]
$t$	time [sec]
$T_s$	general settling time [sec]
$T_t$	torque provided by the wind turbine [N·m]
$T_{base}$	base torque [N·m]
$T_{em}$	electromagnetic torque produced by the generator (positive motoring) [N·m]
$T_{load}$	torque applied to shaft of generator (positive motoring) [N·m]
$T_{mech}$	torque provided by the wind turbine referred to the generator shaft (positive generating) [N·m]
$T_{s1}$	target inner loop settling time [sec]
$T_{s2}$	target outer loop settling time [sec]
$TR$	effective turns ratio between stator and rotor windings [dimensionless]
$V$	peak voltage of time waveforms [V]
$v_w$	wind velocity [m/sec]
$V_{LLrms}$	line to line three phase rated voltage of grid [V (rms)]
$V_{r,rated}$	three phase line to line rated actual rotor voltage [V]
$v_{rd,comp}$	$d$ -axis compensation rotor voltage components [V]
$v'_{rd}, v'_{rq}$	$d$ and $q$ -axis compensated rotor voltage components [V]
$v'^{*}_{rd}, v'^{*}_{rq}$	$d$ and $q$ -axis reference compensated rotor voltage components [V]
$v_{rD}, v_{rQ}$	$D$ and $Q$ -axis rotor voltage components (referred to stator frame) [V]
$v_{rd}, v_{rq}$	$d$ and $q$ -axis rotor voltage components (referred to synchronous frame) [V]
$v^*_{rd}, v^*_{rq}$	$d$ and $q$ -axis reference rotor voltage components [V]



$v_{rd}^{KI}, v_{rq}^{KI}$	$d$ and $q$ -axis inner loop PI integrator outputs [V]
$v_{rq,comp}$	$q$ -axis compensation rotor voltage components [V]
$v_{sD}, v_{sQ}$	$D$ and $Q$ -axis stator voltage components (referred to stator frame) [V]
$v_{sd}, v_{sq}$	$d$ and $q$ -axis stator voltage components (referred to synchronous frame) [V]
$v_{w,in}$	cut-in wind velocity [m/sec]
$v_{w,out}$	cut-out wind velocity [m/sec]
$v_{w,rated}$	rated wind velocity [m/sec]

# Chapter 1

## Introduction

Although the amount of energy derived from the wind is relatively small compared to that of other sources [1], the install capacity of wind turbines is increasing at an accelerating pace in various parts of the world [2]. The Global Wind Energy Council has reported an increase over tenfold since the turn of the century [3].

The doubly-fed induction generator (DFIG) has established itself as the standard generator configuration used by industry. Despite the recent trend towards permanent magnet generator solutions, the DFIG remains a relevant and important technology for the wind industry, accounting for roughly 50% of the installed capacity in 2011 [4]. Three of the top six turbine manufacturers, Sinovel, Goldwind and GE, offer a doubly-fed solution.

The main advantage of this machine over any other configuration is the ability to use a partial sized converter in the rotor to control the power flowing through the whole machine [5]. This, coupled with the added ability of precisely controlling the reactive power flow and thus power factor make the DFIG a competitive choice for turbine manufacturers.

### 1.1 Standard Wind Turbine Generator Configurations

Wind turbines can be categorized into two main groups: fixed speed and variable speed. Although simple and robust, fixed speed turbines suffer from the unavoidable disadvantage that they cannot operate to efficiently capture the energy in the wind [6]. This is because they can only operate at one speed and wind speed is variable. Every turbine has aerodynamic characteristics similar to those shown in Figure 1.1. For each wind speed there is a certain turbine shaft speed that produces maximum power. A fixed speed turbine can only operate at maximum aerodynamic efficiency for one particular wind speed. As the wind varies from this speed the efficiency of the wind turbine is reduced. Therefore to capture the most amount of power from the wind, the turbine must be made to operate at variable speeds and to follow the curve of maximum power extraction.

Most generator types have a fixed relationship between the frequency of the power they produce

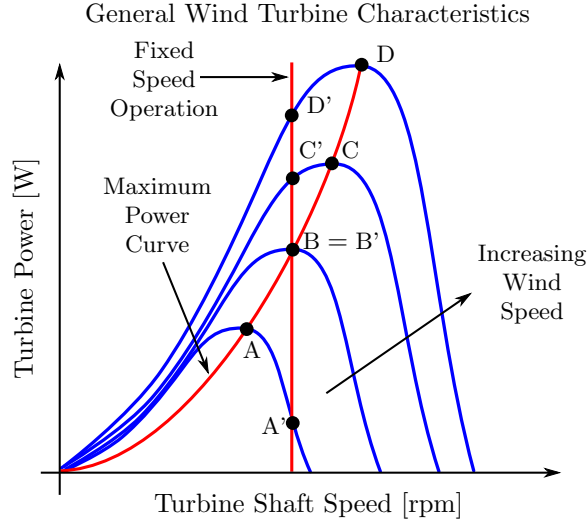


Figure 1.1: General Turbine Characteristics: A variable speed turbine capable of tracking the maximum power curve will extract more power than a fixed speed turbine for every wind speed except one, (B = B') in the diagram.

and the speed of their shafts.

$$f_{grid} = \frac{n_m \cdot P_p}{60}, \quad (1.1)$$

where  $f_s$  is the output frequency in Hz,  $n_m$  is the speed of the shaft in rpm, and  $P_p$  is the number of pole pairs. Keeping the frequency a steady 50 or 60 Hz to match the power grid is a requirement for the wind turbine to connect to the grid. However, if the speed of the shaft is varying along with the wind speed, then so will the frequency. This means a power converter needs to be placed in between the turbine's generator and the grid. Figure 1.2 shows this configuration. This converter needs to handle the entire power that the turbine produces. This type of configuration is necessary for wound rotor and permanent magnet synchronous generators.

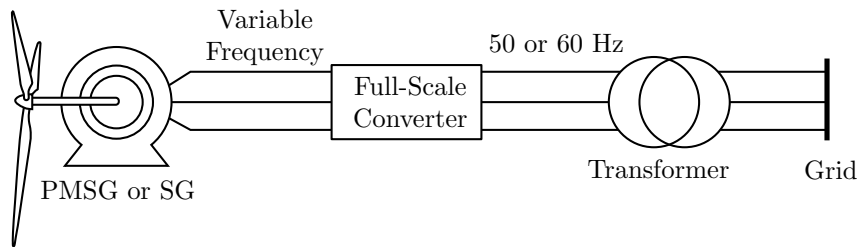


Figure 1.2: Turbine Configuration Using Full-Scale Converters and Synchronous Generators

### 1.1.1 The Doubly-Fed Induction Generator Configuration

A significant improvement in terms of converter size can be made by employing the use of a wound rotor induction machine (WRIM). In this machine, the windings on the rotor are taken out through

terminals by the use of slip rings. Direct access to the rotor windings increases the flexibility of the control of this generator. The major drawback of other types of generators is that their rotors have a fixed field, exerted by permanent magnets or direct currents. That means whatever speed their rotors are turned is the same speed that the rotor field will sweep over the stator windings and thus the frequency of the power available at the stator windings is directly related to that rotor speed. With the ability to directly inject variable frequency alternating current into the spinning rotor windings, the WRIM can ensure that the addition of the variable speed shaft and its field add to a constant 60 or 50 Hz. This will be explained in Section 2.1.2. The consequence is that the stator can be directly connected through a converter to the grid, as can be seen in Figure 1.3. The advantage of moving the converter from the stator to the rotor is that its size can be dramatically reduced, making it cheaper. The next section explains this in detail.

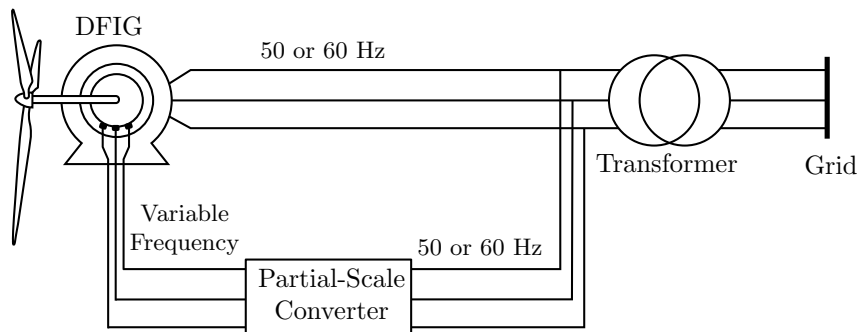


Figure 1.3: DFIG Configuration Using Partial-Scale Converters

#### 1.1.1.1 The Advantage of a DFIG Configuration

As stated, the main advantage of employing a DFIG is that the converter needed to control the machine is moved to the rotor, and the rotor can be made to handle significantly less power than the stator but still be able to control the power through the stator.

The power handled by the rotor is roughly proportional to the slip or relative speed difference from synchronous speed. This will be shown in Section 2.2.1. The relationship between the frequency and rotor speed of a WRIM is the same as that of any other machine, given in Equation 1.1, if its rotor is supplied with direct currents. As the rotor speed spins slower or faster than synchronous, the slip begins to increase. The power flowing stays proportional to this slip and everything keeps working if the proper frequency alternating currents are injected into the rotor. Now by limiting the speed range around synchronous, the power flow through the rotor is limited as well. If the speed range was extended all of the way to zero, or all of the way to twice synchronous, then the rotor would have to handle full power and the advantage would be lost. Fortunately, to cover the normal range of wind speeds that exist in nature, it has been found that the slip range only needs to extend about 30% above or below synchronous, so the power converter can be reduced to 30% as well [7].

Beyond the main advantage of reduced power converter size, the power flow that naturally occurs in the machine is ideally suited to wind energy conversion. This stems from the fact that the DFIG

can generate both below and above synchronous speed [7]. In Section 2.3.1 it will be explained how the DFIG can generate power from its stator for all speeds. Above synchronous speed additional power is generated by the rotor (supersynchronous generation) and below synchronous speed power is required to be injected into the rotor to sustain generation (subsynchronous generation). The fraction of power flowing through the rotor in either direction is related to the slip or speed difference from synchronous speed. This division of power through the rotor and stator is ideal for wind energy conversion.

More power is dealt with by the system as a whole for supersynchronous generation because the wind speed, generator speed and power in the wind are higher here. In fact, it will be demonstrated in Chapter 4 how the maximum power in the wind is proportional to the cube of the generator shaft speed. Therefore all stresses and limits imposed on the system's power handling capabilities are set in this region.

The generator and turbine are sized together so that the rated power of the generator is not exceeded. Since a known proportion of the power will be carried by the rotor, the generator can be sized smaller than the maximum target turbine power by that same proportion. For example, see Figure 1.4, if a generator is rated at 2MW and the rotor converter is sized to handle 30% of that (600 kW), then the generator as a whole can be expected to produce 2.6 MW in total. The generator's shaft speed is chosen through a gearbox ratio to achieve this target power at a speed that corresponds to 30% over synchronous. By setting this condition, the turbine and generator are now matched up well to gather maximum power for a large range of wind speeds. In the supersynchronous region, the power is split between the stator and rotor. At the rated wind speed the turbine is delivering its maximum target power, the stator provides most of it with its rated power and the rotor converter handles the rest, operating near its maximum capacity as well. Any speed in the supersynchronous region below this maximum speed results in a lower power level overall which does not overload either component.

When the wind speed falls low enough that the system enters the subsynchronous region, to sustain the generation, power must be injected into the rotor. This injected power is not wasted by the generator, rather it is recovered at the other side, through the stator terminals. Now the stator needs to handle the mechanical power from the wind and that of the rotor converter, which has been pulled from the grid to sustain the generation. It is not overloaded however because in this region, the total power available from the wind is far less than the stator's rated power, so it can easily handle the added load. Note also that since the power is so low, there is no risk of overloading the rotor converter, so it can operate at a much lower speed (higher slip) than it could in the supersynchronous region. Thus the DFIG can generate all the way down to the lowest usable wind speed that the turbine can operate with, often at a slip as high as 0.5 [6]. Furthermore, note that neglecting losses, regardless of the complicated power flow, the grid is supplied with the power converted from the wind.

### Suitability of the DFIG for Wind Energy Conversion

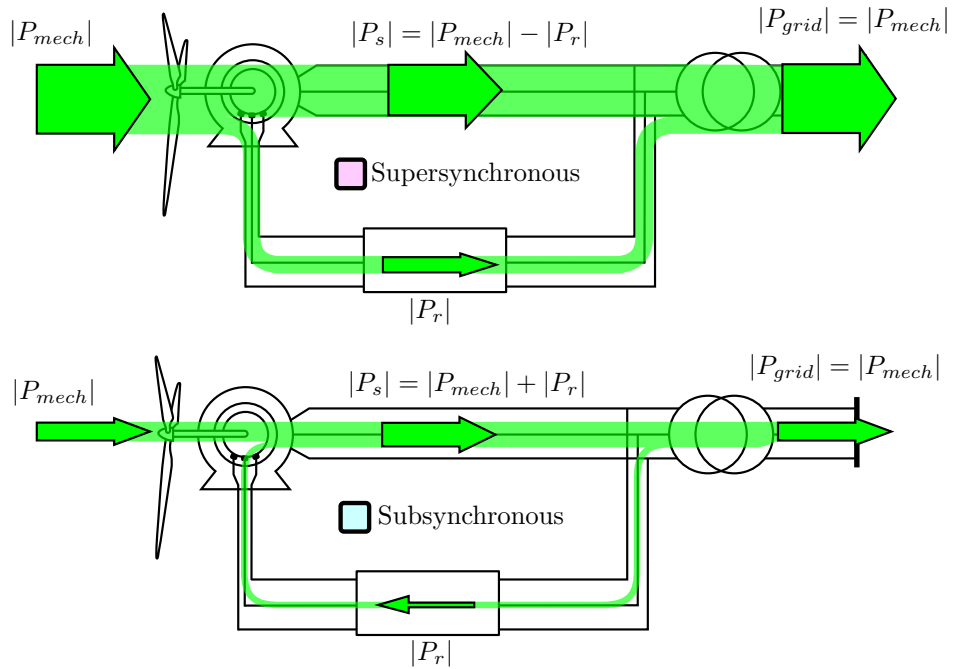
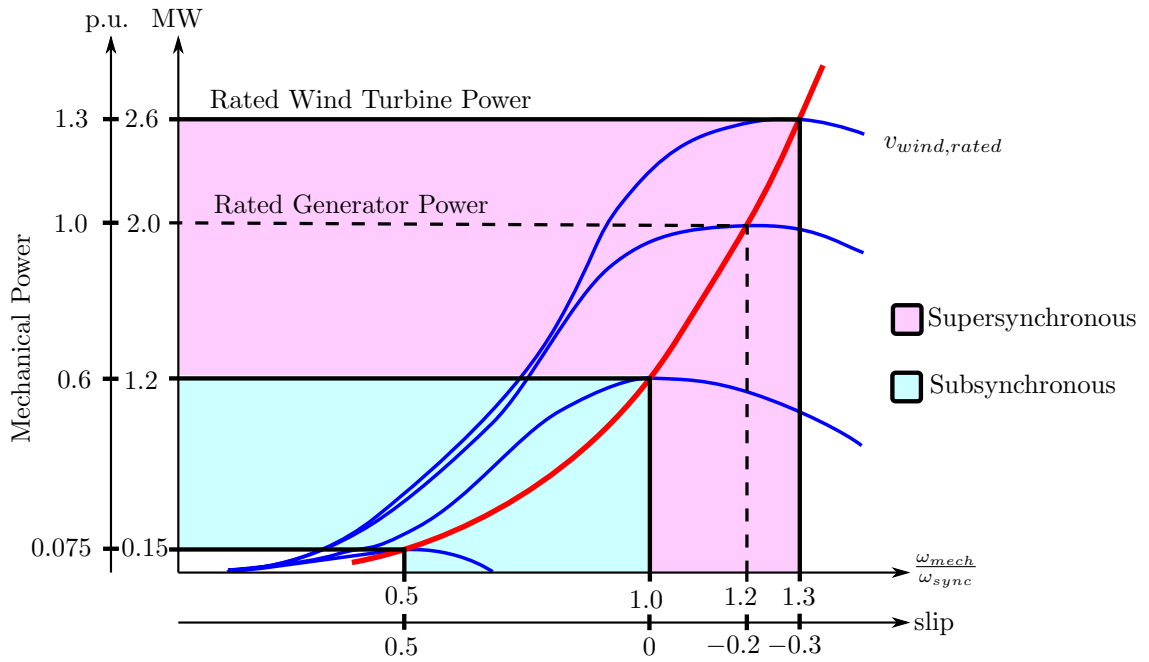


Figure 1.4: A generator rated at 2MW is connected to a wind turbine. The rated power of the generator is selected approximately 30% lower than the rated output of the turbine and it is not overrated. The extra power at high wind speeds is processed by the rotor. At low speeds the rotor needs to be injected with power to sustain generation. The stator also needs to process this extra power, but is not overloaded because the mechanical input power is smaller as well.

## 1.2 Control Strategies for DFIGs

A few main control methodologies have become popular for DFIGs in wind turbine applications. The most prevalent in literature are vector control, and direct torque or power control. Control of the torque constitutes control of any rotating machinery [8]. Direct torque control is a technique that aims to control the magnitude and angle of the rotor flux, to directly control torque. Since torque is the cross product of stator and rotor flux, and since the stator is connected to the grid, the stator flux is almost constant, and thus the rotor flux is the chosen control variable. This technique has been applied with success [9]. Its main drawback is the non-constant switching frequency it imposes on the converter [7].

### 1.2.1 Vector Control

Vector control was the first technique proposed for DFIGs in wind applications [10] and is still the most common in literature [7]. In this technique the rotor current is separated into two components, one responsible for the torque and the other for the magnetization of the machine. In this way the aim is to emulate the simple control structure of a DC machine [11]. To break the current into two components different reference frames can be used. The two most common are aligning to the stator flux [10] or the stator voltage [12]. Stator flux oriented vector control is the classical method and will be studied in Chapter 5.

Once the torque and flux are under control, the currents are related to the real and reactive powers of the machine. This is easier to do if the stator voltage reference frame has been used [7], but it has been achieved in the stator flux oriented frame by several researchers including *Tapia et al.* [13]. This decoupling or separate control of power is ideal for a wind turbine. The real power can be set to extract the maximum available power from the turbine and the power factor can be independently regulated [6].

## 1.3 Thesis Overview

In the textbook “*Advanced Electric Drives: Analysis, Control and Modeling using Simulink®*,” *Mohan et al.* establishes a working model of a vector controlled induction machine [8]. In that work, the gaps between theory and practical simulation are completely filled with clear explanations. The simulations are proven with provided scripts and models. This makes learning the subject manageable for new students in the area. The undertaking in this dissertation aims to extend this treatment to a DFIG wind turbine system. It is the intention of the author to quickly get the reader familiar with the mathematical constructs, the basic physics of the machines and the control theory necessary to construct a working model. Provided along with the theory is a working simulation model in the Simulink® environment with initializing scripts, on the accompanying CD-ROM.

Every chapter is geared towards understanding the system for simulation purposes. First, in Chapter 2, the steady state of the DFIG is studied to provide an understanding of the basic working

principals and also to solve the steady state operating point for the system. Next in Chapter 3, the mathematical concept of space vectors and reference frames, which are central to the simulation are presented. Furthermore the dynamic equations of the DFIG are derived. The model of the wind turbine is given in Chapter 4, along with a discussion on how to populate it with manufacturer data. The control equations are derived in Chapter 5, along with a controller design procedure proposed by *Tapia et al.* that has been proven effective [13]. Chapter 6 provides details on the simulation blocks and initialization script. Finally, Chapter 7 validates the model by comparing simulation results to published literature.



## Chapter 2

# Steady State Analysis

There are two main purposes for studying the steady state operation of the system. The first is purely for a deeper understanding of the characteristics, modes of operations and power flow. The second is to solve for a steady state operating point and calculate the values of all variables needed to initialize the dynamic model. This initialization procedure will be covered in Section 2.5.

### 2.1 The Steady State Equivalent Circuit of a DFIG

The steady state equivalent circuit of an induction machine is a widely known topic cover thoroughly by many authors. Figure 2.1 shows the standard model for a caged machine [14, 15, 16]. The

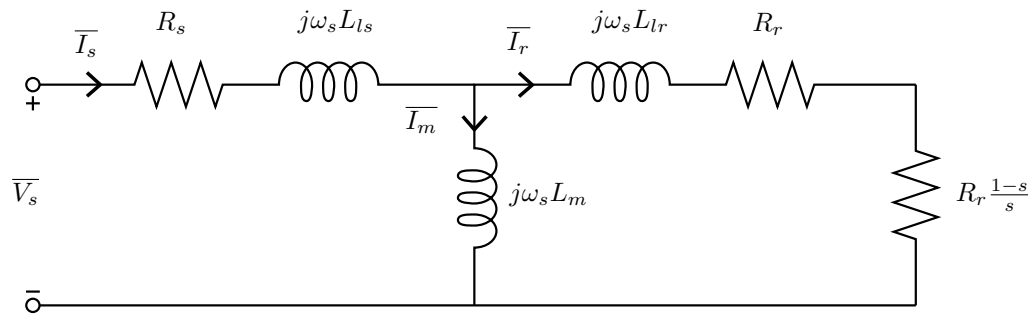


Figure 2.1: Caged Rotor Induction Machine Equivalent Circuit

modification for a doubly fed operation is simply to include the rotor voltage  $\bar{V}_r$ , see Figure 2.2, [7, 6]. Note that it is necessary to divide it by the slip to bring the frequency of the rotor to that of the stator. Furthermore notice that all rotor parameters are referred in magnitude to the stator by an equivalent turns ratio. This concept will be detailed in Section 2.1.3.

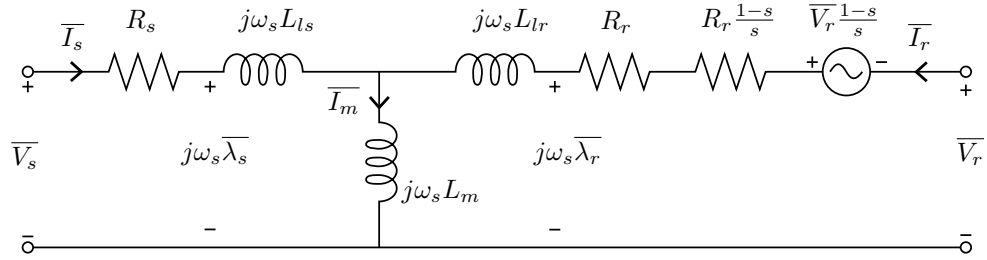


Figure 2.2: Doubly Fed Induction Machine Equivalent Circuit

### 2.1.1 Elementary Two Pole Machine

Due to symmetry, the same interaction of variables occurs in each set of the machine's poles. Calculations of the electrical variables for all sets of poles would be redundant, so they are done on just one pole pair. Mechanically the speed and torque of the machine depend on all the poles, so their quantities need to be adjusted.

Mathematically, this simplification is implemented by defining a new angle in “electrical radians” to replace the physical angle measured in “mechanical radians”;

$$\theta_m = P_p \theta_{mech}, \quad (2.1)$$

where  $P_p$  is the number of pole pairs in the machine,  $\theta_m$  is the position of the machine shaft in electrical radians and  $\theta_{mech}$  is the actual position of the machine shaft in mechanical radians. This has the effect of stretching one pole pair over the circumference of the whole machine, see Figure 2.3. As a consequence, the electrical phase lag angle of sinusoids in the machine will correspond one to one with the position of the space vector representing them, see Section 3.3.1.3. It is important to note that for the remainder of the thesis every angular position and consequently every angular velocity has been defined in this fictitious two pole environment. When it is necessary to find the machine's speed or torque, they need to be scaled by the appropriate  $P_p$  constant. Thus the mechanical speed of the shaft is given by

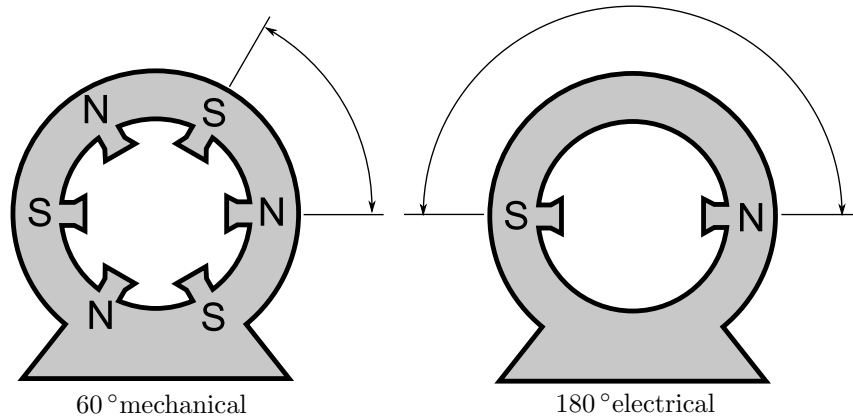


Figure 2.3: Two Pole Fundamental Machine

Quantity	Mechanical Radians per Second	Electrical Radians per Second
rotor angular velocity	$\omega_{mech}$	$\omega_m$
rotor angular frequency	$\omega_{rotor}$	$\omega_r$
stator angular frequency	$\omega_{stator}$	$\omega_s$
synchronous angular frequency	$\omega_{sync}$	$\omega_g$

Table 2.1: Angular Velocity and Frequency Notations

$$\omega_{mech} = \frac{\omega_m}{P_p}, \quad (2.2)$$

where  $\omega_m$  is the angular velocity of the machine shaft in electrical radians per second and  $\omega_{mech}$  is the actual angular velocity of the machine shaft in mechanical radians per second. To be clear, Table 2.1 denotes the notations used for the angular velocities and frequencies that are expressed in both mechanical and electrical radians per second.

The torque derived in Section 2.4 and Section 3.4.4 must have the constant  $P_p$  as well because it is derived from 2-pole variables. Each pole pair will contribute the same amount of torque so multiplying the torque for two poles by the number of pole pairs will give the total machine torque.

### 2.1.2 Slip and Frequency Relations

The frequency of the waveforms in the stator and rotor winding are related to the speed of the machine. In the most general sense the relationship is expressed by [17],

$$\omega_{mech} = \omega_{stator} \pm \omega_{rotor} \quad (2.3)$$

where  $\omega_{mech}$  is the angular velocity of the shaft and  $\omega_{stator}$  and  $\omega_{rotor}$  are the angular frequencies of the waveforms in the stator and rotor windings respectively. The negative sign applies when the phase sequence of the rotor is the same as the stator and the positive sign applies when the stator and rotor are in phase opposition.

With a wound rotor induction machine, both the stator and rotor are free to be injected directly with any frequency or phase sequence desired and the resulting shaft speed is given by Equation 2.3. In the doubly fed configuration for wind turbine applications, see Figure 1.3, the stator terminals are tied to the grid and the shaft is connected to the turbine. The rotor terminals are connected to an inverter capable of injecting any frequency or phase sequence.

Since the stator is tied directly to the grid, its frequency is constant and determined by the frequency of the grid. The stator excitation establishes the rotating magnetic field in the machine, and the speed at which it rotates is known as synchronous speed. Its speed depends also on the number of poles in the machine [14],

$$\omega_{stator} = \omega_{sync} = \frac{2\pi f_{grid}}{P_p}, \quad (2.4)$$

where  $\omega_{sync}$  is the synchronous speed in mechanical radians per second,  $f_{grid}$  is the grid frequency in Hz and  $P_p$  is the number of pole pairs in the machine.

With the stator frequency and shaft speed determined, the rotor frequency that should be injected can be determined by rearranging Equation 2.3,

$$\omega_{rotor} = \begin{cases} \omega_{mech} - \omega_{sync}, & \text{phase equivalence} \\ \omega_{sync} - \omega_{mech}, & \text{phase opposition} \end{cases} \quad (2.5)$$

The need for the rotor frequency to switch phase sequence is illustrated in Figure 2.4. The stator

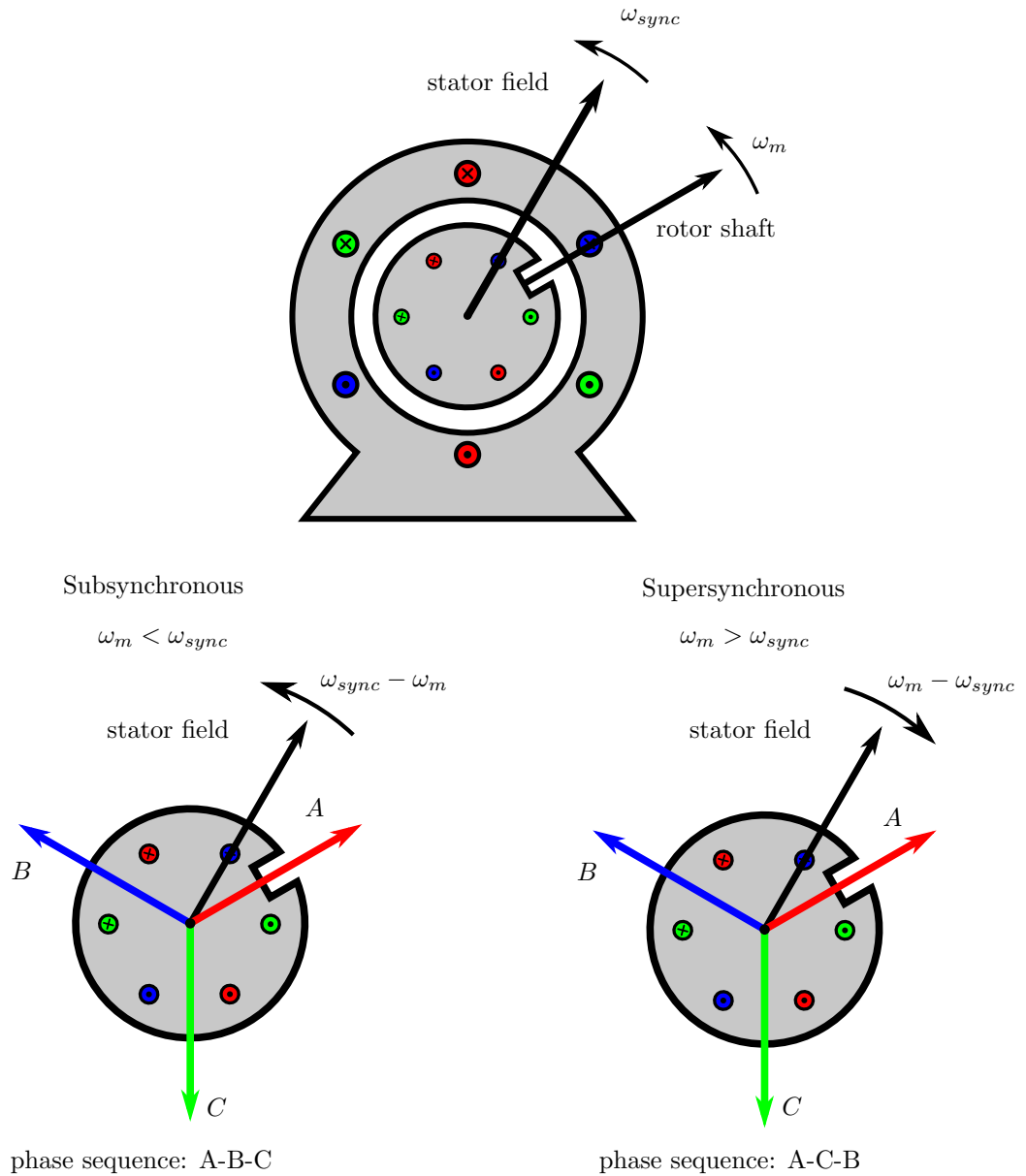


Figure 2.4: Reversal of Rotor Phase Sequence as Rotor Crosses Synchronous Speed

field rotates counter-clockwise at  $\omega_{sync}$ . The rotor also rotates counter-clockwise at  $\omega_{mech}$ . The speed at which the rotor spins relative to the stator field is important, it determines which mode the

machine is working in. The images at the bottom of Figure 2.4 are referenced to the rotor. That is the observer is placed on the rotor and thus the rotor is viewed as stationary. Now the observer will see the stator field rotating at a relative speed. In the first case the rotor is spinning slower than synchronous speed. The rotor would see the stator field, still travelling counter-clockwise but at the slower relative speed  $\omega_{sync} - \omega_{mech}$ . The stator field would sweep over the rotor coils in the sequence A-B-C and induce voltages of that sequence. For the second case, the rotor is spinning faster than the stator field. Now an observer on the rotor would see the stator field travelling clockwise at a speed of  $\omega_{mech} - \omega_{sync}$  relative to the stationary rotor, even though it is actually travelling counter-clockwise relative to the stator. Thus the stator field would sweep over the rotor coils in the sequence A-C-B, and reverse the phase sequence of the induced voltages.

The relative speed difference from synchronous is so important to the operation of an induction machine that a new variable denoted as slip ( $s$ ) is defined [14],

$$s = \frac{\omega_{sync} - \omega_{mech}}{\omega_{sync}}. \quad (2.6)$$

Notice that if the rotor speed is less than synchronous speed, the slip is positive and if the rotor speed exceeds synchronous speed the slip becomes negative. It is useful to express angular frequencies and velocities to each other using the slip for derivations later on,

$$\omega_{rotor} = s\omega_{sync}, \quad (2.7a)$$

$$\omega_r = s\omega_s, \quad (2.7b)$$

$$\omega_{mech} = (1 - s)\omega_{sync}, \quad (2.7c)$$

$$\omega_m = (1 - s)\omega_s. \quad (2.7d)$$

### 2.1.3 Equivalent Turns Ratio

Throughout this work, the rotor voltages and currents will be calculated with the parameters shown in Figure 2.2. However, the magnitudes will not be what actually exists in the machine. The rotor parameters  $R_r$  and  $L_{lr}$  are referred to the stator. This is standard practice for an induction machine; the rotor's parameters usually have to be measured on the stator side because there is no access to the rotor. The rotor parameters of a WRIM can be measured directly from the rotor's terminals. However it is still beneficial to refer the rotor parameters to the stator to simplify the calculations. A definite turns ratio exists between the stator and rotor windings [7],

$$\frac{EMF_s}{EMF_r} = s \frac{k_r N_r}{k_s N_s} = \frac{s}{TR}, \quad (2.8)$$

where  $EMF_s$  and  $EMF_r$  are the induced electromotive forces (emfs) in the windings,  $N_s$  and  $N_r$  are the number of turns of the windings,  $K_s$  and  $K_r$  are winding factors which depend on the geometry of the machine and are slightly smaller than 1,  $s$  is the slip and  $TR$  is the equivalent turns ratio. Note that the quotient  $\frac{k_s}{k_r} \approx 1$  and the slip  $s$  depends on the speed of the machine; at standstill

$s = 1$  and the turns ratio of the windings is expressed as,

$$TR = \frac{K_s N_s}{K_r N_r} \approx \frac{N_s}{N_r}, \quad (2.9)$$

The actual value of the rotor's parameters are

$$R_{r,act} = \frac{R_r}{(TR)^2}, \quad (2.10)$$

and

$$L_{lr,act} = \frac{L_{lr}}{(TR)^2}. \quad (2.11)$$

Since all calculations are done with the referred values, the only purpose of these equations would be to refer the rotor parameters to the stator side if they were measured directly from the rotor's terminals. The actual voltages and currents in the rotor are important. The machine's rotor windings are rated for specific voltages and currents, so determining what the coils are actually subjected to is necessary. The actual voltage and current in the rotor can be calculated with

$$\bar{V}_{r,act} = \frac{\bar{V}_r}{TR}, \quad (2.12)$$

and

$$\bar{I}_{r,act} = \bar{I}_r \cdot TR. \quad (2.13)$$

As a final note, all calculations done in this work use the rotor parameters referred to the stator, thus Equations 2.12 and 2.13 would be necessary for practical implementation.

#### 2.1.4 Steady State Equations

The equations can be found by applying Kirchoff's voltage and current laws to the equivalent circuit in Figure 2.2. The stator voltage is given by,

$$\bar{V}_s = R_s \bar{I}_s + j\omega_s \bar{\lambda}_s, \quad (2.14)$$

where  $\bar{\lambda}_s$  is the stator flux linkage phasor. The rotor voltage is given by,

$$\bar{V}_r = R_r \bar{I}_r + j\omega_r \bar{\lambda}_r, \quad (2.15)$$

where  $\bar{\lambda}_r$  is the rotor flux linkage phasor. The stator and rotor flux linkages are given by,

$$\begin{aligned} \bar{\lambda}_s &= L_m(\bar{I}_s + \bar{I}_r) + L_{ls} \bar{I}_s \\ &= L_s \bar{I}_s + L_m \bar{I}_r, \end{aligned} \quad (2.16)$$

where  $L_s = L_{ls} + L_m$  and,

$$\begin{aligned}\bar{\lambda}_r &= L_m(\bar{I}_s + \bar{I}_r) + L_{lr}\bar{I}_r \\ &= L_m\bar{I}_s + L_r\bar{I}_r,\end{aligned}\tag{2.17}$$

where  $L_r = L_{lr} + L_m$ . These four equations fully describe the interaction of voltage, current and flux linkage in the machine. Often it is useful to solve for the current explicitly,

$$\bar{I}_s = \frac{\begin{vmatrix} \bar{\lambda}_s & L_m \\ \bar{\lambda}_r & L_r \end{vmatrix}}{\begin{vmatrix} L_s & L_m \\ L_m & L_r \end{vmatrix}} = \frac{L_r\bar{\lambda}_s - L_m\bar{\lambda}_r}{L_sL_r - L_m^2} = \bar{\lambda}_s \frac{1}{\sigma L_s} - \bar{\lambda}_r \frac{L_m}{\sigma L_s L_r},\tag{2.18}$$

$$\bar{I}_r = \frac{\begin{vmatrix} L_s & \bar{\lambda}_s \\ L_m & \bar{\lambda}_r \end{vmatrix}}{\begin{vmatrix} L_s & L_m \\ L_m & L_r \end{vmatrix}} = \frac{L_s\bar{\lambda}_r - L_m\bar{\lambda}_s}{L_sL_r - L_m^2} = \bar{\lambda}_r \frac{1}{\sigma L_r} - \bar{\lambda}_s \frac{L_m}{\sigma L_s L_r},\tag{2.19}$$

where  $\sigma = 1 - \frac{L_m^2}{L_s L_r}$  is the total leakage factor.

## 2.2 Power Balance Relations

The equivalent circuit in Figure 2.2 completely neglects any mechanical power losses and the electrical core losses. This model has been chosen to match up with the complexity of the dynamic model required for control [7], so that it can be used in Section 2.5 for initialization of the model through a steady state solution. It is still more than detailed enough to describe the basic power balance and flow through the machine. The purpose of this section is to give an idea how power flows in the four different modes introduced in Section 2.3.

### 2.2.1 Active Power Balance

This discussion will concentrate on the active power in the machine. Figure 2.5 shows where each power is accounted for in the equivalent circuit and shows the direction which corresponds to the power flow that results when the respective power is positive.

First of all there are three places active power can be injected or removed from the machine; the stator terminals, the rotor terminals and the rotor shaft. Additionally some active power is dissipated as heat from the stator and rotor winding resistances. Notice the assumed current directions in Figure 2.5, both stator and rotor currents are assumed to be entering the machine, that is they are in motoring convention. This means that a positive  $P_s$  or  $P_r$  implies the machine is consuming power from the respective terminals and negative  $P_s$  and  $P_r$  implies the machine is supplying power from the respective terminals,

$$P_s = 3\text{Re}\{\bar{V}_s \bar{I}_s^*\},\tag{2.20}$$

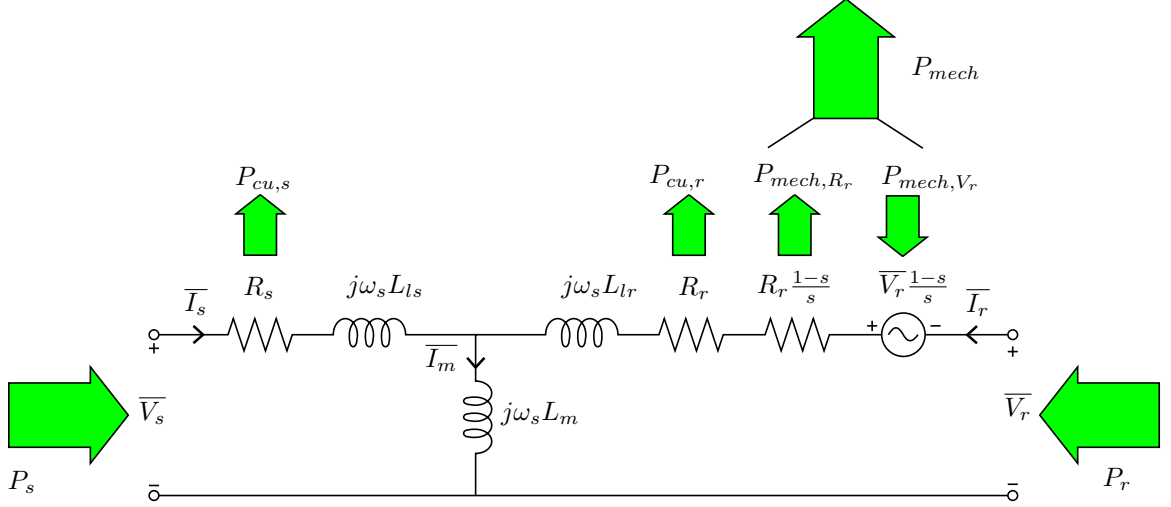


Figure 2.5: Active Power Associated with Each Equivalent Circuit Parameter

$$P_r = 3\text{Re}\{\bar{V}_r \bar{I}_r^*\}. \quad (2.21)$$

In the motoring convention,  $P_{mech}$  is chosen positive for motoring power; that is  $P_{mech} > 0$  implies that the machine is producing mechanical torque.  $P_{mech} < 0$  implies that the machine requires mechanical power from an outside source, the prime mover. In the equivalent circuit  $P_{mech}$  is represented by the two terms with slip in them;  $R_r \left(\frac{1-s}{s}\right)$  and  $\bar{V}_r \left(\frac{1-s}{s}\right)$ . Care must be taken when writing the expression for mechanical power modelled by this source. The mechanical power modelled by the resistor  $R_r \left(\frac{1-s}{s}\right)$  is

$$P_{mech,R_r} = 3|\bar{I}_r|^2 R_r \left(\frac{1-s}{s}\right). \quad (2.22)$$

When  $P_{mech,R_r}$  is positive it represents dissipation of electrical power, which matches the definition of  $P_{mech}$  where electrical power is converted to mechanical for positive values. Note that a negative value of slip will make  $P_{mech,R_r}$  negative, which means it is supplying electrical power. The mechanical power modelled by the voltage source  $\bar{V}_r \left(\frac{1-s}{s}\right)$  is

$$P_{mech,V_r} = 3 \left(\frac{1-s}{s}\right) \text{Re}\{\bar{V}_r \bar{I}_r^*\}. \quad (2.23)$$

Notice the voltage is in source convention; the current is leaving the positive terminal. This is in opposition to the definition of  $P_{mech}$  since a positive value of  $P_{mech,V_r}$  means electrical power is injected into the circuit. The reason for choosing this polarity for  $\bar{V}_r \left(\frac{1-s}{s}\right)$  was to match with the polarity of  $\bar{V}_r$  when separating  $\frac{\bar{V}_r}{s}$  into  $\bar{V}_r$  and  $\bar{V}_r \left(\frac{1-s}{s}\right)$ . Now the full expression for mechanical power can be written,

$$\begin{aligned} P_{mech} &= P_{mech,R_r} - P_{mech,V_r} \\ &= 3|\bar{I}_r|^2 R_r \left(\frac{1-s}{s}\right) - 3 \left(\frac{1-s}{s}\right) \text{Re}\{\bar{V}_r \bar{I}_r^*\}. \end{aligned} \quad (2.24)$$



Finally, the power dissipation from the stator and rotor winding resistances are given as,

$$P_{cu,s} = 3|\bar{I}_s|^2 R_s, \quad (2.25)$$

and

$$P_{cu,r} = 3|\bar{I}_r|^2 R_r. \quad (2.26)$$

respectively.

The power in the stator and rotor pass to each other through the air gap. For motoring convention, positive power at the air gap implies power flowing from the stator to the rotor. On the stator side,

$$P_{ag} = P_s - P_{cu,s}, \quad (2.27)$$

on the rotor side,

$$-P_{ag} = P_r - P_{cu,r} - P_{mech}, \quad (2.28)$$

therefore the power balance of the entire machine is,

$$P_s + P_r = P_{cu,r} + P_{cu,s} + P_{mech}. \quad (2.29)$$

All power on the stator side is electrical in nature while the rotor is host to both mechanical and electrical power. Electrical power in the rotor is sometimes referred to as slip power [18],

$$\begin{aligned} P_{slip} &= P_{cu,r} - P_r \\ &= 3|\bar{I}_r|^2 R_r - 3\text{Re}\{\bar{V}_r \bar{I}_r^*\}. \end{aligned} \quad (2.30)$$

because its magnitude is proportional to slip. The balance of mechanical power in the rotor can be seen by comparing Equations 2.30 and 2.24 to the total power passing through the rotor, (see Figure 2.1),

$$-P_{ag} = 3|\bar{I}_r|^2 \frac{R_r}{s} - 3\text{Re}\{\bar{V}_r \bar{I}_r^*\} \frac{1}{s}. \quad (2.31)$$

Now it is apparent to see,

$$P_{slip} = sP_{ag}, \quad (2.32)$$

and,

$$P_{mech} = (1 - s)P_{ag}. \quad (2.33)$$

## 2.2.2 Reactive Power Balance

Reactive power is necessary to magnetize the machine windings. Unlike a conventional induction machine that must draw reactive power from its stator, the DFIG can inject reactive power through the rotor to better utilize the copper in its windings. That is the reactive power load of the machine, which constitutes an increase in current can be shared by both windings [13]. By looking at the

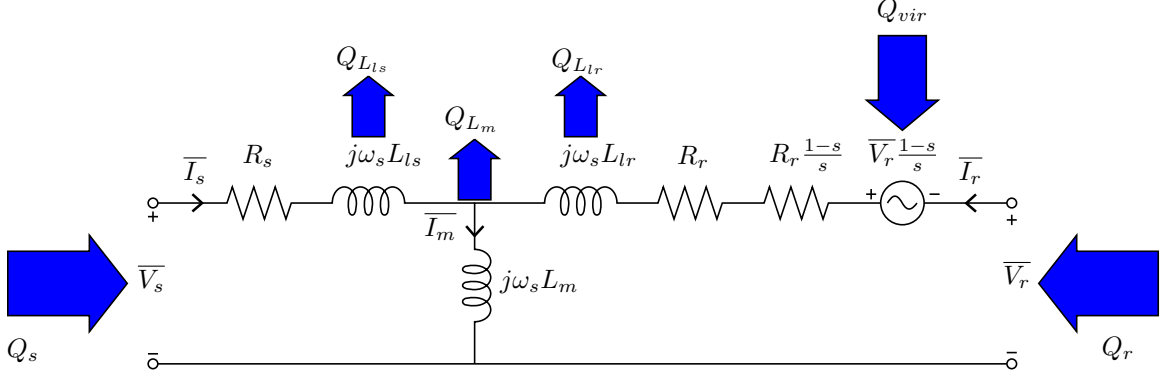


Figure 2.6: Reactive Power Associated with Each Equivalent Circuit Parameter

equivalent circuit it is seen where reactive power flows in the machine. Figure 2.6 shows which elements consume reactive power and where it is injected in the model. The leakage and magnetizing inductances  $L_{ls}$ ,  $L_{lr}$  and  $L_m$  consume reactive power denoted by  $Q_{L_{ls}}$ ,  $Q_{L_{lr}}$  and  $Q_{L_m}$  respectively. The stator and rotor terminals are ports that can exchange (either consume or supply) the reactive power  $Q_s$  and  $Q_r$ . Additionally there is a voltage source  $V_r \frac{1-s}{s}$  which can exchange the reactive power  $Q_{vir}$ . By analysing the model in a completely mathematical sense, the reactive power balance is seen as,

$$Q_{L_{ls}} + Q_{L_{lr}} + Q_{L_m} = Q_s + Q_r + Q_{vir}, \quad (2.34)$$

where,

$$Q_s = 3\text{Im}\{\bar{V}_s \bar{I}_s^*\}, \quad (2.35)$$

$$Q_r = 3\text{Im}\{\bar{V}_r \bar{I}_r^*\}, \quad (2.36)$$

$$Q_{L_{ls}} = 3|\bar{I}_s|^2 \omega_s L_{ls}, \quad (2.37)$$

$$Q_{L_{lr}} = 3|\bar{I}_r|^2 \omega_s L_{lr}, \quad (2.38)$$

$$Q_{L_m} = 3|\bar{I}_s + \bar{I}_r|^2 \omega_s L_m, \quad (2.39)$$

$$Q_{vir} = 3\text{Im}\left\{\frac{1-s}{s} \bar{V}_r \bar{I}_r^*\right\}. \quad (2.40)$$

Note that  $Q_{L_{ls}}$ ,  $Q_{L_{lr}}$ ,  $Q_{L_m}$ ,  $Q_s$  and  $Q_r$  have physical meaning, where as  $Q_{vir}$  is more obscure. According to [19] the term  $Q_{vir}$  which arises from the voltage source  $\frac{1-s}{s} V_r$  is a virtual effect of the external circuit and is necessary to include when the circuit manipulations to reduce the rotor to the stator are applied. The reactive power introduced to the circuit from this modelling element actually comes from the external circuit (the power converter).

## 2.3 Modes of Operation

A wound rotor induction machine is able to operate in modes that a caged induction machine cannot because of the added flexibility provided by the access to the rotor terminals. It is able to achieve a full four quadrant operation for a uni-directional shaft rotation. This is different from the usual definition of four quadrant operation. All machines are capable of working in the four quadrant

operation depicted on the left of Figure 2.7, provided they are connected to a capable drive. That is they can motor and generate in the forward and reverse directions. The ability to reverse direction

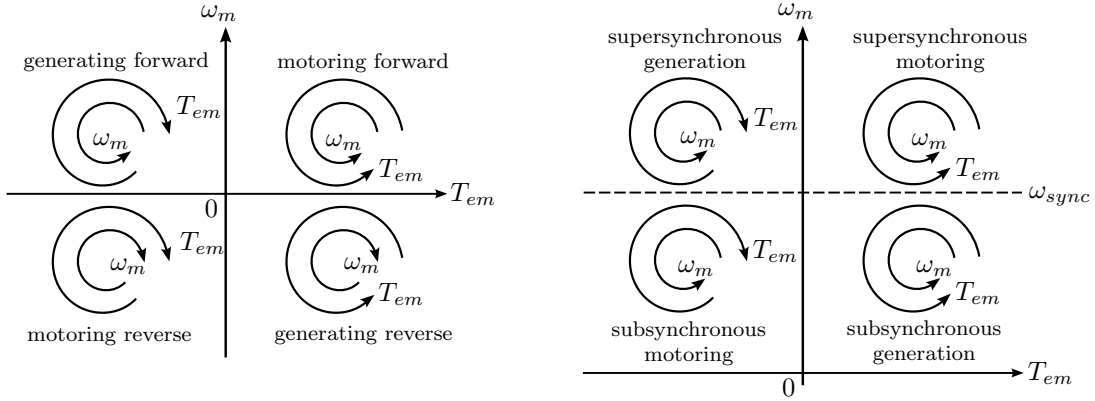


Figure 2.7: Left: Standard Definition of Four Quadrant Operation, Right: Four Quadrant Operation in One Direction

is unnecessary in wind turbine applications; the turbine blades will always spin the shaft in the same direction. There is however still a relevant four quadrant operating region that can be defined for uni-directional rotation, see the right of Figure 2.7. Induction machines are designed to operate around their synchronous speed. When the shaft spins slower than synchronous speed it is known as subsynchronous operation and the machine can only motor. When the shaft spins faster than synchronous speed it is known as supersynchronous operation and the machine can only generate. This is because the direction of the induced torque in an induction machine depends on the speed. A wound rotor machine can be made to generate or motor above or below synchronous speed and thus achieves this sort of four quadrant operation.

### 2.3.1 Power Flow

The exchange of power through the terminals of a wound rotor machine can be explained by examining Equations 2.32 and 2.33. It will be seen that the intrinsic nature of the flow is well suited for variable speed generation. For this discussion, the dissipated power in the stator and rotor resistances will be neglected to simplify the explanation and make the fundamental points clear.

#### 2.3.1.1 Subsynchronous Motoring

This mode is characterized by  $P_{mech} > 0$ , that is mechanical power is available at the shaft, and a slip in the range of  $0 < s < 1$ . From Equation 2.33,

$$P_{ag} = \frac{P_{mech}}{1-s} \Rightarrow P_{ag} > 0 \text{ and } |P_{ag}| > |P_{mech}|.$$

From Equation 2.32,

$$P_{slip} = sP_{ag} \Rightarrow P_{slip} > 0.$$

Therefore power flows across the air gap from stator to rotor side. There is more power at the air gap than available at the shaft, and the extra power is present at the rotor terminals.

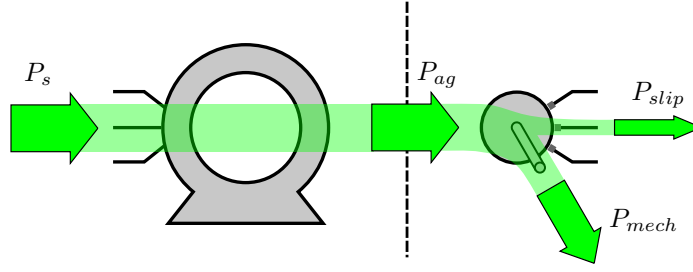


Figure 2.8: Power Flow in the Subsynchronous Motoring Mode

### 2.3.1.2 Supersynchronous Motoring

This mode is characterized by  $P_{mech} > 0$  and a slip in the range of  $-1 < s < 0$ . From Equation 2.33,

$$P_{ag} = \frac{P_{mech}}{1-s} \Rightarrow P_{ag} > 0 \text{ and } |P_{ag}| < |P_{mech}|.$$

From Equation 2.32,

$$P_{slip} = sP_{ag} \Rightarrow P_{slip} < 0.$$

As with subsynchronous motoring,  $P_{ag}$  is still positive, it flows across the air gap from the stator to the rotor. This time it is less than  $P_{mech}$  and the power required to sustain motoring must be input to the rotor; this is seen by  $P_{slip}$  becoming negative.

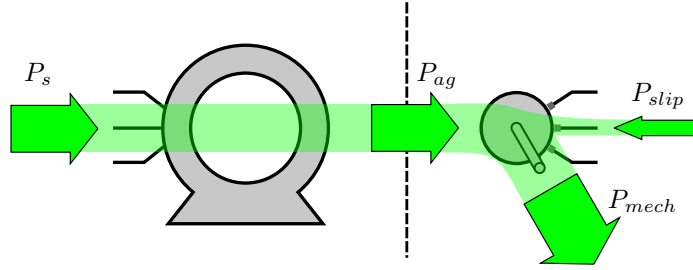


Figure 2.9: Power Flow in the Supersynchronous Motoring Mode

### 2.3.1.3 Supersynchronous Generating

This mode is characterized by  $P_{mech} < 0$ , that is mechanical power needs to be input to the shaft, and a slip in the range of  $-1 < s < 0$ . From Equation 2.33,

$$P_{ag} = \frac{P_{mech}}{1-s} \Rightarrow P_{ag} < 0 \text{ and } |P_{ag}| < |P_{mech}|.$$

From Equation 2.32,

$$P_{slip} = sP_{ag} \Rightarrow P_{slip} > 0.$$

The main input to the system is in the rotor now, reversing the direction of  $P_{ag}$  to transfer power to the stator. The input mechanical power is greater than the air gap power and the extra power is available from the rotor terminals.

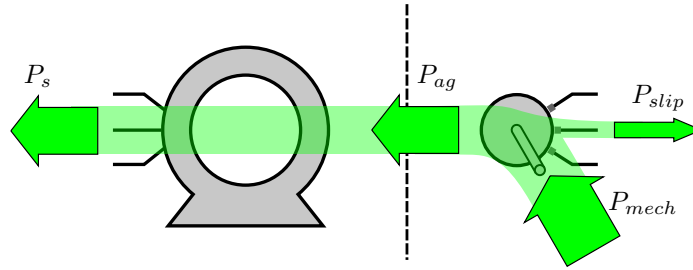


Figure 2.10: Power Flow in the Supersynchronous Generating Mode

### 2.3.1.4 Subsynchronous Generating

This mode is characterized by  $P_{mech} < 0$  and a slip in the range of  $0 < s < 1$ . From Equation 2.33,

$$P_{ag} = \frac{P_{mech}}{1 - s} \Rightarrow P_{ag} < 0 \text{ and } |P_{ag}| > |P_{mech}|.$$

From Equation 2.32,

$$P_{slip} = sP_{ag} \Rightarrow P_{slip} < 0.$$

As with supersynchronous generation  $P_{ag} < 0$  and power is transferred from the rotor to the stator. This time the mechanical power is less than the air gap power and extra power must be injected into the rotor to sustain the generating mode. Electrical power in the rotor is sometimes referred to as slip power.

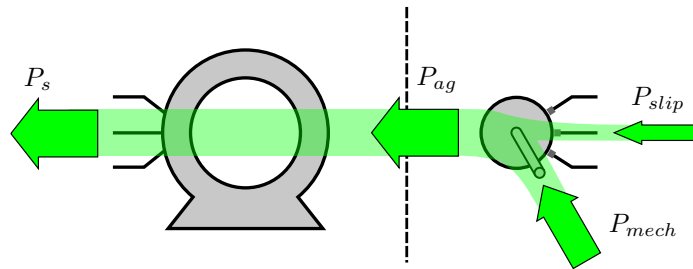


Figure 2.11: Power Flow in the Subsynchronous Generating Mode

## 2.4 Steady State Torque

The torque is one of the most important variables to consider when studying any machine as it is the connection between mechanical and electrical domains. Mechanically torque is defined in terms

of power and speed,

$$T_{em} = \frac{P_{mech}}{\omega_{mech}}. \quad (2.41)$$

The simplest way to derive the torque in terms of electrical quantities is described in [7]. The mechanical power is written in terms of currents only employing Equations 2.24, 2.17 and 2.15. The result is derived in Appendix A.1,

$$T_{em} = 3P_p L_m \text{Im}\{\overline{I_s} \overline{I_r}^*\}. \quad (2.42)$$

It is also possible to express the torque in terms of flux linkage. This way the expression can be directly compared to the dynamic torque equation, Equation 3.36 in Section 3.4.4. Using Equations 2.18 and 2.19,

$$T_{em} = 3P_p \frac{L_m}{L_s L_r \sigma} \text{Im}\{\overline{\lambda_s} \overline{\lambda_r}^*\}. \quad (2.43)$$

The derivation is also given in Appendix A.1.

## 2.5 Steady State Solution

The complete steady state solution of the DFIG is obtained from solving Equations 2.14 through 2.19 and then solving for the power or torque desired. Since the actual machine is excited by applying voltages at the stator and rotor terminals, it seems logical to start with  $\overline{V_s}$  and  $\overline{V_r}$  as known input values and then calculate the current and flux linkage. This solution path is not useful for the purpose of initializing the dynamic model because the rotor voltage will be determined by a controller and depends on other known values. In the dynamic model, the stator voltage is known and the rotor voltage will be controlled to achieve a target stator real and reactive power set point.

To start the solution, all parameters of the machine must be known. Since this is a steady state solution, a speed must be chosen as well. After the model for the wind turbine has been specified, the speed of the generator and its developed power will be derived from its characteristics. For this analysis, this amounts to  $s$  and  $P_s$  being known values. Additionally the desired reactive power  $Q_s$  which can be chosen to make the machine conform to any power factor must be specified. The stator voltage is also known, because it is fixed to the grid voltage, it will be taken as reference in the calculations.

Step 1: The stator phase voltage is specified from the rms line-to-line voltage of the grid,  $V_{LL,rms}$  and set as the reference:

$$\overline{V_s} = \frac{V_{LL,rms}}{\sqrt{3}} \angle 0^\circ. \quad (2.44)$$

Step 2: The stator current is calculated from the reference power requirements, the total complex power exchanged at the stator is

$$P_s^{ref} + jQ_s^{ref} = 3\overline{V_s} \overline{I_s}^*. \quad (2.45)$$

Rearranging, the current is found,

$$\overline{I_s} = \frac{P_s^{ref} - jQ_s^{ref}}{\overline{V_s}^*} \quad (2.46)$$

Step 3: Using Equation 2.16, the stator flux linkage is found:

$$\bar{\lambda}_s = \frac{\bar{V}_s - R_s \bar{I}_s}{j\omega_s} \quad (2.47)$$

Step 4: Using Equation 2.19, the rotor current is found:

$$\bar{I}_r = \frac{\bar{\lambda}_s - L_s \bar{I}_s}{L_m} \quad (2.48)$$

Step 5: Using Equation 2.17, the rotor flux linkage is found:

$$\bar{\lambda}_r = L_m \bar{I}_s + L_r \bar{I}_r \quad (2.49)$$

Step 6: Using Equation 2.15, the rotor voltage is found:

$$\bar{V}_r = j\omega_r \bar{\lambda}_r + R_r \bar{I}_r \quad (2.50)$$

Once these six variables are known, calculating any power or torque is trivial. Finding the steady state rotor voltage to achieve a particular  $P_s^{ref}$  and  $Q_s^{ref}$  also sets the stage for the machine initialization procedure in Section 6.3.1.

## Chapter 3

# Dynamic Model of a Wound Rotor Induction Machine

### 3.1 Brief Introduction to the Model

The dynamic model chosen for this work is a standard used for induction machines by many authors in the field of machine analysis [8, 11, 20]. Like all dynamic models it consists of coupled differential equations. The model is of fifth order; four equations describe the interaction of electrical variables and one is used to characterize the mechanical subsystem. Electromagnetic torque is the single most important variable as it is the link between electrical and mechanical subsystems. The number of equations used to define each aspect shows that this model favours the electrical side and treats the mechanical side as fundamentally as possible.

### 3.2 Simplifying Assumptions

The end purpose of this model is to be used for the control of the machine. As such it is idealized to contain only the most important interaction of variables and ignores complicating features.

The machine is treated as though it is symmetrical down its entire axis, no end effects are taken into account. This allows for all information about the machine to be contained in two dimensions, in a cross section of the machine. The air gap is considered smooth with no slotting effects. The windings are idealized as being perfectly sinusoidally distributed. The flux in the air gap is directly entirely radially. The permeability of iron is infinite and there are no iron losses. There are no mechanical losses, friction or any forms of saturation taken into account.

Furthermore the machine is considered to be perfectly symmetrical and balanced, all waveforms entering or leaving it are assumed to be balanced three phase sets.



### 3.3 Mathematical Concepts

This model relies on the use of space vectors and reference frames to define the variables in the equations. Many authors treat these concepts slightly differently. This section will serve to introduce these concepts, describing what they physically represent in the machine, and how they are used in the model. Furthermore it will clearly denote all notations and conventions for the rest of the thesis.

#### 3.3.1 The Space Vector

The dynamic analysis and control of any electric machine is greatly aided by the mathematical construct known as a space vector. Mathematically a space vector is identical to any arbitrary vector, having a length and angle. It will be shown that they can be used to simultaneously represent the flux linkage, current or voltage in three phases allowing for compact equations. Furthermore they prove useful for easily writing the equations for the control of the machine and actually form the basis for the technique of vector control applied in this thesis.

##### 3.3.1.1 Physical Interpretation of a Space Vector

The flux density in the air gap from an ideally sinusoidally distributed, two pole coil is shown in Figure 3.1. It is sinusoidally distributed and directed radially [8]. The region of maximum flux density defines the direction for the axis of the coil; the positive direction is chosen for flux pointing from the rotor to the stator. A space vector is used to represent this complex distribution. The direction of the vector is pointed along the axis of the winding; the space where the flux density is highest. The length or magnitude of the vector is proportional to the flux density of the field at a particular time. That is, a space vector is an instantaneous quantity, capable of representing variables at each instant of time, as they change. Note that the fact that the field is sinusoidally distributed around its peak is unimportant for the dynamic model leading to the control of the machine, and does not need to be represented by the space vector; only the magnitude of the field density and its position are of concern. Also note that the distributed coil is treated as a single concentrated winding.

Since the stator is unmoving and the windings are mounted inside it, the axis for any coil is also

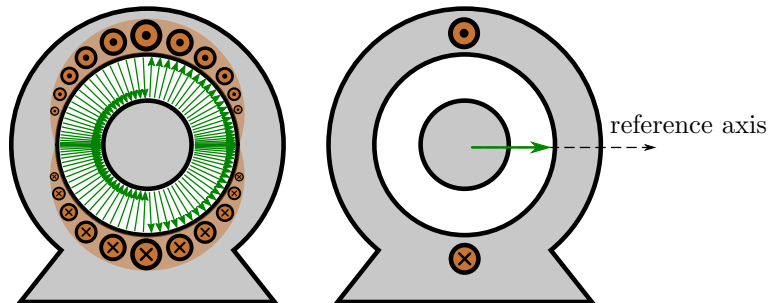


Figure 3.1: Physical Definition of a Space Vector

locked in position. As a sinusoidal excitation is applied to the winding, the peak flux density remains in the same direction, but the magnitude varies sinusoidally, see Figure 3.2.

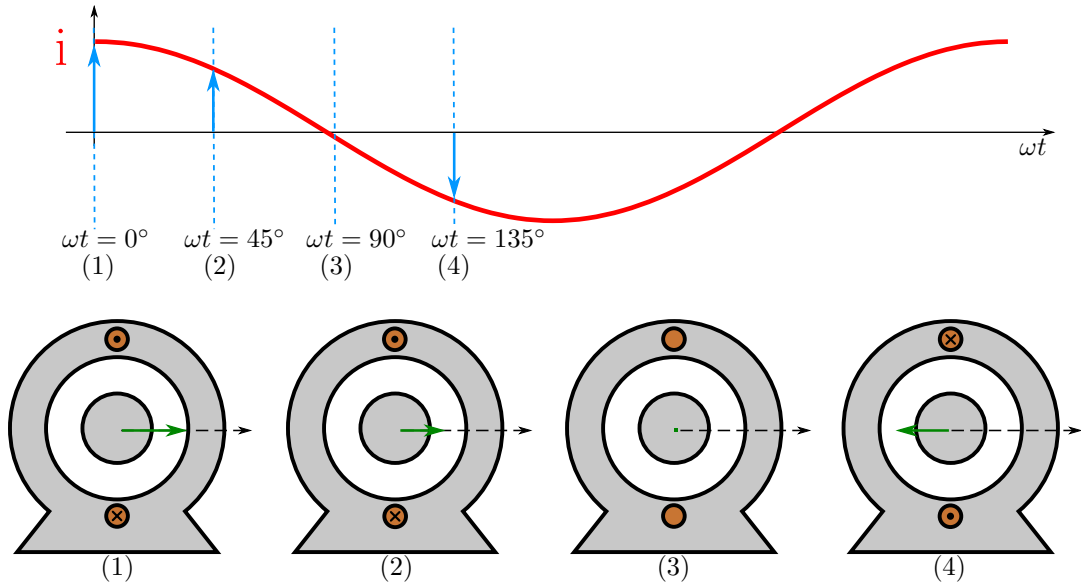


Figure 3.2: Space Vector Representing Instantaneous Field Density from One Winding

The machine under study in this work is a three phase wound rotor induction machine. It contains three windings on the stator and rotor. The machine is constructed such that the axis of the coils will be separated  $120^\circ$  electrically from each other, see Figure 3.3.

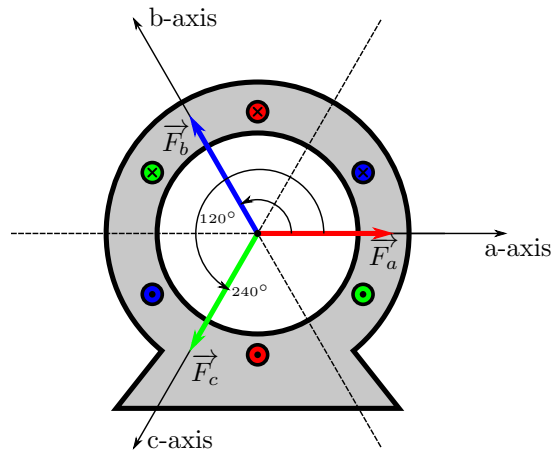


Figure 3.3: Three Phase Axis Placement in Electrical Degrees

Each winding can only create a flux distribution peaking along its own axis as before. The resultant field will be the sum of all component fields. By representing each component field by a space vector it is now an easy task to perform vector addition and find the resultant field distribution. Figure 3.4 demonstrates how three component fields situated  $120^\circ$  apart, when excited with a three phase excitation create a rotating magnetic field, and how this is easily represented with space vectors. Note that at each instant of time the three space vectors add to a resultant that is the same length at every time instant and that changes position in space by the same number of degrees as the

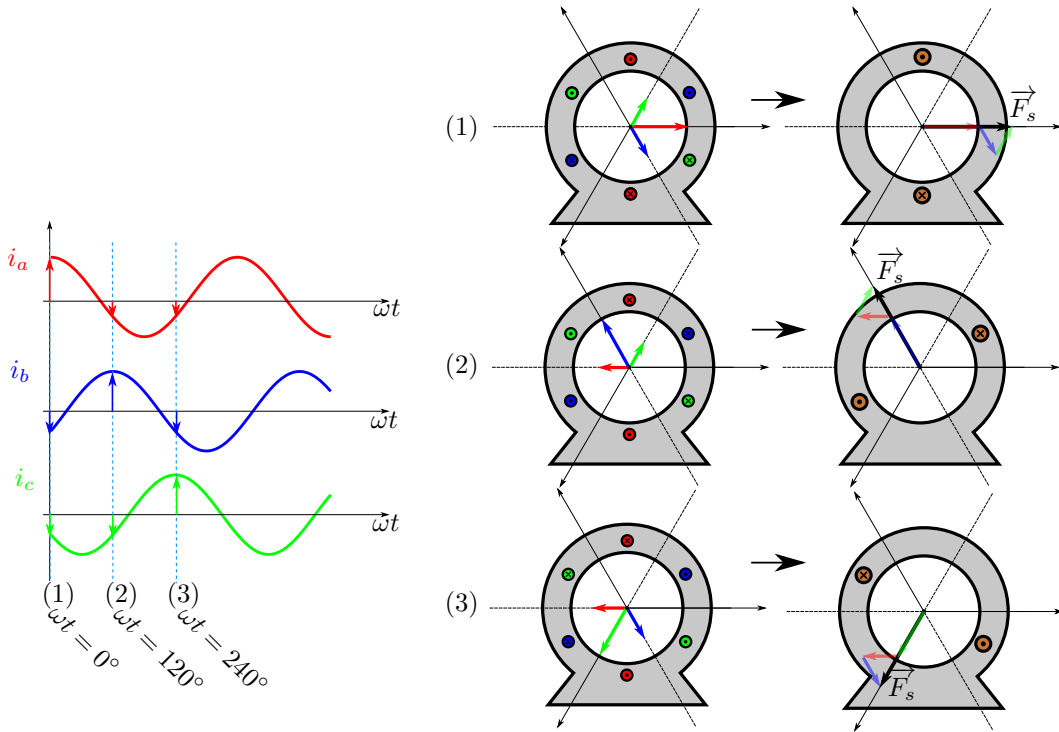


Figure 3.4: Three Phase Rotating Space Vector

electrical phase lag in the excitation waveforms.

Although only the magnetic fields physically exist in space, the space vector concept can extend to describe current and voltage. Note in Figure 3.4 that the three windings can be replaced with just one fictitious winding that is larger and oriented to the resultant field. Now a fictitious current and voltage in and across this coil, that would be responsible for this resultant field can be defined. For modelling purposes these space vectors are a tool which allow the machine equations to be written compactly, with contributions from all three phases in just one variable. The instantaneous value of any variable can quickly be found by projecting the space vector back onto each respective axis and multiplying it by a constant as defined in the following sections.

### 3.3.1.2 Definition of Space Vector Notation

For this work space vectors are used to represent three phase flux linkage ( $\lambda$ ), voltage ( $v$ ) and current ( $i$ ) on both the stator ( $s$ ) and rotor ( $r$ ). The angle of the space vector must be referenced to some axis or known position to make sense. For this purpose coordinate axes, known as reference frames are used. The frames themselves will be described in detail in Section 3.3.2.3. Space vectors will be referenced to either the stator ( $s$ ), the rotor ( $r$ ) or a synchronously rotating general vector ( $g$ ). The letter ( $g$ ) will be replaced with the specific vector that is being aligned to, or it will be kept as ( $g$ ) if the vector is not aligned to any particular vector. The notation is written with an arrow over the variable, the member of the machine subscripted and the reference frame superscripted. An example of the notation showing the stator voltage referenced to the rotor's reference frame is seen

in Figure 3.5.

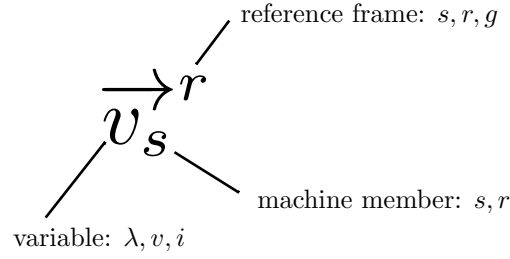


Figure 3.5: Space Vector Notation

### 3.3.1.3 Mathematical Description of a Space Vector

A space vector, having a magnitude and phase is expressed as a complex number, and is similar to the well known time phasor. The first major difference is that the magnitude varies with time, so it is a function of time. Secondly, the phase represents a physical angular displacement and must be referenced to some axis in space. For the stator, the positive a-axis is taken as the reference, see Figure 3.3. Therefore, the space vector components along each phase axis are<sup>1</sup>

$$\vec{v}_a^s = v_a(t) \underline{0^\circ} = v_a(t) e^{j0}, \quad (3.1a)$$

$$\vec{v}_b^s = v_b(t) \underline{120^\circ} = v_b(t) e^{j\frac{2\pi}{3}}, \quad (3.1b)$$

$$\vec{v}_c^s = v_c(t) \underline{240^\circ} = v_c(t) e^{j\frac{4\pi}{3}}. \quad (3.1c)$$

The space vector is found by adding the contributions from each phase

$$\begin{aligned} \vec{v}_s^s &= \vec{v}_a^s + \vec{v}_b^s + \vec{v}_c^s \\ &= v_a(t) e^{j0} + v_b(t) e^{j\frac{2\pi}{3}} + v_c(t) e^{j\frac{4\pi}{3}} \\ &= v_s(t) e^{j\theta_{v_s}}. \end{aligned} \quad (3.2)$$

Now  $v_a(t)$ ,  $v_b(t)$ ,  $v_c(t)$  are a balanced set;

$$v_a(t) = V \cos(\omega t + \phi), \quad (3.3a)$$

$$v_b(t) = V \cos(\omega t + \phi - \frac{2\pi}{3}), \quad (3.3b)$$

$$v_c(t) = V \cos(\omega t + \phi - \frac{4\pi}{3}). \quad (3.3c)$$

Substituting Equation 3.3 into 3.2<sup>2</sup>,

<sup>1</sup>stator voltage is taken for example

<sup>2</sup>see Appendix A.2 for the complete derivation

$$\begin{aligned}\vec{v}_s^s &= V \cos(\omega t + \phi)e^{j0} + V \cos(\omega t + \phi - \frac{2\pi}{3})e^{j\frac{2\pi}{3}} + V \cos(\omega t + \phi - \frac{4\pi}{3})e^{j\frac{4\pi}{3}} \\ &= \frac{3}{2}V e^{j(\omega t + \phi)}.\end{aligned}\tag{3.4}$$

First it is important to note that the magnitude of the space vector is  $\frac{3}{2}$  that of the peak of the input sinusoids. Second, the position of the space vector depends on time, and thus is rotating counter-clockwise at an angular speed  $\omega$ . Figure 3.6 shows the space vector at an arbitrary time  $t$ . Note that any phase shift in the input sinusoids shows up as the initial position of the space vector at time  $t = 0$ , this property will be exploited in Section 3.3.3 to find the correspondence between a space vector and the time phasor.

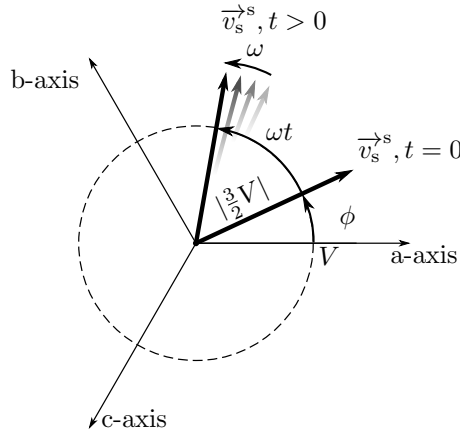


Figure 3.6: Graphic Representation of Space Vector in Equation 3.4

### 3.3.2 Reference Frames and the Two-Axis Transformation

Examining a space vector, it is clear that the contributions from three axes can be represented with just two; a space vector contains the information from three axes in two dimensional space. The equations needed to describe the three phase machine windings can be reduced if the space vector is projected onto a set of two axis instead of onto the set of three axis physically present in the machine. Furthermore it has been known for almost a century since R.H. Park [21] first referred stator variables to the rotor that choosing an appropriate frame of reference can simplify machine equations immensely. The reason is an electric machine is basically comprised of electric circuits in relative motion linked by mutual inductances. The inductances vary with rotor position through time, however if the frame of reference is rotated at the proper speed the inductances will appear constant and the machine model is simplified. P.C Krause [20] has a thorough treatment of reference frame theory. His transformation matrices simultaneously reduce to two axes and apply the proper rotation to the desired reference frame. It has been found beneficial to separate these two steps and thus this thesis follows the work laid out by P. Vas [11] and N. Mohan [8, 22].

### 3.3.2.1 Clarke Transformation

The Clarke transformation is probably the simplest form of two-axis transformation available. It maps the contributions from three axes directly to two. Figure 3.7 shows the axis placement for the Clarke transformation for stator and rotor quantities. For the stator, the  $D$ -axis is directly in line with the a-axis; the  $Q$ -axis leads it by  $90^\circ$ . The matrix which maps the components is

$$\begin{bmatrix} F_D \\ F_Q \end{bmatrix} = c \begin{bmatrix} 1 & -\frac{1}{2} & -\frac{1}{2} \\ 0 & \frac{\sqrt{3}}{2} & -\frac{\sqrt{3}}{2} \end{bmatrix} \begin{bmatrix} F_a \\ F_b \\ F_c \end{bmatrix}, \quad (3.5)$$

where  $F$  is just a general variable which could represent voltage, current or flux linkage. The entries in the matrix are easy to understand. The  $D$ -axis is directly in line with the a-axis so its contribution is 1. The b and c axes are both  $30^\circ$  off the perpendicular to the  $D$  axis, in the opposite direction so they both contribute  $-\sin(30^\circ) = -\frac{1}{2}$ . The  $Q$ -axis is completely orthogonal to the a-axis so there is 0 contribution. The b and c axes are  $30^\circ$  off the positive and negative  $Q$ -axis respectively, so their contributions are  $\cos(30^\circ) = \frac{\sqrt{3}}{2}$  and  $-\cos(30^\circ) = -\frac{\sqrt{3}}{2}$  respectively.

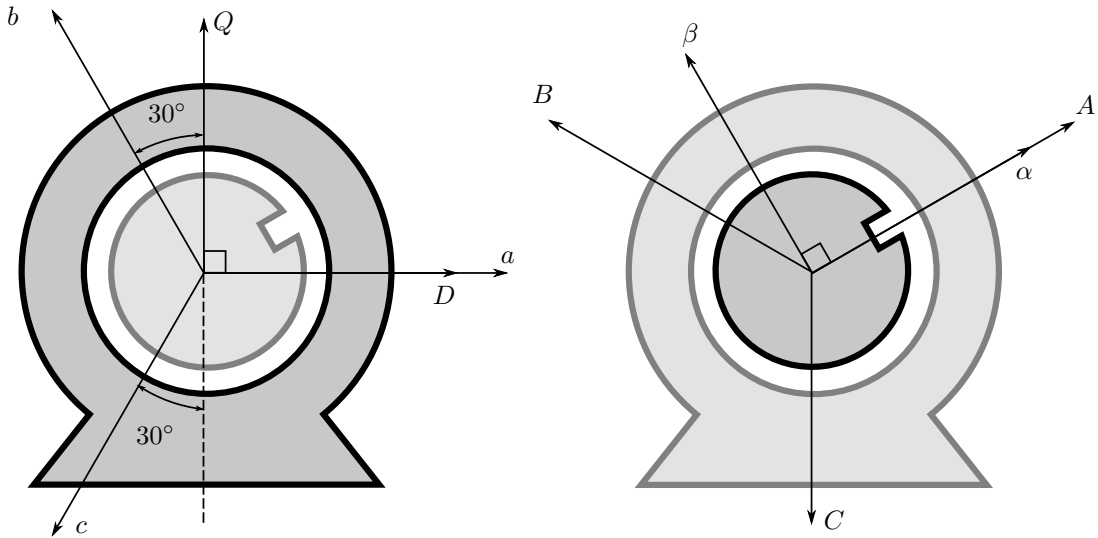


Figure 3.7: Stator and Rotor Reference Frames Overlaid on their Respective Three Phase Axes

There is a constant of proportionality  $c$  in Equation 3.5 which has not been defined yet. By transforming 3 axes to 2, the variables in their equations no longer represent real magnitudes. In fact the transformation creates a fictitious calculation environment which is separate from the real world; as long as the relative magnitudes of the components remain proper, when they are converted back with the inverse transform, everything will work out. This leaves a degree of freedom when performing the transformation, it can be scaled by any number and it will work when transformed back. There are however advantages to choosing certain values and the most prevalent are  $c = \frac{2}{3}$  and  $c = \sqrt{\frac{2}{3}}$ . The first choice allows the peak values of the variables in the two axis frame to equal those in the three axis frame. Recall Equation 3.4 where the space vector for a balanced three phase set was derived. Its magnitude was  $\frac{3}{2}$  that of the peak of the input sinusoids, so by choosing  $c = \frac{2}{3}$ , this

effect is cancelled out and the peak of the two axis components are equal to the peak values of the phase quantities. One disadvantage of this is that the power will not be the same in the two axis frame as it was in the three axis frame. It can be shown, see Appendix A.3, that choosing  $c = \sqrt{\frac{2}{3}}$  will ensure the power is equal, but loses the convenience of the peak values being equal. In the end some value for  $c$  must be chosen and in this work uses  $c = \frac{2}{3}$  to follow the original definition of the Clarke transform [23]. This means that power and torque formulae in any two axis environment will have an extra constant of proportionality of  $\frac{3}{2}$  as will be seen in Section 3.4.4. Appendix A.3 also details how that number arises.

The inverse Clarke transform will take the two axis components back to the real abc frame. It is derived by taking the inverse<sup>3</sup> of equation 3.5 with  $c = \frac{2}{3}$ ,

$$\begin{bmatrix} F_a \\ F_b \\ F_c \end{bmatrix} = \begin{bmatrix} 1 & 0 \\ -\frac{1}{2} & \frac{\sqrt{3}}{2} \\ -\frac{1}{2} & -\frac{\sqrt{3}}{2} \end{bmatrix} \begin{bmatrix} F_D \\ F_Q \end{bmatrix}. \quad (3.6)$$

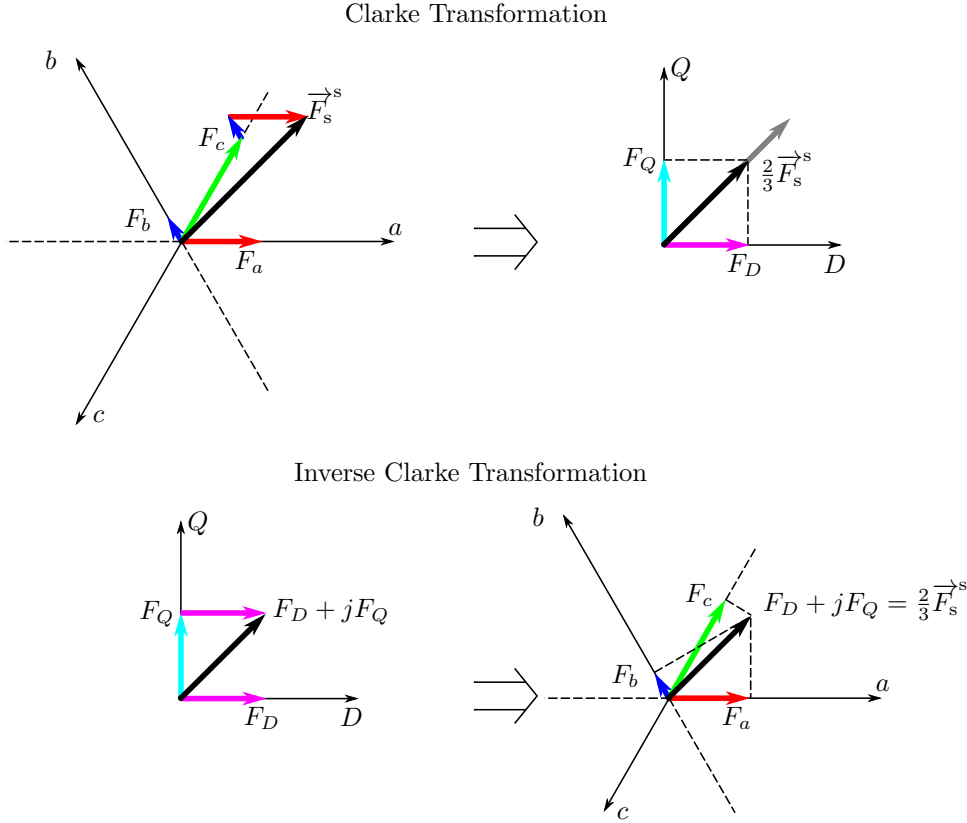


Figure 3.8: Graphical Representation of Clarke Transformation and its Inverse

Graphically the Clarke transformation is shown in Figure 3.8. The abc components are added into a space vector, then the space vector is scaled by  $\frac{2}{3}$  and then projected onto the  $D$ ,  $Q$  axes. Similarly for the inverse Clarke transformation, given the  $D$  and  $Q$  components, a space vector is made, and projected back onto the abc axes. From Figure 3.8 it can be seen that the components in either

<sup>3</sup>see Appendix A.3 to take the inverse of a non-square matrix

frame can be visualized as space vectors but it is not necessary to do this as the Clarke transform goes directly from one set of axes to the other. The space vector is just a concept that visualizes these components.

The Clarke transformation has been shown thus far for stator quantities. It forms a two axis representation referenced to the stator, that is the two components are locked to the stator's reference frame, along the  $D$  and  $Q$  axes shown in Figure 3.7. If the Clarke transform is used on a rotor quantity, it performs a similar function. The two axis components are now in the rotor's reference frame. Recall that in a wound rotor machine that the rotor also has a three phase winding, locked to the moving rotor. The rotor's reference frame is defined in a similar way to the stator's, the  $\alpha$ -axis is in line with the rotor's A-axis and the  $\beta$  axis leading by  $90^\circ$ , see Figure 3.7. The transformation matrices are exactly the same for both the rotor and stator, it just needs to be kept in mind that the Clarke transformation will automatically reference any stator quantity to the stator and any rotor quantity to the rotor.

### 3.3.2.2 Rotational Transform

The Clarke transform was able to take a three axis quantity and represent it in two axes. Furthermore it automatically references the quantities to their natural reference frames; the stator reference frame for stator quantities and the rotor reference frame for rotor quantities. To simultaneously solve equations of a system, they must all be written in the same frame. Also there are advantages for operating in certain reference frames, this will be explained in Section 3.3.2.3. For these reasons, being able to write quantities and equations in any reference frame is necessary. At any instant of time, the only difference between reference frames is the angle that they are aligned to, so to change from one to another all that is required is a rotational transform.

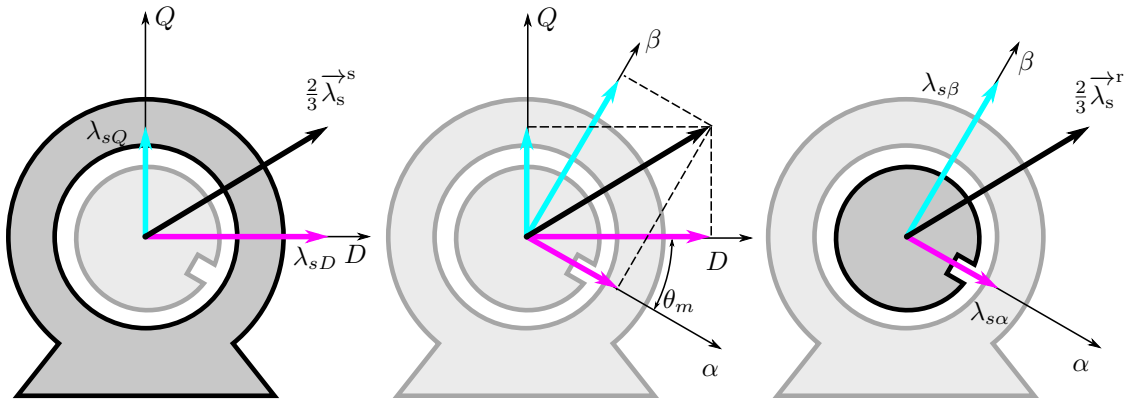


Figure 3.9: Changing from Stator to Rotor Reference Frames

Before looking into the mathematics of the rotational transform, it can be visualized easily with space vectors. Given the components in one frame, a space vector is constructed, then it is projected onto the axes of the new frame. Consider the situation depicted in Figure 3.9. Suppose the quantity shown represents stator flux linkage. In the first image the stator flux is referenced to the stator's reference frame, as if it had just been transformed with the Clarke transform from abc quantities. In the next image the position of the rotor is seen to be  $\theta_m$  radians clockwise from the stator. The



rotor's reference frame, being locked to the rotor is also at this position. To obtain the stator flux referenced to the rotor, the space vector is simply projected onto the rotor reference frame axes. It is important to note that the physical alignment of the stator flux never moved only the frame of reference changed to be aligned with the rotor.

Mathematically this operation is defined as

$$e^{j\theta} = \begin{bmatrix} \cos \theta & -\sin \theta \\ \sin \theta & \cos \theta \end{bmatrix}, \quad (3.7)$$

which is usually interpreted as having the property of rotating a vector counter-clockwise by  $\theta$  radians, without scaling the magnitude. However as noted above, space vectors represent some quantity and its position in space, and the quantity does not change position as the observer changes their frame of reference. It is better to interpret a rotational transform as rotating the frame of reference in the opposite direction (clockwise) by  $\theta$ . Figure 3.10 demonstrates that rotating a vector counter-clockwise by  $\theta_m$  radians produces the same results as rotating the reference frame in the opposite direction (clockwise) by the same angle  $\theta_m$ , that is, the magnitudes of the components after the transformation are the same in both cases<sup>4</sup>. It is just that interpreting the operation as a rotation of reference frame instead of a rotation of the vector better matches what is physically happening, see Figure 3.9.

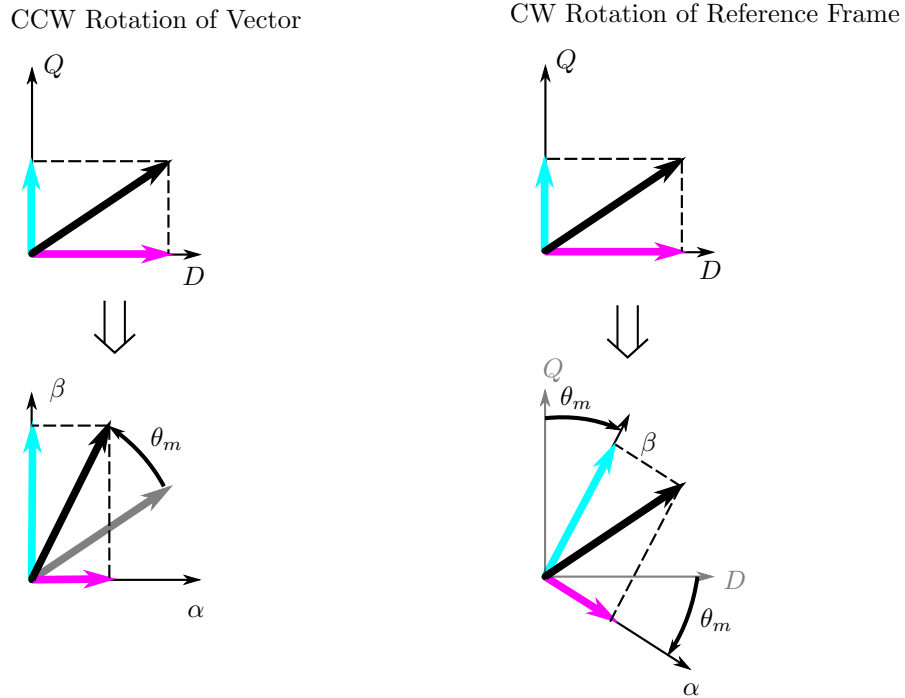


Figure 3.10: Different Interpretations of the Rotation Transformation

<sup>4</sup>of course they have to be since the same operator  $e^{j\theta}$  is being applied in both cases

### 3.3.2.3 Definition of Reference Frames

A reference frame in this work refers to a set of two orthogonal axes on which space vectors are defined. Two reference frames have already been introduced. The stator reference frame which is unmoving and locked to the stator and the rotor reference frame which is locked to the moving rotor, and therefore rotates at the rotor's angular velocity  $\omega_m$ . There is one more reference frame of interest, the general synchronous reference frame.

The general synchronous reference frame is distinguished by its speed, which is synchronous angular velocity in the two pole environment,  $\omega_g = \omega_s$ . This speed is defined by the speed of rotation of the stator's magnetic field. For an induction machine this speed is very important because under balanced conditions and when referenced to the stator, all quantities will rotate at synchronous speed, regardless of which member of the machine they exist in. Since this frame rotates at the same speed as all space vectors in the machine, the components of all vectors are constant, instead of sinusoidal. This is an important fact that is exploited for control later. Notice that the initial position of the synchronous frame has not been defined yet. That is why this frame is denoted in the superscript by the letter (g)<sup>5</sup>, it is left undefined so it can be aligned to any vector. By aligning this frame with an arbitrary space vector at time  $t = 0$ , the reference frame will always stay aligned to that vector because they are both rotating at synchronous speed.

Some authors, including "P. Vas," [11], define another reference frame called the general reference frame, which they use for aligning to arbitrary vectors. They do this to cover the case in which everything is not balanced, and the vectors do not spin at synchronous speed. Since this work assumes only balanced conditions, all vectors will rotate at synchronous speed when viewed from the stator, so a separate general reference frame with an arbitrary speed of rotation is unnecessary.

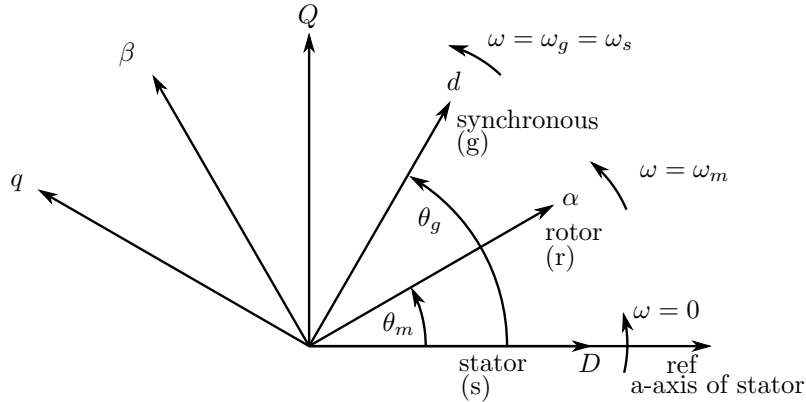


Figure 3.11: Definition of Reference Frames

To be explicit and clear, two properties fully define a reference frame; its angular velocity and its initial alignment at  $t = 0$ . Figure 3.11 defines all frames and their notations. The stator reference frame axes are labelled with DQ and it is denoted as the superscript (<sup>s</sup>) when referred to in a space vector. It is not moving, ( $\omega = 0[\frac{\text{rad}}{\text{sec}}]$ ). and it is initialized at  $\theta = 0[\text{rad}]$ , where  $0[\text{rad}]$  is defined as the positive a-axis of the stator. The rotor reference frame is labelled with  $\alpha\beta$  and is assigned

<sup>5</sup>g stands for general

From↓ To→	stator	rotor	synchronous
stator	-	$e^{-j\theta_m}$	$e^{-j\theta_g}$
rotor	$e^{j\theta_m}$	-	$e^{-j(\theta_g-\theta_m)}$
synchronous	$e^{j\theta_g}$	$e^{j(\theta_g-\theta_m)}$	-

Table 3.1: Rotational Transforms to Change Between Reference Frames

the superscript ( $r$ ) in the space vector notation. It is spinning at  $\omega = \omega_m [\frac{\text{rad}}{\text{sec}}]$ . The displacement from the stator reference frame is measured by  $\theta_m$ . The rotor is free to spin and its initial position for this work is unimportant and is arbitrarily chosen to coincide with the a-axis of the stator at  $t = 0$ , that is  $\theta_m(0) = 0[\text{rad}]$  which means that the rotor's A-axis is chosen to be in line with the stator's a-axis at  $t = 0$ . The general synchronous reference frame, labelled with  $dq$  and superscripted with ( $g$ ), rotates at  $\omega = \omega_g = \omega_s [\frac{\text{rad}}{\text{sec}}]$ . Its initial alignment  $\theta_g(0)$  is left undefined so that it can be aligned to whatever space vector is necessary for the analysis. Table 3.1 gives the rotational transform necessary to convert from one reference frame to another.

### 3.3.3 The Relationship Between Time Phasors and Space Vectors

The reason for finding the relationship between phasors and space vectors is for the initialization of the model from any steady state. The steady state solution of an induction machine is easily solved with phasors, then the results can be applied to initialize all the space vectors in the machine [8]. Equation 3.2 and Figure 3.6 show the correspondence. In terms of magnitude a space vector is  $\frac{3}{2}$  larger than the peak of the input sinusoids. A phasor's magnitude is the rms quantity of an input sinusoid. Recall Equation 3.3

$$v_a(t) = V \cos(\omega t + \phi), \quad (3.3a)$$

$$v_b(t) = V \cos(\omega t + \phi - \frac{2\pi}{3}), \quad (3.3b)$$

$$v_c(t) = V \cos(\omega t + \phi - \frac{4\pi}{3}). \quad (3.3c)$$

The space vector for this three phase set is, (Recall equation 3.4)

$$\vec{v}_s^s = \frac{3}{2} V e^{j(\omega t + \phi)}. \quad (3.4)$$

Its magnitude is

$$|\vec{v}_s^s| = \frac{3}{2} V. \quad (3.9)$$

The phasor for Equation 3.3a is

$$\bar{V}_a = \frac{V}{\sqrt{2}} \angle \phi. \quad (3.10)$$

Its magnitude is

$$|\bar{V}_a| = \frac{V}{\sqrt{2}}. \quad (3.11)$$

Thus the relationship between magnitudes is

$$|\vec{v}_s^s| = \frac{3}{\sqrt{2}} |\bar{V}_a|. \quad (3.12)$$

The phase angle  $\phi$  in the phasor is equal to the space angle  $\phi$  of the space vector at  $t = 0$ . After  $t = 0$  the space vector begins rotating and the correspondence is lost, but for initialization, the relationship only needs to hold at  $t = 0$ . The phase angle is equal to the space angle at  $t = 0$ , but this holds true only if everything is defined the way it has been. For instance the three phase balanced set is referenced to cosine, which has its positive peak for an argument of zero. This causes the space vector to develop in the direction of the a-axis at  $t = 0$ . If the three phase set was defined with sine instead, it would develop  $90^\circ$  lagging the a-axis and this shift would have to be accounted for.

Therefore, ensuring that the input three phase balanced sinusoids are referenced to cosine, the magnitudes of the time phasor and space vector are related by Equation 3.12 and the space angle is equal to the phase shift of the a-phase phasor at time  $t = 0$ .

### 3.4 Interaction of Electrical Variables

The main purpose of the electrical subsystem is to define the relationship between the electrical variables in the machine and the torque, so it can be connected to the mechanical subsystem. Additionally it is important that all intermediate electrical variables are characterized instantaneously through time so that information of energy flow in the machine is known for all time. The machine under study, being a wound rotor induction machine, has a three phase winding set with terminal access on both the stator and rotor, the latter through slip rings. All windings are characterized by their self and mutual inductances, which interact magnetically with other windings in the machine. The voltages ( $v$ ) subjected to or developed from the coils, along with the currents ( $i$ ) flowing through them and the magnetic flux linked ( $\lambda$ ) are the principal electrical variables of interest.

#### 3.4.1 Electrical Equations in their Natural Reference Frames

The derivation of the electrical equations of an induction machine is a topic covered extensively by many authors [8, 11, 20]. Both [11] and [20] explicitly show the position varying mutual inductances that link each winding and how using a proper reference frame removes this complication. [8] skips this and goes directly to into space vectors and avoids the complex arithmetic. This work follows that approach and the voltage and flux equations written with space vectors will be the starting point.

The model takes voltage to be the input and then will calculate the currents and flux linkages. The voltage across the stator and rotor windings is written as a voltage drop across the winding resistance and the voltage due to a change in flux linkage through the winding [8];

$$\vec{v}_s^s = R_s \vec{i}_s^s + \frac{d}{dt} \vec{\lambda}_s^s, \quad (3.13)$$

$$\vec{v}_r^r = R_r \vec{i}_r^r + \frac{d}{dt} \vec{\lambda}_r^r, \quad (3.14)$$

where  $R_s$  and  $R_r$  are the resistance of the stator and rotor windings in one phase respectively. Note

that in the stator voltage equation, the voltage current and flux linkage are referenced to the stator and similarly in the rotor, they are referenced to the rotor. Next the relationship between the current and flux linkage is given as [8]

$$\vec{\lambda}_s^s = L_s \vec{i}_s^s + L_m \vec{i}_r^s, \quad (3.15)$$

$$\vec{\lambda}_r^r = L_m \vec{i}_s^r + L_r \vec{i}_r^r, \quad (3.16)$$

where  $L_m$  is the per phase magnetizing inductance,  $L_s = L_{ls} + L_m$  is the total stator inductance,  $L_{ls}$  is the stator leakage inductance,  $L_r = L_{lr} + L_m$  is the total rotor inductance and  $L_{lr}$  is the rotor leakage inductance.

### 3.4.2 Electrical Equations in the General Synchronously Rotating Reference Frame

The equations are simple when written in their natural reference frames, but they cannot be solved simultaneously in this form. They must be brought to the same frame. Some equations are in the stator reference frame, Equations 3.13 and 3.15, and others are in the rotor reference frame, Equations 3.14 and 3.16. Instead of transforming the stator referenced equations to the rotor, or the rotor referenced equations to the stator, all equations will be referenced to a general frame. This will make it simple to change reference frames and align to particular space vectors. As stated before in Section 3.3.2.3 this general reference frame rotates at synchronous speed and is not aligned to any particular vector, until necessary. The rotational transformations to take the stator or rotor referenced equations to the general synchronous reference frame can be found in Table 3.1.

The stator quantities are brought to the general synchronous reference frame by multiplying them by the rotational transform  $e^{-j\theta_g}$ ;

$$\vec{v}_s^g = \vec{v}_s^s e^{-j\theta_g} \implies \vec{v}_s^s = \vec{v}_s^g e^{j\theta_g}, \quad (3.17a)$$

$$\vec{i}_s^g = \vec{i}_s^s e^{-j\theta_g} \implies \vec{i}_s^s = \vec{i}_s^g e^{j\theta_g}, \quad (3.17b)$$

$$\vec{\lambda}_s^g = \vec{\lambda}_s^s e^{-j\theta_g} \implies \vec{\lambda}_s^s = \vec{\lambda}_s^g e^{j\theta_g}. \quad (3.17c)$$

Similarly the rotor quantities are brought to the synchronous frame with the rotational transform  $e^{-j(\theta_g - \theta_m)}$ ;

$$\vec{v}_r^g = \vec{v}_r^r e^{-j(\theta_g - \theta_m)} \implies \vec{v}_r^r = \vec{v}_r^g e^{j(\theta_g - \theta_m)}, \quad (3.18a)$$

$$\vec{i}_r^g = \vec{i}_r^r e^{-j(\theta_g - \theta_m)} \implies \vec{i}_r^r = \vec{i}_r^g e^{j(\theta_g - \theta_m)}, \quad (3.18b)$$

$$\vec{\lambda}_r^g = \vec{\lambda}_r^r e^{-j(\theta_g - \theta_m)} \implies \vec{\lambda}_r^r = \vec{\lambda}_r^g e^{j(\theta_g - \theta_m)}. \quad (3.18c)$$

The flux linkages of the stator and the rotor in their own frames from Equations 3.15 and 3.16 can be expressed in the same frame:

$$\vec{\lambda}_s^g = L_s \vec{i}_s^g + L_m \vec{i}_r^g, \quad (3.19)$$

$$\vec{\lambda}_r^g = L_m \vec{i}_s^g + L_r \vec{i}_r^g. \quad (3.20)$$

These expressions will be useful to develop the control equations later.

Now the transformed variables in Equations 3.17 and 3.18 are substituted into the voltage Equations 3.13 and 3.14;

$$\vec{v}_s^g e^{j\theta_g} = R_s \vec{i}_s^g e^{j\theta_g} + \frac{d}{dt} (\vec{\lambda}_s^g e^{j\theta_g}), \quad (3.21)$$

$$\vec{v}_r^g e^{j(\theta_g - \theta_r)} = R_r \vec{i}_s^g e^{j(\theta_g - \theta_r)} + \frac{d}{dt} (\vec{\lambda}_r^g e^{j(\theta_g - \theta_r)}). \quad (3.22)$$

The derivatives are important and lead to the motional electromotive force (emf) terms in the final equations, their step by step solutions are given in Appendix A.4. The voltage equations become

$$\vec{v}_s^g = R_s \vec{i}_s^g + \frac{d}{dt} \vec{\lambda}_s^g + j\omega_g \vec{\lambda}_s^g, \quad (3.23)$$

$$\vec{v}_r^g = R_r \vec{i}_r^g + \frac{d}{dt} \vec{\lambda}_r^g + j(\omega_g - \omega_m) \vec{\lambda}_r^g. \quad (3.24)$$

At this point a choice must be made for the state variables. Either currents or flux linkages (or a combination of both) must be chosen. In the end, only four variables are needed to describe the system of electrical equations because it is fourth order. Through experience it has been determined that choosing flux linkage as the state variables has a considerable advantage. The flux linkage varies much slower than the currents and thus time steps for the simulation can be chosen larger and the simulation speed can be drastically improved. Equations 3.15 and 3.16 are solved for  $\vec{i}_s^g$  and  $\vec{i}_r^g$ ,

$$\vec{i}_s^g = \frac{\begin{vmatrix} \vec{\lambda}_s^g & L_m \\ \vec{\lambda}_r^g & L_r \end{vmatrix}}{\begin{vmatrix} L_s & L_m \\ L_m & L_r \end{vmatrix}} = \frac{L_r \vec{\lambda}_s^g - L_m \vec{\lambda}_r^g}{L_s L_r - L_m^2} = \vec{\lambda}_s^g \frac{1}{\sigma L_s} - \vec{\lambda}_r^g \frac{L_m}{\sigma L_s L_r}, \quad (3.25)$$

$$\vec{i}_r^g = \frac{\begin{vmatrix} L_s & \vec{\lambda}_s^g \\ L_m & \vec{\lambda}_r^g \end{vmatrix}}{\begin{vmatrix} L_s & L_m \\ L_m & L_r \end{vmatrix}} = \frac{L_s \vec{\lambda}_r^g - L_m \vec{\lambda}_s^g}{L_s L_r - L_m^2} = \vec{\lambda}_r^g \frac{1}{\sigma L_r} - \vec{\lambda}_s^g \frac{L_m}{\sigma L_s L_r}, \quad (3.26)$$

where  $\sigma = 1 - \frac{L_m^2}{L_s L_r}$  is the total leakage factor. Substituting  $\vec{i}_s^g$  and  $\vec{i}_r^g$  from Equations 3.25 and 3.26 into Equations 3.23 and 3.24 yields the voltage equations in the general synchronous frame in terms of flux linkage;

$$\begin{aligned} \vec{v}_s^g &= \left( \vec{\lambda}_s^g \frac{1}{\sigma L_s} - \vec{\lambda}_r^g \frac{L_m}{\sigma L_s L_r} \right) R_s + \frac{d}{dt} \vec{\lambda}_s^g + j\omega_g \vec{\lambda}_s^g \\ &= \frac{d}{dt} \vec{\lambda}_s^g + \left( \frac{R_s}{\sigma L_s} + j\omega_g \right) \vec{\lambda}_s^g + \frac{L_m R_s}{\sigma L_s L_r} \vec{\lambda}_r^g, \end{aligned} \quad (3.27)$$

$$\begin{aligned}
\vec{v}_r^{\rightarrow g} &= \left( \vec{\lambda}_r^{\rightarrow g} \frac{1}{\sigma L_r} - \vec{\lambda}_s^{\rightarrow g} \frac{L_m}{\sigma L_s L_r} \right) R_r + \frac{d}{dt} \vec{\lambda}_r^{\rightarrow g} + j(\omega_g - \omega_m) \vec{\lambda}_r^{\rightarrow g} \\
&= \frac{d}{dt} \vec{\lambda}_r^{\rightarrow g} + \left( \frac{R_r}{\sigma L_r} + j(\omega_g - \omega_m) \right) \vec{\lambda}_r^{\rightarrow g} + \frac{L_m R_r}{\sigma L_s L_r} \vec{\lambda}_s^{\rightarrow g}. \tag{3.28}
\end{aligned}$$

### 3.4.3 Electrical Equations in Scalar Form

Writing the equations as space vectors allowed for easy manipulation and alignment to the general synchronous reference frame. However the equations are not in a form suitable for computer simulation. Furthermore the variables must be scalar to perform standard control laws on them. Decomposing the equations is a trivial task, it involves projecting them onto the axes (dq) of the reference frame they are aligned to. First the voltage equations are written in standard form for a set of first order differential equations, that is the derivatives of flux linkage are isolated in Equations 3.27 and 3.28,

$$\frac{d}{dt} \vec{\lambda}_s^{\rightarrow g} = \vec{\lambda}_s^{\rightarrow g} \left( -\frac{R_s}{\sigma L_s} - j\omega_g \right) + \vec{\lambda}_r^{\rightarrow g} \left( \frac{L_m R_s}{\sigma L_s L_r} \right) + \vec{v}_s^{\rightarrow g}, \tag{3.29}$$

$$\frac{d}{dt} \vec{\lambda}_r^{\rightarrow g} = \vec{\lambda}_s^{\rightarrow g} \left( \frac{L_m R_r}{\sigma L_s L_r} \right) + \vec{\lambda}_r^{\rightarrow g} \left( -\frac{R_r}{\sigma L_r} - j(\omega_g - \omega_m) \right) + \vec{v}_r^{\rightarrow g}. \tag{3.30}$$

Next the equations are projected onto the  $dq$  axes. Each space vector is broken down into its component vectors; for example  $\vec{\lambda}_s^{\rightarrow g} = \lambda_{sd} + j\lambda_{sq}$ .

$$\frac{d}{dt} (\lambda_{sd} + j\lambda_{sq}) = (\lambda_{sd} + j\lambda_{sq}) \left( -\frac{R_s}{\sigma L_s} - j\omega_g \right) + (\lambda_{rd} + j\lambda_{rq}) \left( \frac{L_m R_s}{\sigma L_s L_r} \right) + (v_{sd} + jv_{sq}), \tag{3.31}$$

$$\frac{d}{dt} (\lambda_{rd} + j\lambda_{rq}) = (\lambda_{sd} + j\lambda_{sq}) \left( \frac{L_m R_r}{\sigma L_s L_r} \right) + (\lambda_{rd} + j\lambda_{rq}) \left( -\frac{R_r}{\sigma L_r} - j(\omega_g - \omega_m) \right) + (v_{rd} + jv_{rq}). \tag{3.32}$$

The  $d$  and  $q$  axes are orthogonal in space, so any value on one axis has no effect on the other. The result is that a separate differential equation of flux linkage can be written for each axis on both the stator and rotor, making four scalar differential equations. The brackets in Equations 3.31 and 3.32 are expanded and the result is separated by grouping all real terms with the  $d$ -axis equations and all imaginary terms with  $q$ -axis equations;

$$\frac{d}{dt} \lambda_{sd} = -\frac{R_s}{\sigma L_s} \lambda_{sd} + \omega_g \lambda_{sq} + \frac{L_m R_s}{\sigma L_s L_r} \lambda_{rd} + v_{sd}, \tag{3.33a}$$

$$\frac{d}{dt} \lambda_{sq} = -\omega_g \lambda_{sd} - \frac{R_s}{\sigma L_s} \lambda_{sq} + \frac{L_m R_s}{\sigma L_s L_r} \lambda_{rq} + v_{sq}, \tag{3.33b}$$

$$\frac{d}{dt} \lambda_{rd} = \frac{L_m R_r}{\sigma L_s L_r} \lambda_{sd} - \frac{R_r}{\sigma L_r} \lambda_{rd} + (\omega_g - \omega_m) \lambda_{rq} + v_{rd}, \tag{3.33c}$$

$$\frac{d}{dt} \lambda_{rq} = \frac{L_m R_r}{\sigma L_s L_r} \lambda_{sq} - (\omega_g - \omega_m) \lambda_{rd} - \frac{R_r}{\sigma L_r} \lambda_{rq} + v_{rq}. \tag{3.33d}$$

In matrix form, the state equations for the electrical subsystem are

$$\frac{d}{dt} \begin{bmatrix} \lambda_{sd} \\ \lambda_{qd} \\ \lambda_{rd} \\ \lambda_{rq} \end{bmatrix} = \begin{bmatrix} -\frac{R_s}{\sigma L_s} & \omega_g & \frac{L_m R_s}{\sigma L_s L_r} & 0 \\ -\omega_g & -\frac{R_s}{\sigma L_s} & 0 & \frac{L_m R_s}{\sigma L_s L_r} \\ \frac{L_m R_r}{\sigma L_s L_r} & 0 & -\frac{R_s}{\sigma L_r} & \omega_g - \omega_m \\ 0 & \frac{L_m R_r}{\sigma L_s L_r} & -(\omega_g - \omega_m) & -\frac{R_s}{\sigma L_r} \end{bmatrix} \begin{bmatrix} \lambda_{sd} \\ \lambda_{qd} \\ \lambda_{rd} \\ \lambda_{rq} \end{bmatrix} + \begin{bmatrix} v_{sd} \\ v_{qd} \\ v_{rd} \\ v_{rq} \end{bmatrix}. \quad (3.34)$$

### 3.4.4 Electromagnetic Torque Equation

As stated before, the electromagnetic torque is the single most important variable of the induction machine. It forms the link between electrical and mechanical systems. Physically torque arises from the forces present when a current carrying conductor passes through a magnetic field. Torque is proportional to the cross product of the rotor flux linkage space vector and the rotor current space vector in any general reference frame [11],

$$T_{em} = -\frac{3}{2} P_p \vec{\lambda}_r^g \times \vec{i}_r^g. \quad (3.35)$$

The factor of  $\frac{3}{2}$  is necessary for power equivalence between two axis and three axis variables, see Appendix A.3. The torque is directly proportional to  $P_p$ , the number of pole pairs, because the space vectors only account for one pole pair as explained in Section 2.1.1. The negative sign is necessary to ensure the cross product conforms with the conventions taken by the author in [11] and creates a torque which acts in the counter-clockwise direction when positive. The cross product is formally defined for three dimensional vectors but can also be applied to two dimensional space vectors, see Appendix A.5. Since the state variables were chosen as flux linkage, it is advantageous to calculate the torque directly from these variables. The torque expression can easily written in terms of any desired variables by using the flux and current relations given explicitly in Equations 3.15, 3.16, 3.25 and 3.26. Replacing the rotor current in Equation 3.35 with the expression in Equation 3.26 yields

$$\begin{aligned} T_{em} &= -\frac{3}{2} P_p \vec{\lambda}_r^g \times \left( \vec{\lambda}_r^g \frac{1}{\sigma L_r} - \vec{\lambda}_s^g \frac{L_m}{\sigma L_s L_r} \right) \\ &= -\frac{3}{2} P_p \left( \vec{\lambda}_r^g \times \vec{\lambda}_r^g \frac{1}{\sigma L_r} - \vec{\lambda}_r^g \times \vec{\lambda}_s^g \frac{L_m}{\sigma L_s L_r} \right) \\ &= \frac{3}{2} P_p \frac{L_m}{\sigma L_s L_r} \vec{\lambda}_r^g \times \vec{\lambda}_s^g \\ &= \frac{3}{2} P_p \frac{L_m}{\sigma L_s L_r} (\lambda_{rd} \lambda_{sq} - \lambda_{rq} \lambda_{sd}). \end{aligned} \quad (3.36)$$



### 3.4.5 Dynamic Power Expressions

To complete the model it is necessary to compute the real and reactive power in the stator and rotor. The equations are similar to the steady state forms, see Equations 2.5, 2.5, 2.5 and 2.5, with the exceptions of the factor of  $\frac{3}{2}$  explained in Appendix A.3. The dynamic power expressions in terms of space vectors and their components are:

$$P_s = \frac{3}{2} \text{Re} \left\{ \vec{v}_s^g \vec{i}_s^g \right\} = \frac{3}{2} (v_{sd} i_{sd} + v_{sq} i_{sq}), \quad (3.37)$$

$$Q_s = \frac{3}{2} \text{Im} \left\{ \vec{v}_s^g \vec{i}_s^g \right\} = \frac{3}{2} (v_{sq} i_{sd} - v_{sd} i_{sq}), \quad (3.38)$$

$$P_r = \frac{3}{2} \text{Re} \left\{ \vec{v}_r^g \vec{i}_r^g \right\} = \frac{3}{2} (v_{rd} i_{rd} + v_{rq} i_{rq}), \quad (3.39)$$

$$Q_r = \frac{3}{2} \text{Im} \left\{ \vec{v}_r^g \vec{i}_r^g \right\} = \frac{3}{2} (v_{rq} i_{rd} - v_{rd} i_{rq}). \quad (3.40)$$

## 3.5 The Mechanical Subsystem

The mechanical subsystem is treated as simply as possible, as it is not the focus of this model. Only the most basic interaction between the acceleration and torque balance is considered [20],

$$T_{em} - T_{load} = J \frac{d}{dt} \omega_{mech}. \quad (3.41)$$

where  $T_{load}$  is the torque on the shaft originating from mechanical means and  $J$  is the inertia on the shaft. Substituting  $\omega_m$  for  $\omega_{mech}$  using Equation 2.2 puts the equation into the 2-pole domain and allows it to be directly coupled with the electrical equations,

$$\begin{aligned} \frac{d}{dt} \frac{\omega_m}{P_p} &= \frac{1}{J} (T_{em} - T_{load}) \\ \frac{d}{dt} \omega_m &= \frac{P_p}{J} (T_{em} - T_{load}). \end{aligned} \quad (3.42)$$

Notice that  $T_{em}$  has been chosen positive and  $T_{load}$  has been subtracted from it, to emphasize the fact that these torques are always in opposition to each other. The convention is that a positive  $T_{em}$  and  $T_{load}$  correspond to the motoring mode and a negative  $T_{em}$  and  $T_{load}$  correspond to a generating mode. Of course a machine can be made to motor or generate in either direction but this model is intended to be used with a wind turbine which is always made to spin in the same direction, assumed counter-clockwise in this model. Thus when  $T_{em} > 0$  then it is in the counter-clockwise sense, the torque and angular velocity are in the same direction and the machine is motoring. When  $T_{em} < 0$  then it is in the clockwise sense, opposite to the direction of the angular velocity and the machine is generating. This also implies that applying a load torque for motoring to the machine requires  $T_{load} > 0$  and applying a prime mover torque for generating requires  $T_{load} < 0$ .

### 3.6 The Complete Fifth Order Model

This section brings together all equations necessary for the simulation. The electrical and mechanical equations given in Equations 3.33 and 3.42 form the state equations of the machine:

$$\frac{d}{dt}\lambda_{sd} = -\frac{R_s}{\sigma L_s}\lambda_{sd} + \omega_g\lambda_{sq} + \frac{L_m R_s}{\sigma L_s L_r}\lambda_{rd} + v_{sd}, \quad (3.33a)$$

$$\frac{d}{dt}\lambda_{sq} = -\omega_g\lambda_{sd} - \frac{R_s}{\sigma L_s}\lambda_{sq} + \frac{L_m R_s}{\sigma L_s L_r}\lambda_{rq} + v_{sq}, \quad (3.33b)$$

$$\frac{d}{dt}\lambda_{rd} = \frac{L_m R_r}{\sigma L_s L_r}\lambda_{sd} - \frac{R_s}{\sigma L_r}\lambda_{rd} + (\omega_g - \omega_m)\lambda_{rq} + v_{rd}, \quad (3.33c)$$

$$\frac{d}{dt}\lambda_{rq} = \frac{L_m R_r}{\sigma L_s L_r}\lambda_{sq} - (\omega_g - \omega_m)\lambda_{rd} - \frac{R_s}{\sigma L_r}\lambda_{rq} + v_{rq}, \quad (3.33d)$$

$$\frac{d}{dt}\omega_m = \frac{P_p}{J}(T_{em} - T_{load}). \quad (3.42)$$

The torque in terms of the flux, Equation 3.36, is an axillary equation which links the two systems;

$$T_{em} = \frac{3}{2}P_p \frac{L_m}{\sigma L_s L_r}(\lambda_{rd}\lambda_{sq} - \lambda_{rq}\lambda_{sd}). \quad (3.36)$$

### 3.7 Wound Rotor Induction Machine Parameters

To use the dynamic model presented in this chapter, it is necessary to populate it with parameters. Obtaining the required parameters from manufacturer nameplates or data sheets is not sufficient. Parameter determination experiments must be run on the machine to determine the equivalent circuit parameters. Instead, the values reported by *Abad et al.* for a 2MW wound rotor induction machine are used in this work [7]. They are shown in Table 3.2.

A 2 MW generator was chosen as it will be of sufficient size to be matched to a multi-megawatt turbine, which will be chosen in Section 4.4. This machine is also ideally suited for doubly-fed operation. As explained in Section 1.1.1.1, DFIGs realize their main advantage by limiting their slip about 30% around synchronous speed. According to Equation 2.8, the stator and rotor voltages (neglecting voltage drops across  $R_s$  and  $R_r$ ) are related by,

$$\frac{\overline{V}_s}{\overline{V}_r} = \frac{s}{TR}. \quad (3.44)$$

Thus at its maximum operating speed the rotor voltage is approximately 30% of the stator voltage, if the turns ratio is one. This presents a problem of mismatched voltage level requirements for the stator and rotor windings. The rotor does not generate or require as much voltage as the stator, and a transformer is needed between the connection of the back to back converter attached to the rotor and the grid [7]. To balance the voltages, a wound rotor induction machine intended for doubly-fed configuration will normally be built with an effective turns ratio of about 0.3. Removing the transformer is not the only advantage of the higher rotor turns; by stepping up the rotor voltage, the

Parameter	Symbol	Value	Unit
rated power	$P_{rated}$	2	MW
rated stator frequency	$f_s$	50	Hz
rated stator current (rms)	$I_{s,rated}$	1760	A
rated stator voltage (line-to-line, rms)	$V_{LLrms}$	690	V
rated rotor voltage (line-to-line, rms)	$V_{r,rated}$	2070	V
effective turns ratio	$TR$	0.34	dimensionless
number of pole pairs	$P_p$	2	dimensionless
stator resistance	$R_s$	2.6	m $\Omega$
stator leakage inductance	$L_{ls}$	0.087	mH
rotor resistance (referred)	$R_r$	2.9	m $\Omega$
rotor leakage inductance (referred)	$L_{lr}$	0.087	mH
magnetizing inductance	$L_m$	2.5	mH
system inertia	$J$	98.26	Kg · m <sup>2</sup>

Table 3.2: Wound Rotor Induction Generator Parameters [7, 6].

machine becomes easier to control. As the speed of the system approaches synchronous, the rotor voltage diminishes in proportion. However, all control is done through the rotor, and if the voltage becomes too low, approaching zero, control is lost. This problem has been addressed by *Cadiraci et al.* [24], and is alleviated by increasing the rotor voltage magnitude. Note that the rotor voltage winding rating is about three times as high as the stator's to accommodate triple the voltage which could be impressed upon the rotor if the machine came to stop ( $s = 1$ ) while connected to the grid.

The inertia  $J$  presented is a fictitious value that has been reduced from the real value to speed up simulations [6]. Large MW scale turbines have very large moments of inertia because of the heavy spinning blades and hub assembly attached to their rotor; in turn the speed changes very slowly. Thus to see dynamics in the system, very long simulations in the order of minutes need to be run. Reducing  $J$  will allow the same dynamic behaviour in much less time, on the order of a few seconds; the results must be interpreted with this in mind.

## Chapter 4

# Aerodynamic Model of the Wind Turbine

The complex behaviour of the atmosphere and wind patterns is not of concern in this work. Any aerodynamic phenomenon present in the turbine beyond what is necessary for the simulation is ignored. Only the most simplified and basic characteristics are accounted for.

The turbine is the prime mover of the system. The power extracted from the wind is seen by the generator as an input torque. The torque provided by the turbine depends on the parameters of the turbine itself, the speed of its own shaft and the speed of the wind.

### 4.1 Turbine Construction

The basic features of a modern wind turbine are necessary to understand its capabilities and how it is controlled under different circumstances. Figure 4.1 depicts the main components. The nacelle is the housing for the generator. It is able to rotate about its yaw axis so that the wind turbine is always squarely facing the direction of the incoming wind. In the equations, this simply means that the direction of the wind is not a variable.

Another feature is the ability to pitch the blades in and out of the wind. Pitching means twisting the blades about the hub. If the pitch angle ( $\beta$ ) is 0, it means the blades are facing so they gather as much wind as possible. As  $\beta$  increases the blades are turned out of the wind so they gather less power. The pitching of blades is necessary when the wind becomes so strong that the turbine would spin above its rated speed, and the power needs to be shed. The angle does effect the turbine characteristics as will be seen in the equations. However in this work  $\beta$  will always be kept at zero so that the blades are always capturing as much wind as possible and the pitch angle does not appear in the model.

The turbine shaft is much slower than that of the generator's rated speed, so a gear box is necessary. The gear ratio is fixed, there is no transmission, so the variable speed is handled by the generator

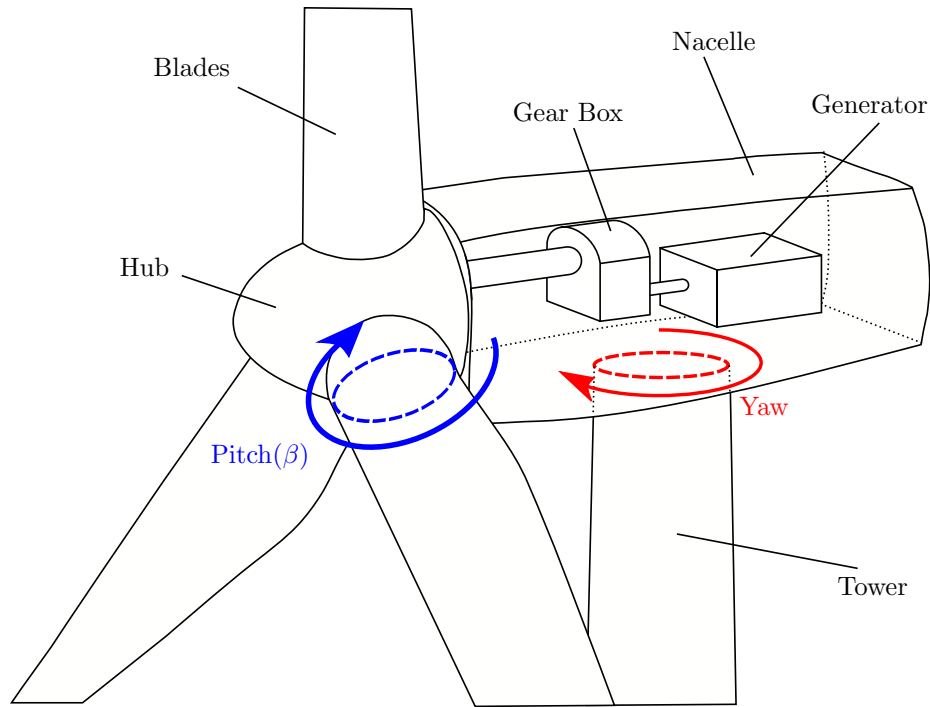


Figure 4.1: Main Structural Features of a Wind Turbine

and converter. The blades always spin in the same direction.

## 4.2 Turbine Operating Regions

Depending on wind speed the turbine is controlled differently with different goals and set points. There are four main regions [6], shown in Figure 4.2.

Region 1: There is a minimum wind speed that the turbine can operate with. Below the cut-in speed the turbine cannot cover its own losses or the small power that is produced is not profitable. In this area the turbine is held stationary with a mechanical brake.

Region 2: For the wind speeds between cut-in and rated, the turbine is controlled to extract the maximum power possible from the wind. It is known as the Maximum Power Point Tracking (MPPT) region. At the rated wind speed the turbine delivers its rated power.

Region 3: Here the wind speed is increasing, providing more power, but the rated power of the turbine is already being produced. The extra power is shed by pitching the turbine blades out of the wind.

Region 4: At the cut-out speed, the wind is too strong for safe operation of the turbine, and it is stopped completely with a mechanical brake.

This work concentrates on Region 2 and the MPPT problem exclusively. This means the control of the wind turbine's pitch to shed power is not covered.

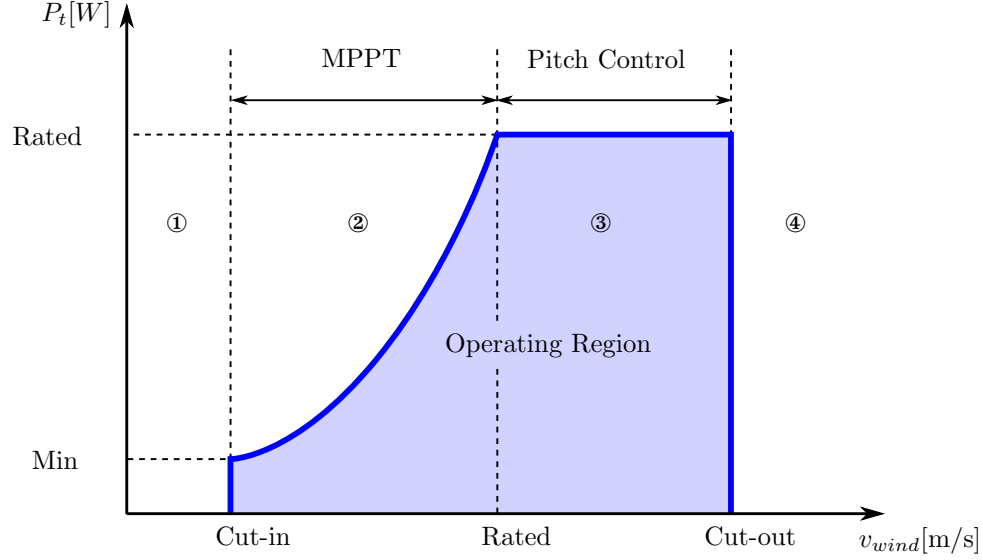


Figure 4.2: Operating Regions of a Wind Turbine

### 4.3 Aerodynamic Turbine Model

The purpose of this study is to come up with an expression of torque at the shaft of the generator from the wind turbine.

The power contained in the air is given by [25],

$$P_{wind} = \frac{1}{2}\rho A v_w^3 = \frac{1}{2}\rho\pi r_t^2 v_w^3. \quad (4.1)$$

Where  $\rho$  is the density of air in  $\text{kg/m}^3$ ,  $v_w$  is the air speed in  $\text{m/s}$ ,  $r_t$  is the radius of the wind turbine (length of blade) in  $\text{m}$  and  $A = \pi r_t^2$  is the cross sectional area of wind swept by the blades.

The power extracted by a wind turbine is always only a fraction of what exists in the wind. No turbine can extract all of it; the portion is expressed by the coefficient of performance  $C_p$ ,

$$P_t = C_p P_{wind} = \frac{1}{2}C_p \rho \pi r_t^2 v_w^3. \quad (4.2)$$

The coefficient of performance depends on the geometry of the turbine, the speed of the turbine's shaft, the speed of the wind and the pitch of the blades  $\beta$ . The first three parameters are combined into one variable known as the tip speed ratio,

$$\lambda = \frac{r_t \omega_t}{v_w}, \quad (4.3)$$

where  $\omega_t$  is the angular velocity of the wind turbine shaft measured in mechanical radians per second.  $\lambda$  is dimensionless, and expresses a ratio of how fast the tip of the blade is moving relative to how fast the wind is blowing. It is a convenient parameter that manufacturers use to plot and convey the coefficient of performance for each particular turbine. The relationship between  $C_p$ ,  $\lambda$  and  $\beta$  is nonlinear and is obtained by curve fitting experimental data. A curve fit for the MOD-2 type

turbine is given in [26], and will be used to show the effect of pitch angle,

$$\begin{cases} \frac{1}{\lambda_i} &= \frac{1}{\lambda+0.08\beta} - \frac{0.035}{\beta^3+1}, \\ C_p(\lambda, \beta) &= 0.5176 \left( \frac{116}{\lambda_i} - 0.4\beta - 5 \right) e^{-\frac{21}{\lambda_i}} + 0.0068\lambda. \end{cases} \quad (4.4)$$

Figure 4.3 shows the function in Equation 4.4 plotted for several values of  $\beta$ . Note that as  $\beta$  increases the coefficient of performance generally decreases. This is how power is shed in the high wind region, by making the air turbine less aerodynamically efficient in capturing the power of the wind. This work does not deal with this region so for the remainder of the text the wind turbine will only be examined at its highest efficiency where  $\beta = 0^\circ$ . By evaluating Equation 4.2, using Equation 4.3 and 4.4 for all values of wind speed and turbine angular velocity, a set of power curves for the turbine can be found. They will be very similar in shape to the  $C_p$  vs  $\lambda$  characteristic since it is a major factor in Equation 4.2. Before the power curves can be evaluated, the parameters from the manufacturer need to be known, a topic which will be covered in Section 4.4. However without evaluating the curves specifically the torque available at the turbine shaft can be calculated from the power,

$$T_t = \frac{P_t}{\omega_t}. \quad (4.5)$$

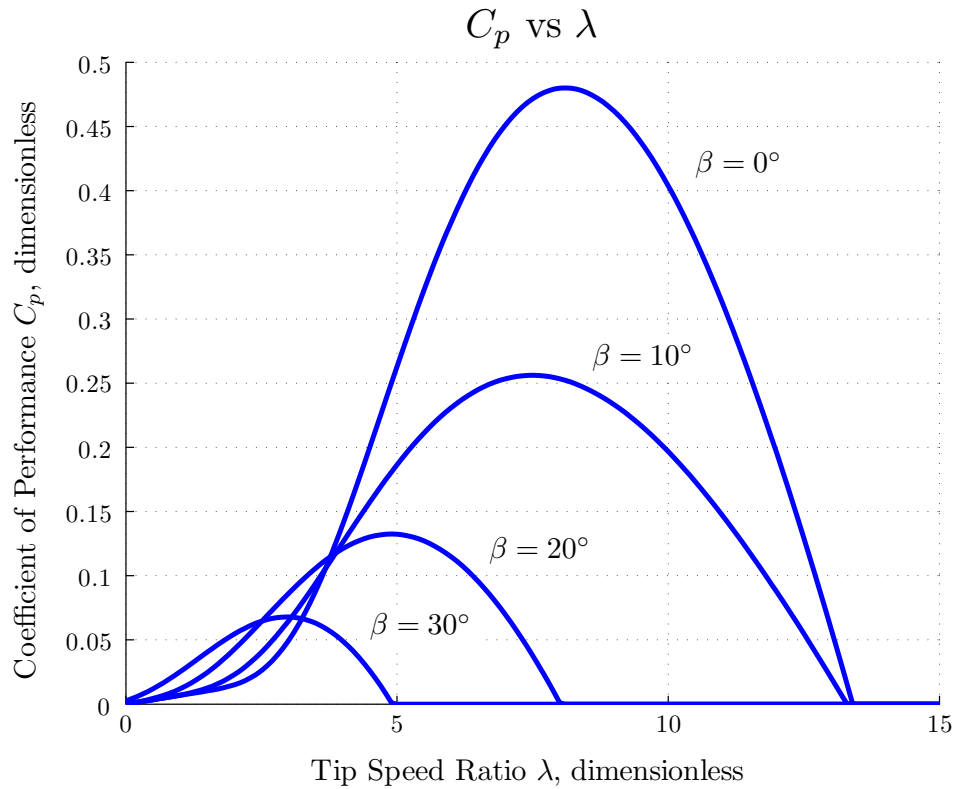


Figure 4.3: Coefficient of Performance Vs Tip Speed Ratio for Several Pitch Angles

### 4.3.1 Turbine Gearbox

The torque and speed of the turbine,  $T_t$  and  $\omega_t$ , are converted through a gear box to the torque and speed at the generator shaft,  $T_{mech}$  and  $\omega_{mech}$ . The gearbox is assumed to be ideal, with no friction or power losses, therefore,

$$P_{mech} = P_t. \quad (4.6)$$

The gearbox will gear down the turbine's shaft to the generator's shaft. That is, the turbine shaft has high torque and low speed, and the gearbox increases the speed by the same factor it decreases the torque as it transmits the same power to the generator's shaft. This factor is known as the gear ratio,  $GR$ . The torques and angular velocity on both sides of the gearbox are given by,

$$T_{mech} = \frac{T_t}{GR}, \quad (4.7)$$

$$\omega_{mech} = GR\omega_t. \quad (4.8)$$

Where variables subscripted with “*mech*” are on the generator side and variables subscripted with “*t*” are on the turbine side. A gearbox is necessary because a large turbine spins much slower than the rated speed of any standard generator, and also has a much higher torque.

## 4.4 Modelling a Wind Turbine From Manufacturer Data

Wind turbines are designed together with a specific generator type and size. Manufacturers usually provide minimal data for the turbine and its generator as noted by [7]. It is possible to come up with the simple aerodynamic model of the turbine using just the  $C_p$  vs.  $\lambda$  characteristic and a few other mechanical parameters. Unfortunately the generator data provided is not complete enough to parametrize the model of Section 3.6. Thus the approach taken in this work is to select the parameters of a generator from an alternative source, see Section 3.7, and then match a turbine of similar power to it as best as possible.

The generator chosen in Section 3.7 is rated at 2 MW. Since in supersynchronous operation a DFIG is normally operated to a maximum speed of 30% over synchronous, the maximum power that the machine will produce out of both the stator and rotor can be roughly seen by applying Equations 2.27 , 2.32 and 2.29 and ignoring losses,

$$P_r + P_s \approx P_{mech} = P_{ag}(1 - s) \approx P_s(1 - s) = 2M(1 + 0.3) = 2.6 \text{ MW}. \quad (4.9)$$

Therefore a turbine that can deliver around 2.6 MW around the generator's maximum speed within its rated wind speed range should be roughly matched. Relevant data for the wt2000df turbine from AMSC's Windtec Solutions [27] is provided in table 4.1. The coefficient of performance, shown in Figure 4.4 is found in a related document [28] for the D49 Blades used in the turbine. For the purpose of modelling the wind turbine, a curve fit will not be necessary since the result will eventually be put into a numerical look-up table anyway. The data is extracted from the plot and stored as an array; see the file *CpVsTSR\_49.xls* on the accompanying CD. To calculate the power



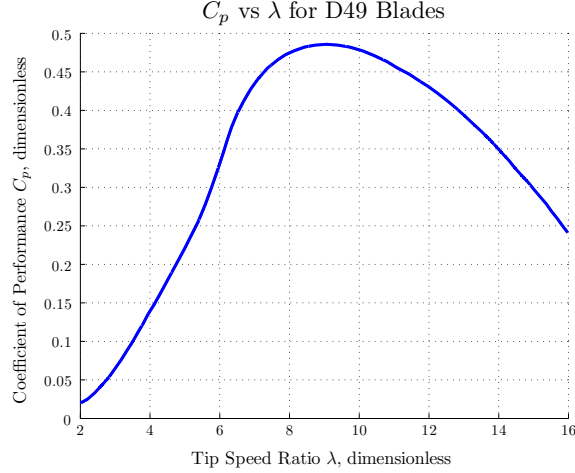


Figure 4.4: Coefficient of Performance Vs Tip Speed Ratio for D49 Blades

Parameter	Description	Value	Units
$r_t$	blade length	48.63	m
$\omega_{t,rated}$	rated rotational speed	15.7	rpm
$\rho$	air density	1.21	kg/m <sup>3</sup>
$v_{w,in}$	cut in wind speed	3	m/s
$v_{w,out}$	cut out wind speed	20	m/s
$v_{w,rated}$	rated wind speed	11	m/s

Table 4.1: Parameters of the wt2000df Turbine, from: [27] and [28]

curves the wind speed will be varied from 3 to 11 m/s. Beyond 11 m/s, the turbine enters the third control region, see Figure 4.2, where power needs to be shed. To get the complete curves, the range for the turbine shaft's angular velocity can be found from Equation 4.3.  $\lambda$  ranges from 2 to 16 and  $v_w$  ranges from 3 to 11. Therefore the smallest and largest value of  $\omega_t$  is:

$$\omega_t = \frac{\lambda v_w}{r} \implies \left[ \frac{2 \cdot 3}{48.63}, \frac{16 \cdot 11}{48.63} \right] = [0.1234, 3.6192] \text{ rad/sec.}$$

With these ranges for  $v_w$  and  $\omega_t$  the power curves for the turbine are calculated by evaluating Equation 4.2 over both independent variables. The code to perform the calculation is provided in Appendix B; the results are plotted in Figure 4.5.

The final parameter needed to connect the turbine to the generator is the gear ratio, which was not given in the data sheet. This is fine as it can be chosen to ensure that the speeds of the generator and turbine match properly. The generator has 4 poles, supplying a grid with 50 Hz frequency. Limiting the slip to 30% and using Equations 2.4 and 2.7c gives a speed range of 1050 to 1950 rpm. The peak of the power curves reach 2.6 MW around  $\omega_t = 18.9$  rpm. The gear ratio will be chosen so that 18.9 rpm on the turbine translates to about 1950 rpm on the generator, from Equation 4.8,

$$GR = \frac{\omega_{mech}}{\omega_t} = \frac{1950}{18.9} = 103.2.$$

Therefore the gear ratio is chosen as  $GR = 103.2$ . The torque and speed on both sides of the gearbox,

at the turbine and the generator, are calculated using Equation 4.5 and are shown in Figure 4.6.

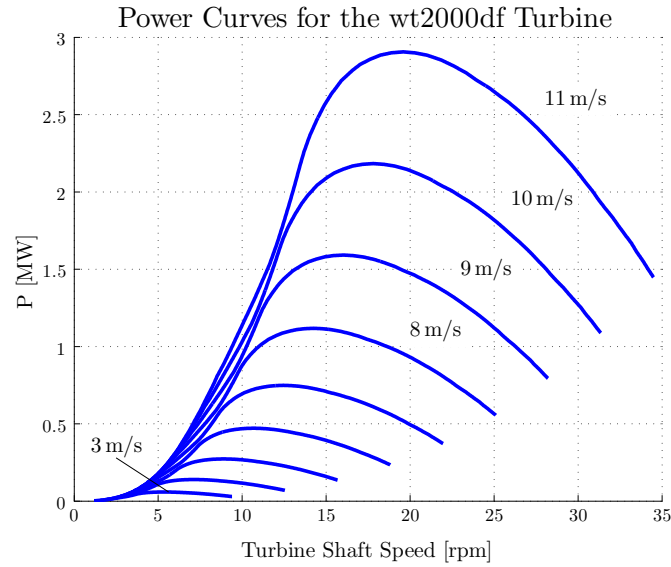


Figure 4.5: Power Curves for the wt2000df Turbine

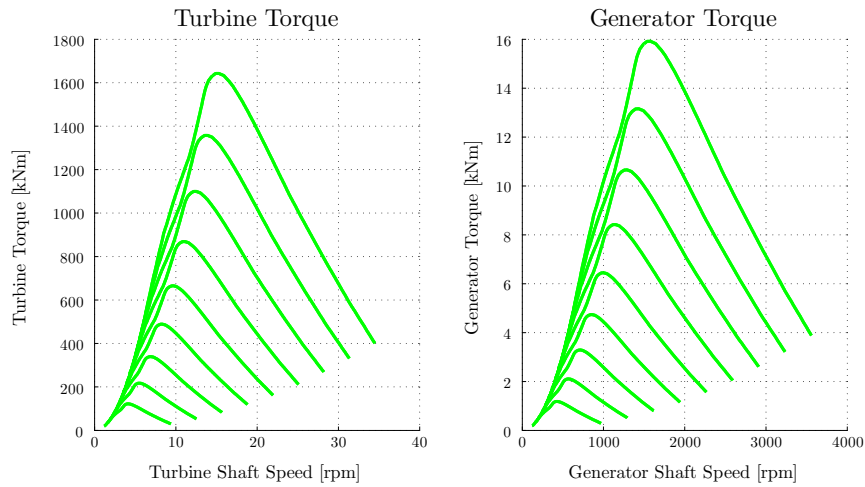


Figure 4.6: Torque Curves for wt2000df Turbine - Left: Torque on turbine shaft, Right: torque on generator's shaft after transformation through the gearbox with gear ratio of 103.2. Note that the curves correspond to the wind speeds marked on the power curves in Figure 4.5

## 4.5 Maximum Power Point Tracking (MPPT)

As explained in [6], the goal of the control strategy of a wind turbine is to extract the most amount of power from the wind as possible, when the wind speed is low enough that the turbine extracts less than rated power. From Figure 4.5 it can be seen that for every wind speed the turbine produces

the maximum power at a specific rotational speed. By finding the rotational speed that yields the maximum power at each wind speed, the maximum power point curve is found, see Figure 4.7. The set of points follows a cubic regression, which can be explained by the fact that the maximum power in the wind is proportional to the cube of wind speed, see Equation 4.1. The data is fit to the

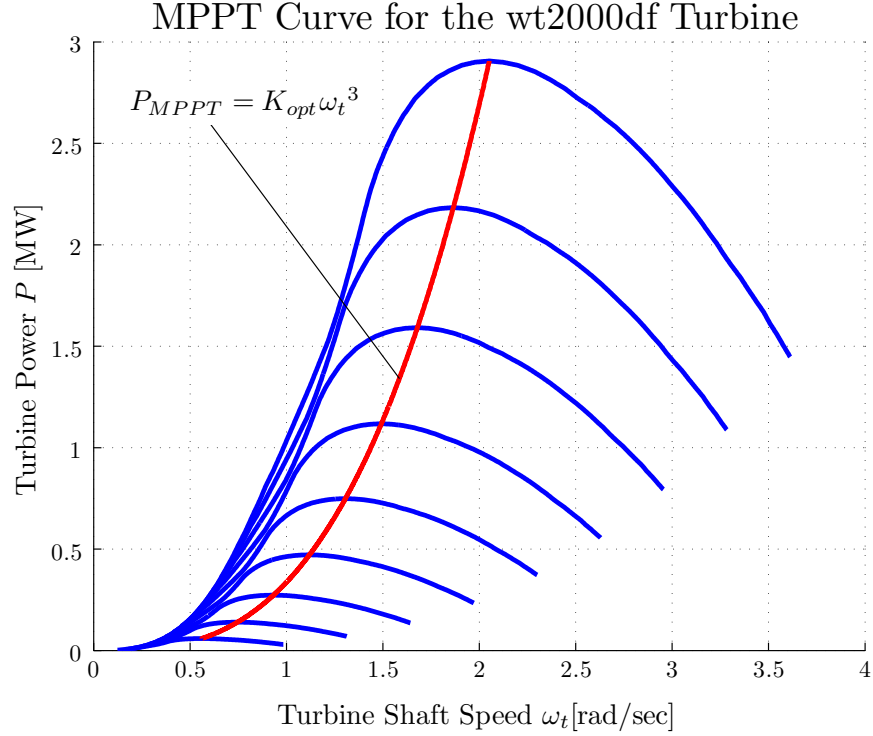


Figure 4.7: Maximum Power Point Tracking Curve

following function,

$$P_{MPPT}(\omega_t) = K_{opt}\omega_t^3, \quad (4.10)$$

where  $K_{opt}$  is the coefficient which satisfies the curve for a specific turbine characteristic. For the wt2000df wind turbine in Figure 4.5 cubic regression yields,

$$K_{opt} = 3.364 \times 10^5. \quad (4.11)$$

#### 4.5.1 Turbine Operation and Stability

To understand how a turbine operates under varying wind conditions, it is helpful to map the maximum power point curve into torque by dividing it by the rotational speed and superimposing it on the torque curves, this is done in Figure 4.8. The system will settle at the intersection of this curve and the curve of the turbine torque corresponding to the particular wind speed. For instance, if the wind speed is 8 m/s the turbine will be operating at point A. If the wind speed suddenly changes to 11 m/s the inertia of the blades and generator will not allow for a sudden change in shaft speed, so the operating point will be moved to point B. Here the turbine torque is greater than the back torque of the generator so the system will speed up. As it speeds up the turbine produces

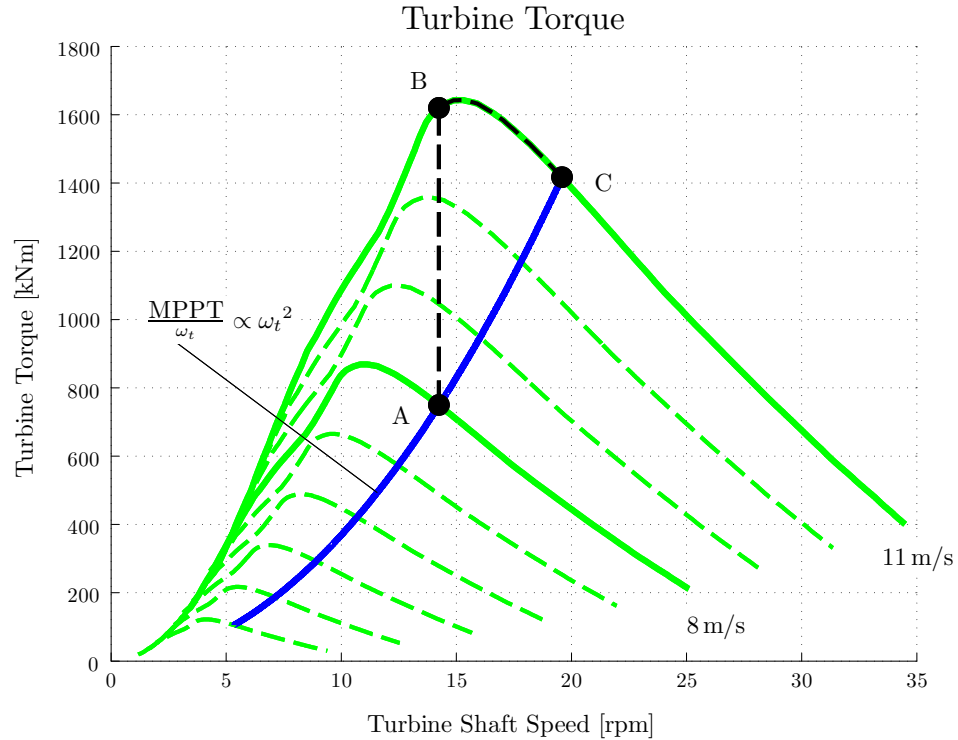


Figure 4.8: Turbine Operation through Wind Speed Change - The torque of the turbine follows the black dotted line along the path A-B-C. The torque of the generator follows the blue curve corresponding to the MPPT profile along the path A-C.

torque according to its curve and the generator according to its own curve imposed by the MPPT algorithm. At point C these curves intersect and the torque is balanced again, at the new steady state operating point.

It is important to note that the operation of a wind turbine around its maximum power point curve is dynamically stable [7]. That is, for a small variation in the turbine speed, the system will naturally tend back towards the set operating point. If the speed becomes slightly too high, then the generator torque becomes greater than the turbine torque and results in the system tending back toward the set operating point. Similarly if the speed becomes slightly slower the generator torque will drop below that of the turbine causing a natural increase in speed and negating the disturbance.

## Chapter 5

# Vector Control of the DFIG and Wind Turbine System

The control of an electromechanical machine ultimately comes down to the control of the electromagnetic torque [8]. The torque of any machine arises as the cross product of the flux in the rotor and the stator. The fluxes are closely related to the currents and the torque is maximized when the two fluxes are perpendicular to each other. In a DC machine, the torque is relatively easy to control; the field flux and armature magneto-motive force (mmf) are developed completely apart from each other with separate field and armature currents. The two fluxes can be kept perpendicular by the mechanical commutator. This means that the torque can be controlled in a linear fashion just by varying one of the current magnitudes.

Obtaining this type of simple control performance for an AC machine is not directly possible. This is because controlling the torque in an AC machine is not trivial. The system inherently has a lot of coupling and interaction between its fluxes and currents which makes it difficult to find a linear relationship between a control variable and the torque. Additionally, without a commutator, the field flux and the armature mmf have to be spatially separated with electronic control instead of with a mechanical structure. It becomes necessary to control not only the magnitude, but also the phase angle of the current [11]. The control of both the magnitude and phase of the control variable means that the complete space vector is controlled. Therefore vector control is a strategy whereby AC machines are forced by electronic control to closely match the characteristics of DC machines in order to achieve a fast torque response and hence full command of the machine.

### 5.1 Vector Control Principals of the Grid Connected DFIG

It was shown in Section 3.3.1.1 that any three phase quantity, whether it be a voltage, current or flux linkage, can be expressed as a single rotating vector. Vector control acts to control these space vectors in magnitude and phase. As shown in Section 3.4.4, the torque is proportional to the cross product of the stator and rotor flux linkages space vectors. It was also shown that it is possible to

express the torque as the cross product of any two different currents, flux linkages or combinations of both. Which two variables are chosen to be the control variables is dependent on the type of machine being controlled, and how it is excited. Many different combinations can work and they each have advantages and disadvantages. For the grid connected DFIG, it is most common to choose the stator flux  $\vec{\lambda}_s^g$  and the rotor current  $\vec{i}_r^g$ . The reason for this is explained as follows. Since the stator terminals are directly connected to the grid where the voltage is fixed and constant, the stator flux will be relatively easy to hold constant as well. Also since the stator is connected directly to the grid, the stator currents cannot be controlled through that side of the machine. All control must be done where the inverter is, at the rotor terminals, by varying the voltages applied there. The impressed voltages cause currents to flow which interact with the stator currents and ultimately dictate the operation of the machine, thus the rotor current is chosen as the control variable.

The basic idea is to mathematically separate the portion of current that contributes to the field flux or magnetization of the machine and the portion which is perpendicular to it which is responsible for the armature mmf and torque production. For a detailed physical explanation please refer the work of *Mohan et al.* [8]. In order to achieve this, the position of the stator flux vector must be found, while the machine is running. The rotor currents can then be separated into two components, the one in line with the stator flux,  $i_{rd}$ , which is responsible for contributing to it, and the other,  $i_{rq}$ , which is orthogonal, see Figure 5.1. The torque can be controlled by varying the magnitude of  $i_{rq}$  while keeping  $i_{rd}$ , and the field flux constant. To do this the magnitude and phase angle with respect to the stator flux vector must be controlled. In this way there is a linear relationship between torque and the control variable. It will be shown that  $i_{rq}$  can further be related to the real power and  $i_{rd}$  to the reactive power, allowing for decoupled control of these important variables.

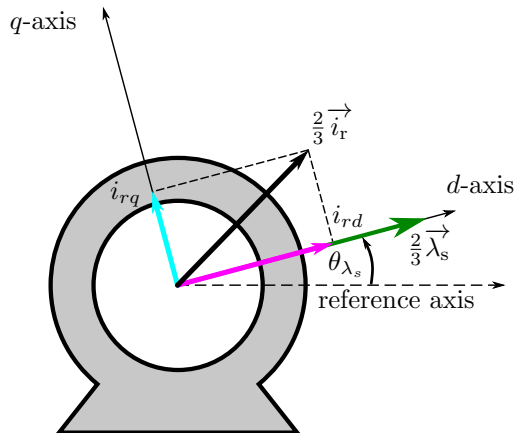


Figure 5.1: Basic Diagram of Vector Control

## 5.2 Cascaded Control Methodology

The cascaded control system is widely used in the machine control industry due to its flexibility and simplistic design [22]. The complex non-linear machine model is broken down into subsystems which

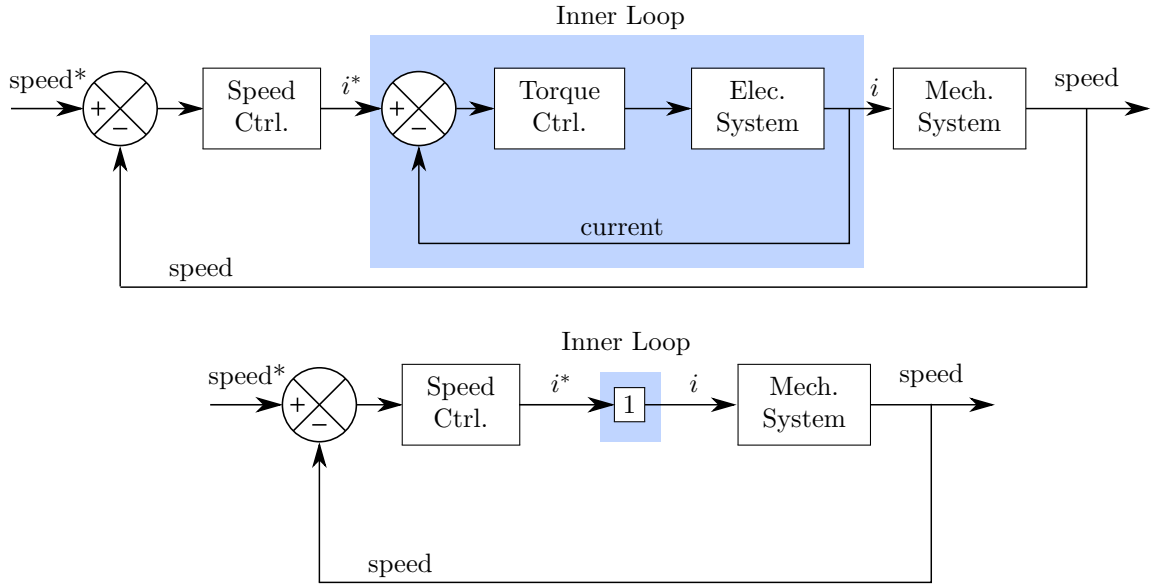


Figure 5.2: Standard Cascading Control Structure - Top: The inner loop is designed with outer loop variables viewed as constants; Bottom: the outer loop is designed neglecting the inner loop dynamics and assuming the references are met in reality instantaneously

are simple and assumed to be linear around their steady state operating points. The controllers can then be designed with linear control theory and applied to the machine successfully. For example, one reason the equations of an induction machine are non-linear is that the mechanical speed, a state variable, is multiplied with the current and fluxes which are also state variables. However the currents and flux vary so much faster than the mechanical speed of the machine, that they can be controlled with such a high bandwidth, that the speed can be taken as a constant. Once the current and flux, and hence the torque is under control, the speed or other slowly changing variables can be dealt with separately in an outer loop with another controller. This controller can safely ignore the dynamics of the inner loop because they are happening so fast in comparison. Figure 5.2 shows this standard cascading structure, and how the outer loop is isolated from the inner loop.

For the DFIG there are two of these cascaded control loops, see Figure 5.3. Vector control acts on the inner loop and regulates the fastest changing electrical variables. The torque producing component  $i_{rq}$  can then be related to real power in the outer loop. The flux producing component  $i_{rd}$  is related in the outer loop to the reactive power of the machine. In this way decoupled control of active and reactive power is achieved.

Outside the outer loop on the  $q$ -axis the reference real power  $P_s^{ref}$  is derived from the MPPT characteristic, so that the maximum power is extracted from the turbine. It is important to note that the speed is an input to this block and thus the speed and real power of the DFIG are related by this curve. It is not possible to independently control the speed and the real power. The reference reactive power  $Q_s^{ref}$  is directly related to the desired power factor of the machine; no third loop is required on this axis.

The cascaded control structure works because the dynamics in the inner loop are orders of magnitude faster than their encompassing loops. In this way the outer loops disregard the inner loop dynamics

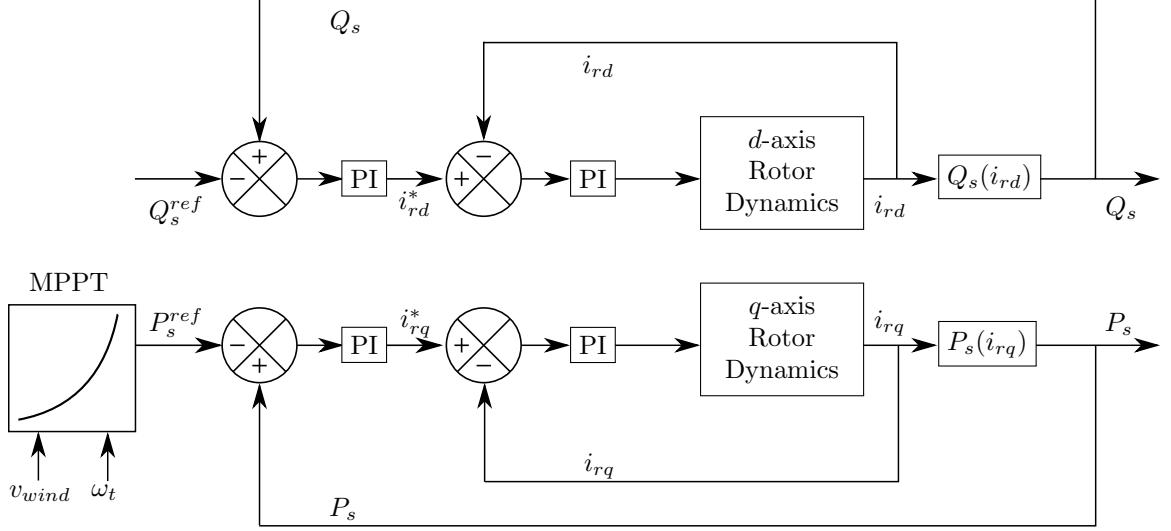


Figure 5.3: Cascaded Control Structure of the DFIG - Top: the  $d$ -axis control loop regulating  $Q_s$ ; Bottom: the  $q$ -axis control loop regulating  $P_s$

and each stage is designed as a low order system. This method is adopted by many prominent authors including [8] and [11]. A slight modification and improvement to this method is provided by *Tapia et al.* [13] in their work with DFIGs. Instead of completely ignoring the inner loops, they approximate them by simple first order systems. In this way the control loops are still separated in a cascaded manner, and development of the control law is still simple, but the inner loop dynamics are seen by the outer loop. This method has proven to be effective and will be followed in this work.

### 5.3 Vector Control Equations of the DFIG

As stated previously, the control of the grid connected DFIG is done completely through the rotor side, because that is where the converter is. It is not surprising then, that the control equations are derived by eliminating all the stator variables, currents and flux linkage, in the rotor voltage equation, replacing them with the rotor current. To make this substitution possible the equations must be aligned to a particular space vector, in this case the stator flux linkage. To perform this alignment the stator flux magnitude and phase which defines the position of the reference frame must be estimated. The estimating equations form naturally by applying the same manipulations to the stator voltage equation that were applied to the rotor voltage.

The end purpose to all of these manipulations is to find the transfer function clearly relating the rotor current dynamics to the rotor voltage. Eventually, in the outer loops, variables  $P_s$  and  $Q_s$  are related to this rotor current. Knowing how to set the rotor voltage properly to impress these desired rotor currents and in turn the real and reactive power of the machine constitutes full control of the system.



### 5.3.1 Stator Flux Orientation

As stated in the previous discussion, the control equations come by finding and separating components of the current that are responsible for magnetizing the machine and generating the torque. This work chooses the variable of stator flux linkage for the reference frame alignment, because it is the most common in the literature [7] and was the first proposed for the DFIG in wind energy systems [10]. Alignment to other space vectors is possible, for instance the stator voltage or rotor flux linkage.

Alignment to the stator flux simply means that the  $d$ -axis of the reference frame is chosen to coincide with the stator flux vector. This causes the  $q$ -axis component to be zero in the equations,

$$\vec{\lambda}_s^{\lambda_s} = \lambda_{sd} + j0 = \lambda_{sd} = |\vec{\lambda}_s|. \quad (5.1)$$

That is, the stator flux linkage aligned to itself lies completely long the  $d$ -axis. To perform this alignment on-line, while the machine is running, an estimator must be present to calculate the angle of the stator flux and its magnitude. The estimator will be derived in Section 5.3.2.2.

Off-line, the stator flux angle can be computed from the  $D$  and  $Q$ -axis components (stator flux vector aligned to stator's reference frame),

$$\theta_{\lambda_s} = \arctan\left(\frac{\lambda_{sQ}}{\lambda_{sD}}\right). \quad (5.2)$$

This relationship will be useful to perform the stator flux alignment during initialization of the simulation.

This stator flux alignment simplifies the stator flux linkage equation allowing a fundamental relationship to be derived between the stator and rotor currents. Aligning Equation 3.19 by applying the expression in Equation 5.1,

$$\begin{aligned} \vec{\lambda}_s^{\lambda_s} &= \lambda_{sd} = L_s \vec{i}_s^{\lambda_s} + L_m \vec{i}_r^{\lambda_s} \\ \implies \vec{i}_s^{\lambda_s} &= \frac{\lambda_{sd}}{L_s} - \frac{L_m}{L_s} \vec{i}_r^{\lambda_s}. \end{aligned} \quad (5.3)$$

Breaking down the expression along the  $d$  and  $q$  axes,

$$i_{sd} = \frac{\lambda_{sd}}{L_s} - \frac{L_m}{L_s} i_{rd}, \quad (5.4)$$

$$i_{sq} = -\frac{L_m}{L_s} i_{rq}. \quad (5.5)$$

These expressions are central to vector control, allowing the stator current to be expressed in terms of the rotor current and the stator flux, which is kept constant.

### 5.3.2 Rotor Voltage Dynamics

The rotor voltage dynamics are derived by aligning the rotor voltage equation to the stator flux. First the rotor voltage is written in terms of current by replacing  $\vec{\lambda}_r^{\rightarrow g}$  in Equation 3.24 with the expression in Equation 3.19:

$$\vec{v}_r^{\rightarrow g} = [R_r + j(\omega_g - \omega_m)]\vec{i}_r^{\rightarrow g} + L_r \frac{d}{dt} \vec{i}_r^{\rightarrow g} + j(\omega_g - \omega_m)L_m \vec{i}_s^{\rightarrow g} + L_m \frac{d}{dt} \vec{i}_s^{\rightarrow g}. \quad (5.6)$$

Next the stator current is eliminated by applying Equation 5.3, which at the same time will align the equation to the stator flux linkage,

$$\begin{aligned} \vec{v}_r^{\rightarrow \lambda_s} &= [R_r + j(\omega_{\lambda_s} - \omega_m)]\vec{i}_r^{\rightarrow \lambda_s} + L_r \frac{d}{dt} \vec{i}_r^{\rightarrow \lambda_s} \\ &+ j(\omega_{\lambda_s} - \omega_m)L_m \left( \frac{\lambda_{sd}}{L_s} - \frac{L_m}{L_s} \vec{i}_r^{\rightarrow \lambda_s} \right) + L_m \frac{d}{dt} \left( \frac{\lambda_{sd}}{L_s} - \frac{L_m}{L_s} \vec{i}_r^{\rightarrow \lambda_s} \right), \\ &= [R_r + j(\omega_{\lambda_s} - \omega_m)\sigma L_r]\vec{i}_r^{\rightarrow \lambda_s} + \sigma L_r \frac{d}{dt} \vec{i}_r^{\rightarrow \lambda_s} + j(\omega_{\lambda_s} - \omega_m) \frac{L_m}{L_s} \lambda_{sd} + \frac{L_m}{L_s} \frac{d}{dt} \lambda_{sd}. \end{aligned} \quad (5.7)$$

Breaking down the expression along the  $d$  and  $q$  axes:

$$v_{rd} = \underbrace{R_r i_{rd} + \sigma L_r \frac{d}{dt} i_{rd}}_{v'_{rd} \text{ (d-axis dynamics)}} - \underbrace{\sigma L_r (\omega_{\lambda_s} - \omega_m) i_{rq}}_{\text{cross coupling term}} + \underbrace{\frac{L_m}{L_s} \frac{d}{dt} \lambda_{sd}}_{\text{disturbance term}} \quad (5.8)$$

$$v_{rq} = \underbrace{R_r i_{rq} + \sigma L_r \frac{d}{dt} i_{rq}}_{v'_{rq} \text{ (q-axis dynamics)}} + \underbrace{\sigma L_r (\omega_{\lambda_s} - \omega_m) i_{rd}}_{\text{cross coupling term}} + \underbrace{(\omega_{\lambda_s} - \omega_m) \frac{L_m}{L_s} \lambda_{sd}}_{\text{disturbance term}} \quad (5.9)$$

$v_{rq,comp}$  (q-axis compensation terms)

These expressions explicitly separate the dynamics of the rotor currents and show how they affect the rotor voltages on the same axis. The actual dynamics are simple, linear, first order systems and are the same for both axes. The compensation terms arise from the cross-coupling of the equations. They do not contain the control variables for their respective axis and thus will be seen as a disturbance for the controller. The block diagram for the machine (plant) of the rotor dynamics is shown in Figure 5.4. The compensation terms need to be dealt with in order for the system to have the expected dynamic performance.

#### 5.3.2.1 Feed-Forward Cancellation

The compensation terms are nullified with a technique known as feed-forward cancellation. The unknown variables are estimated, and then added or subtracted after the controller to cancel their effect and expose the underlying dynamics so the controllers can operate as intended. Figure 5.5 shows how the controller dynamics produce the references  $v_{rd}^*$  and  $v_{rq}^*$ . The compensation terms are added or subtracted to create the the  $d$  and  $q$ -axis rotor voltage references  $v_{rd}^*$  and  $v_{rq}^*$ . These references are fed to an inverter which creates them and in turn feeds the machine. Note that in real applications and in a simulation the  $d$  and  $q$ -axis components must be converted back to

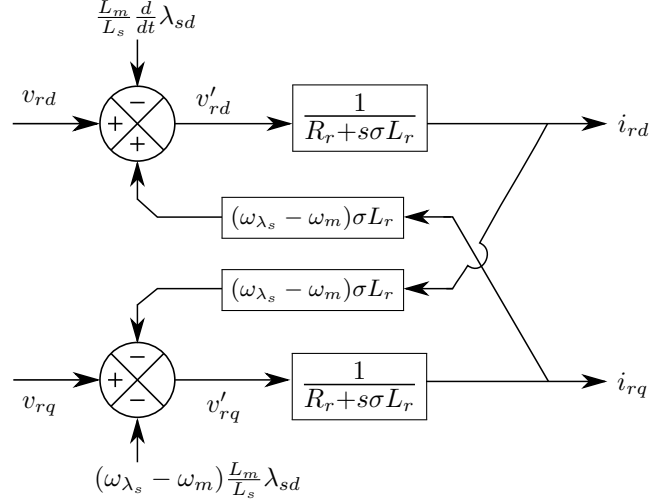


Figure 5.4: Rotor Voltage Dynamics of the Machine (plant)

three phase quantities and produced through pulse width modulation (PWM) techniques. This treatment ignores these complications and treats the inverter as ideal. That is, whatever voltage that is commanded is produced perfectly, with no harmonic content. That is why the inverter is just modelled as a gain block of one. Figure 5.6 shows the effect after feed-forward cancellation: the simple rotor dynamics are exposed.

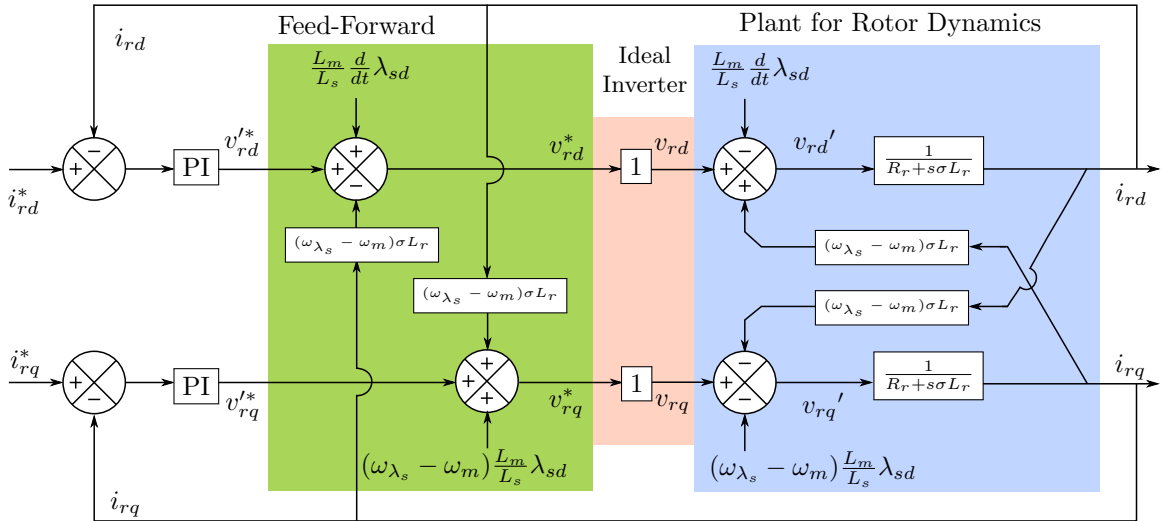


Figure 5.5: Feed-Forward Cancellation

### 5.3.2.2 Estimator

The estimator has two important functions. First, it computes the stator flux angle  $\theta_{\lambda_s}$  and its speed  $\omega_{\lambda_s}$ . This information is necessary to align the  $d$ -axis of the reference frame. Secondly, it calculates the variables needed for the feed-forward compensation, that is  $\lambda_{rd}$  and  $\frac{d}{dt}\lambda_{rd}$ . Since  $\lambda_{rd}$  is held

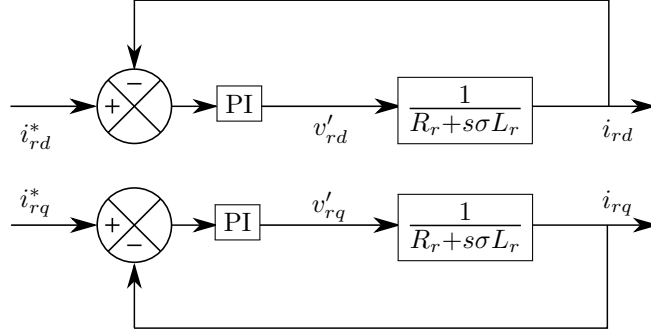


Figure 5.6: System after Feed-Forward Cancellation

constant by the vector control,  $\frac{d}{dt}\lambda_{rd}$  is almost always zero, unless  $\lambda_{rd}$  is undergoing a transition. For this reason, many vector control algorithms ignore this term [8], [11]; this work will however calculate it for completeness.

It is important to note that the estimator must do all of its calculations with physically measurable quantities. The measured variables required by the estimator are the rotor currents, stator voltages and rotor speed. The physical quantities need to be measured with voltage and current sensors and an encoder respectively. There is an approximation many authors make to approximate the stator voltage and remove the need for the voltage sensors; the assumptions are discussed at the end of this section. The equations are derived by applying the same procedure in Section 5.3.2 to the stator voltage equation.

First the stator voltage in Equation 3.23 is written in terms of currents by replacing  $\vec{\lambda}_s^g$  with the expression in Equation 3.19,

$$\vec{v}_s^g = (R_s + j\omega_g)\vec{i}_s^g + L_s \frac{d}{dt}\vec{i}_s^g + j\omega_g L_m \vec{i}_r^g + L_m \frac{d}{dt}\vec{i}_r^g. \quad (5.10)$$

Next the stator current is eliminated by applying Equation 5.3, which also aligns the expression to the stator flux at the same time,

$$\begin{aligned} \vec{v}_s^{\lambda_s} &= (R_s + j\omega_{\lambda_s}) \left( \frac{\lambda_{sd}}{L_s} - \frac{L_m}{L_s} \vec{i}_r^{\lambda_s} \right) + L_s \frac{d}{dt} \left( \frac{\lambda_{sd}}{L_s} - \frac{L_m}{L_s} \vec{i}_r^{\lambda_s} \right) \\ &\quad + j\omega_{\lambda_s} L_m \vec{i}_r^{\lambda_s} + L_m \frac{d}{dt} \vec{i}_r^{\lambda_s}, \\ &= \vec{i}_r^{\lambda_s} \left( -\frac{L_m}{L_s} R_s \right) + \lambda_{sd} \left( \frac{R_s}{L_s} + j\omega_{\lambda_s} \right) + \frac{d}{dt} \lambda_{sd}. \end{aligned} \quad (5.11)$$

Breaking down the expression along the  $d$  and  $q$  axes yields,

$$v_{sd} = -\frac{L_m}{L_s} R_s i_{rd} + \frac{R_s}{L_s} \lambda_{sd} + \frac{d}{dt} \lambda_{sd}, \quad (5.12)$$

$$v_{sq} = -\frac{L_m}{L_s} R_s i_{rq} + \omega_{\lambda_s} \lambda_{sd}. \quad (5.13)$$

From Equation 5.12, the  $d$ -axis stator flux and its derivative are found by solving the differential equation,

$$\frac{d}{dt}\lambda_{sd} + \frac{R_s}{L_s}\lambda_{sd} = v_{sd} + \frac{L_m}{L_s}R_s i_{rd}. \quad (5.14)$$

From Equation 5.13, the stator flux angular velocity and hence reference frame speed  $\omega_{\lambda_s}$  is found,

$$\omega_{\lambda_s} = \frac{v_{sq}}{\lambda_{sd}} + \frac{L_m}{L_s} \frac{R_s}{\lambda_{sd}} i_{rq}. \quad (5.15)$$

To calculate the stator flux angle  $\theta_{\lambda_s}$ , all that is required is to integrate the speed  $\omega_{\lambda_s}$ . It should be noted that most authors assume  $R_s \approx 0$  and thus  $v_{sq} = |\vec{v}_s|$  and  $v_{sd} = 0$ . This means that the practical implementation would not need the voltage sensors. Since this work is purely simulation based, the assumption will not be made unless it significantly reduces the complexity of the equations.

### 5.3.3 Inner Loop Controller Design

The simplest controller possible is purely proportional. If this approach is used and the compensation in the feed-forward section is not perfect, it will lead to steady state errors. Since the compensation is based on estimation, there will certainly be errors, and thus integral action is compulsory.

#### 5.3.3.1 Inner Loop Controller Structure

Figure 5.6 shows that the rotor dynamics are actually identical on both the  $d$  and  $q$  axes, so the design is only done for one and duplicated on the other. Many authors and researchers use a standard proportional-integral (PI) controller to satisfy the inner and outer loops independently according to the method of cascaded control. In this way they completely isolate the control design for each successive loop. As mentioned in Section 5.2, this work will follow that of *Tapia et al.* [13] which uses a slightly modified version of the PI controller. The proportional part is fed directly from the measured value instead of from the error signal. Figure 5.7 shows the standard PI control structure and Tapia's modification.

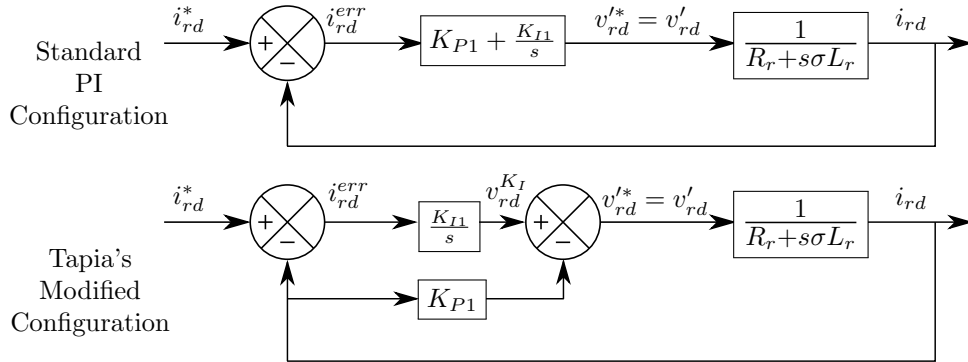


Figure 5.7: PI Controller Structures for the Inner Loop

The advantage to this structure is that the transfer function of the dynamics will be in standard second order form, as opposed to the standard PI structure which leads to a zero in the transfer function. Appendix A.6 derives the inner loop transfer functions for the modified structure in Figure 5.7, the end results are presented here,

$$\text{standard: } \frac{i_{rd}(s)}{i_{rd}^*(s)} = \frac{K_{P1}s + K_{I1}}{s^2\sigma L_r + s(R_r + K_{P1}) + K_{I1}} \quad (5.16)$$

$$\text{Tapia: } \frac{i_{rd}(s)}{i_{rd}^*(s)} = \frac{\frac{K_{I1}}{\sigma L_r}}{s^2 + s\frac{(R_r + K_{P1})}{\sigma L_r} + \frac{K_{I1}}{\sigma L_r}} \quad (5.17)$$

Notice that Tapia's structure results in a transfer function in the standard 2<sup>nd</sup> order form of,

$$G(s) = \frac{\omega_n^2}{s^2 + 2\zeta\omega_n s + \omega_n^2}. \quad (5.18)$$

where  $\omega_n$  is the natural frequency and  $\zeta$  is the damping ratio. The inner loop dynamics can now be subjected to known simple control criteria to determine the values of  $K_{P1}$  and  $K_{I1}$ .

### 5.3.3.2 Calculation of Inner Loop Controller Constants $K_{P1}$ and $K_{I1}$

The first criterion that Tapia's method requires is that the system is critically damped. This sets the following condition,

$$\zeta = 1. \quad (5.19)$$

The inner loop must be critically damped so that it exhibits no overshoot and its second order dynamics can later be approximated accurately with a first order system.

The second criteria that Tapia suggests is to specify the natural frequency  $\omega_n$  by demanding a reasonable settling time. According to [29], the time for a standard second order system to settle with 2% of its final value is,

$$T_s = \frac{4}{\zeta\omega_n}. \quad (5.20)$$

Of course the settling time cannot be chosen too low otherwise the bandwidth of the controller will be too high to realize with a practical inverter. According to [22], the bandwidth of the system should be at least one order of magnitude less than the switching frequency of the inverter. Once the power rating of the inverter is known, a realistically achievable frequency can be determined. This work will assume that requiring an inverter to switch over 5 kHz at the MW power level would be unrealistic. Thus the bandwidth of the inner loop should be less than 500 Hz. According to [29], for a second order system with  $\zeta = 1$ ,

$$\omega_B \approx 0.65\omega_n, \text{ and } \omega_B < 2\pi 500, \quad (5.21)$$

where  $\omega_B$  is the bandwidth of the closed loop system.

Comparing coefficients in Equations 5.17 and 5.18,  $K_{P1}$  and  $K_{P2}$  are determined,

$$\omega_{n1}^2 = \frac{K_{I1}}{\sigma L_r}, \quad (5.22)$$

$$2\zeta\omega_{n1} = \frac{R_r + K_{P1}}{\sigma L_r}. \quad (5.23)$$

Imposing the criteria from Equations 5.19 and 5.20 in Equations 5.22 and 5.23 yields,

$$K_{P1} = \frac{8}{T_{s1}}\sigma L_r - R_r, \quad (5.24)$$

$$K_{I1} = \frac{16}{T_{s1}}\sigma L_r. \quad (5.25)$$

Tapia suggests an inner loop settling time of  $T_{s1} = 40$  ms. Checking the bandwidth criterion in Equation 5.21,

$$\omega_B \approx 0.65 \frac{4}{T_{s1}} = 0.65 \frac{4}{0.04} = 65 < 2\pi 500 \quad (5.26)$$

This settling time is more than conservative enough to be achieved with a 5 kHz inverter.

### 5.3.4 Outer Loop Controller Design

The outer control variables are selected to be the real and reactive power of the stator. These are ideal for a wind turbine as decoupled control of the power is a desired feature. It will allow the turbine to follow the MPPT curve and do so at any desired power factor.

#### 5.3.4.1 Outer Loop Control Equations

The real and reactive power at the stator is given by Equations 3.37 and 3.38,

$$P_s = \frac{3}{2} \text{Re} \left\{ \vec{v}_s^g \vec{i}_s^g \right\} = \frac{3}{2} (v_{sd}i_{sd} + v_{sq}i_{sq}), \quad (3.37)$$

$$Q_s = \frac{3}{2} \text{Im} \left\{ \vec{v}_s^g \vec{i}_s^g \right\} = \frac{3}{2} (v_{sq}i_{sd} - v_{sd}i_{sq}). \quad (3.38)$$

The effect of stator flux orientation is examined on the expressions. Aligning the stator voltage in Equation 3.23 by applying the expression in Equation 5.1,

$$\vec{v}_s^{\lambda_s} = R_s \vec{i}_s^{\lambda_s} + \frac{d}{dt} \lambda_{sd} + j\omega_{\lambda_s} \lambda_{sd} \quad (5.27)$$

To further simplify the stator voltage expression a few assumptions are made. First of all, the term  $\frac{d}{dt} \lambda_{sd}$  can be considered zero. Under vector control  $\lambda_{sd}$  is held constant so its derivative is zero, unless there is a change to the set point of  $i_{sd}$ . While this will happen as the reactive power reference changes, the effect is small as all authors who adopt this method ignore it [7, 8, 11]. Secondly, the stator resistance is considered small enough that  $R_s \approx 0$ . Using these assumptions,

$$\vec{v}_s^{\lambda_s} = j\omega_{\lambda_s} \lambda_{sd}, \quad (5.28)$$

which implies that,

$$v_{sd} = 0, \quad (5.29)$$

$$v_{sq} = j\omega\lambda_s\lambda_{sd} = |\vec{v}_s|. \quad (5.30)$$

It can be inferred from these equations that under stator flux orientation and neglecting  $R_s$ , the stator voltage vector is perpendicular to the stator flux. This simplification can also be applied to the estimator in Section 5.3.2.2 to remove the need for voltage sensors at the stator. Using Equations 5.4, 5.5, 5.29 and 5.30, the expressions for  $P_s$  and  $Q_s$  are simplified,

$$P_s = -\frac{3}{2}\frac{L_m}{L_s}|\vec{v}_s|i_{rq} \quad (5.31)$$

$$Q_s = \frac{3}{2}|\vec{v}_s|\left(\frac{\lambda_{sd}}{L_s} - \frac{L_m}{L_s}i_{sd}\right) = \frac{3}{2}\frac{\lambda_{sd}}{L_s}|\vec{v}_s| - \frac{3}{2}\frac{L_m}{L_s}|\vec{v}_s|i_{rd} \quad (5.32)$$

Therefore after a few assumptions the approximate dynamics between the rotor current and the stator real and reactive power can be found. Note that the reactive power has a term that does not depend on rotor current. It is left to the controller to deal with this term as a disturbance, and no feed-forward structure will be used to cancel it out [13].

#### 5.3.4.2 Outer Loop Controller Structure

The dynamics for the real and reactive power loops are considered to be identical, once the disturbance term in  $Q_s$  is ignored. The most important feature to observe is the negative static gain  $-\frac{3}{2}\frac{L_m}{L_s}|\vec{v}_s|$  between the current component and its respective power. This means that in order to achieve a negative feedback structure, the references must be subtracted from the actual value [13]. Appendix A.7 proves this fact.

As stated before, the inner loop will be approximated with a first order system. This is possible because it was tuned to be critically damped, with no overshoot. The approximation of the inner loop dynamics is given by [13],

$$\frac{i_{rd}(s)}{i_{rd}^*(s)} = \frac{i_{rq}(s)}{i_{rq}^*(s)} = \frac{1}{1 + \frac{T_{s1}}{4}s} \quad (5.33)$$

The outer control loops are shown in Figure 5.8. Note that the reactive power loop is slightly different because of its disturbance term.

#### 5.3.4.3 Calculation of Outer Loop Controller Constants $K_{P2}$ and $K_{I2}$

As noted before, the dynamics on both outer loops are the same if the disturbance in  $Q_s$  is neglected. Again the design will be done for one axis ( $q$ -axis) and duplicated on the other axis ( $d$ -axis). The transfer function for the outer loop is derived in Appendix A.8 and is shown here,

$$\frac{P_s(s)}{P_s^{ref}(s)} = \frac{Q_s(s)}{Q_s^{ref}(s)} = \frac{6\frac{L_m}{L_s}\frac{|\vec{v}_s|}{T_{s1}}K_{I2}}{s^2 + \left(\frac{4}{T_{s1}} + 6\frac{L_m}{L_s}\frac{|\vec{v}_s|}{T_{s1}}K_{P2}\right)s + 6\frac{L_m}{L_s}\frac{|\vec{v}_s|}{T_{s1}}K_{I2}}. \quad (5.34)$$



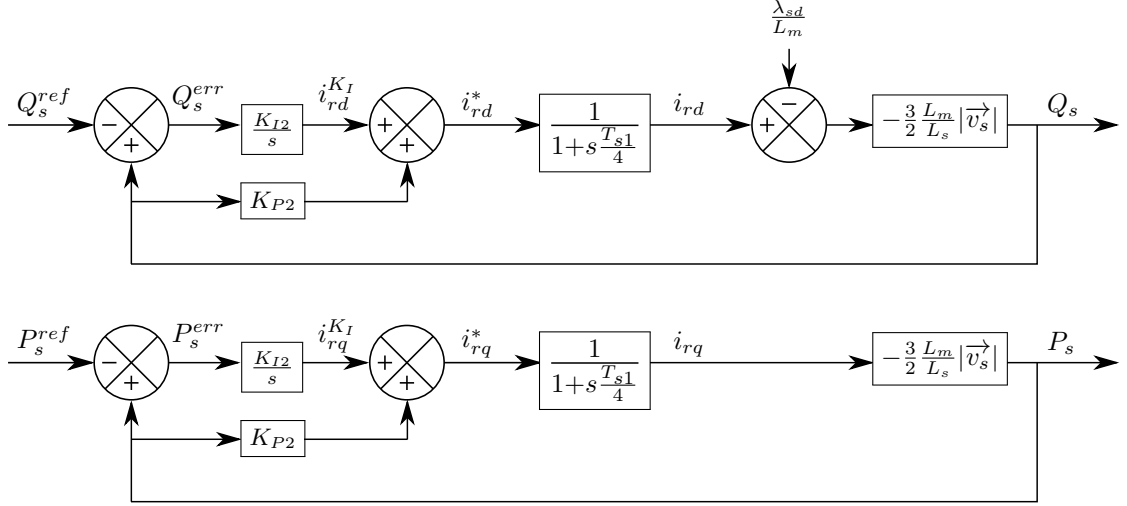


Figure 5.8: Outer Control Loops - Top: reactive power loop; Bottom: real power loop

Again, the transfer function is in standard form for a general second order system. The same procedure applied to the inner loop is used to calculate  $K_{P2}$  and  $K_{I2}$ . This time the settling time is selected to be longer than it was for the inner loop. It does not have to be orders of magnitude larger, because the inner loop dynamics have been accounted for in the outer loop transfer function. Tapia suggests 70 ms for the outer loop settling time.

Comparing coefficients in Equation 5.34 and Equation 5.18,

$$\omega_{n2}^2 = 6 \frac{L_m |\vec{v}_s|}{L_s T_{s1}} K_{I2}, \quad (5.35)$$

$$2\zeta\omega_{n2} = \frac{4}{T_{s1}} + 6 \frac{L_m |\vec{v}_s|}{L_s T_{s1}} K_{P2}, \quad (5.36)$$

Imposing the criteria in Equations 5.19 and 5.20,

$$K_{P2} = \frac{2}{3} \left( \frac{2T_{s1} - T_{s2}}{T_{s2}} \right) \frac{L_s}{L_m} \frac{1}{|\vec{v}_s|}, \quad (5.37)$$

$$K_{I2} = \frac{8}{3} \frac{T_{s1}}{T_{s2}^2} \frac{L_s}{L_m} \frac{1}{|\vec{v}_s|}. \quad (5.38)$$

### 5.3.5 Implementation of MPPT Control

The final step is to cascade one more loop on the real power. The real power reference depends on the turbine speed according to the MPPT curve. The power is proportional to the cube of the mechanical shaft speed, according to Equation 4.10,

$$P_s^{ref} = K_{opt}\omega_t^3, \quad (5.39)$$

where  $K_{opt}$  is a coefficient generated by curve fitting the MPPT curve to a cubic function of turbine shaft speed, see Section 4.5. The diagram for the MPPT control loop is given shown in Figure 5.3. The turbine shaft speed  $\omega_t$  is determined from the generator's mechanical speed by using Equation 4.8.

## Chapter 6

# Simulation Model Description

This chapter brings together all the relevant equations from Chapters 2 through 5 that are necessary to simulate the entire system including the wound rotor generator, the wind turbine and its associated control. It is the intention of this work to provide the reader with a thorough explanation of the model. This model is realized in the Matlab/Simulink environment and is constructed from basic blocks available in the student version of the software. This allows for easy modification of the system at the most basic level. The model is provided in its entirety on the accompanying CD-ROM with the model file “DFIG\_Wind\_Turbine.mdl” and its initialization script “Init\_System.m”.

### 6.1 Description of Simulink Model

There are two main parts to the simulation model. The wind turbine and the generator which constitute the physical subsystems that are being simulated, and the associated control blocks which are governing their behaviour. The physical generator is simulated and then the measurable outputs are fed to the machine estimator, which computes the values of other variables which are not measurable but are necessary for the control. It is important to keep this distinction between physical system and virtual control clear or the user may become confused. This is because every signal in the model is treated as the same and looks the same whether it is a real power signal or an estimated value that would only exist in a microcontroller in the real world.

The boundaries of these environments in the real world are the inverter at the input and the sensors at the output. The inverter dynamics are not studied in this work, so they appear in the model as simply a gain of one. The input to this inverter would be the desired rotor voltage waveforms. Then through PWM techniques the inverter would replicate the signals at the desired power levels, with some harmonic distortion. This reality is neglected by the simulation; the control blocks calculate the required rotor voltage and it is fed directly to the machine. At its output, the generator model calculates every variable within the machine: the torque, speed, flux and current. In reality it is only practical to measure some of these variables: the current, the rotor speed and perhaps the voltages. This is why only these variables are fed back to the estimator and the control. It would be useless

to design a control system that requires all of the variables. Again, any dynamics in the sensors and any realistic concerns such as sampling and analogue to digital conversion are ignored by the model as well. Therefore this model must be taken for what it is: an ideal functional description of a wind turbine connected to a DFIG that treats each component in the most simple and fundamental way possible.

### 6.1.1 System Overview

The two physical components, the generator and the wind turbine, have their shafts coupled by a gearbox. The quantities these systems interchange are the torques and speed of their common shaft. The turbine calculates its torque and outputs it to the generator model based on a wind speed profile and the speed of its shaft. The information of its shaft speed comes from the generator model which computes the speed based on an inertial model and the balance of its own back torque and the torque input of the turbine. Figure 6.1 shows the exchange of torque and speed variables at the gearbox connection between the generator and wind turbine.

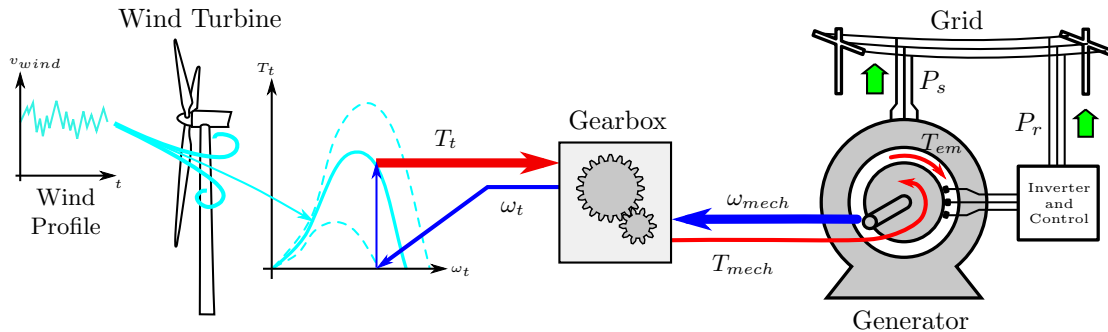


Figure 6.1: Overview of the Simulation

The generator model computes the back torque of the generator  $T_{em}$  which sets the speed of the system based on the control voltages applied at the rotor. Electrically, the real and reactive power flow of the machine is computed at the same time.

## 6.2 Detailed Description of Simulink Blocks

In this section each block in the simulation is described in detail. A table at the beginning of each subsection quickly shows the block input and output signals, the parameters it needs to calculate them and also any initial conditions that the block requires. Some outputs are used as signals to connect to other blocks and some are just output for display.

### 6.2.1 Input Stator Voltage Block

The grid is modelled as an ideal voltage source that can supply or receive infinite power without a change in voltage. It is directly connected to the stator so the stator voltages are considered grid

Inputs	Outputs	Parameters	Initial Conditions
none	$v_{as}, v_{bs}, v_{cs}$	$V_{LL,rms}, f_s$	none

Table 6.1: Simulation Variables of Stator Voltage Input Block

Out	Amp	Freq	Phase	Bias
$v_{as}$	$\sqrt{\frac{2}{3}}V_{LLrms}$	$2\pi f_s$	$\frac{\pi}{2}$	0
$v_{bs}$	$\sqrt{\frac{2}{3}}V_{LLrms}$	$2\pi f_s$	$\frac{\pi}{2} - \frac{2\pi}{3}$	0
$v_{cs}$	$\sqrt{\frac{2}{3}}V_{LLrms}$	$2\pi f_s$	$\frac{\pi}{2} + \frac{2\pi}{3}$	0

Table 6.2: Simulink Parameters for the Voltage Input Block

voltages.

The equations for stator voltage are given in Equation 3.3. Here  $V$  is the peak phase voltage which is related to the rms line to line voltage with

$$V = \frac{\sqrt{2}V_{LLrms}}{\sqrt{3}}. \quad (6.1)$$

The angular frequency  $\omega$  is related to the grid frequency

$$\omega = 2\pi f_s. \quad (6.2)$$

The phase angle  $\phi$  is taken as zero. The consequence is that the stator voltage space phasor starts at the reference position. It is fully aligned with the a-axis of the stator at  $t = 0$ . In Simulink the sine wave block is used to implement these equations. Its form is

$$O(t) = Amp * \sin(Freq * t + Phase) + Bias. \quad (6.3)$$

Thus to generate the voltages of Equation 3.3, Table 6.2 gives the values of all the arguments.

## 6.2.2 Clarke Transformation Blocks

Inputs	Outputs	Parameters	Initial Conditions
$F_a, F_b, F_c$	$F_D, F_Q$	none	none

Table 6.3: Simulation Variables of Clarke Transformation Block

Input	Outputs	Parameters	Initial Conditions
$F_D, F_Q$	$F_a, F_b, F_c$	none	none

Table 6.4: Simulation Variables of Inverse Clarke Transformation Block

These blocks are required whenever three-axis variables need to be converted to the two-axis variables or vice versa. This occurs any time a real world three phase signal is converted to the fictitious two-axis environment. They are thus required on both sides of the machine model, to bring the fictitious

control variables to the real world at the inverter and to convert the real measured variables to two-axis control variables at the machine output. Furthermore they are used in the internal model of the real machine, to bring that model to a fictitious two-axis environment and speed up the calculations. Note that the Clarke transformation and its inverse apply to all three phase variables, on any member of the machine. These blocks directly implement Equations 3.5 and 3.6.

### 6.2.3 Vector Rotation Block

Inputs	Outputs	Parameters	Initial Conditions
$\theta, F_x, F_y$	$F_{x2}, F_{y2}$	none	none

Table 6.5: Simulation Variables of Vector Rotation Block

The purpose of the vector rotation block is to align space vectors (their two-axis components) to the desired reference frame. This is done by realizing which reference frame the variable is currently in and rotating it by the angular difference  $\theta$  to get to the next reference frame. Thus the block takes in the two-axis variables and an angle  $\theta$  that describes the angular separation between the frames and uses Equation 3.7 to perform the calculations. Table 3.1 along with Figure 3.11 defines all the rotation angles required to change between any frame. These blocks are always paired with a Clarke or inverse Clarke block to complete the transformation to the two-axis calculation environment.

### 6.2.4 Wind Turbine Block

Inputs	Outputs	Parameters	Initial Conditions
$\omega_{mech}$ $v_{wind}$	$T_{mech}$	$GR, r_t, \rho$ $C_p$ -vector $\lambda$ -vector $v_{wind}$ -vector $\omega_t$ -vector $Tt$ -matrix	$v_{wind}(0)$

Table 6.6: Simulation Variables of the Wind Turbine Block

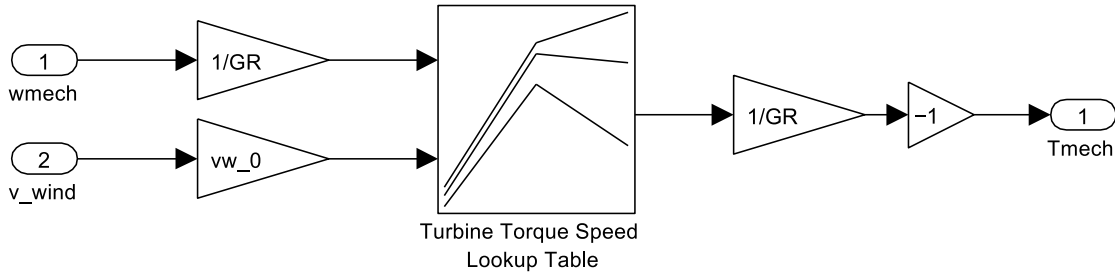


Figure 6.2: Simulink Block Diagram of Wind Turbine

This block implements the aerodynamic model of the wind turbine. The characteristic torque based on wind speed and shaft speed is calculated based on Equations 4.2, 4.3 and 4.5, using the  $C_p$  vs  $\lambda$

characteristic in Figure 4.4. It is stored in the matrix  $T_t$ -matrix and implemented in the Simulink model as a look-up table. Also required by the look-up table are the wind speed and turbine speed vectors. The calculations for all these vectors and the matrix are described in Section 4.4 and performed in the initialization script. The gearbox equations in 4.7 and 4.8 are implemented in gain blocks around the look-up table. Also note that the torque is multiplied with  $-1$  before it exits this subsystem. This is because the turbine torque is actually a prime mover torque and the machine model is expecting a negative load torque. The block diagram for the wind turbine is shown in Figure 6.2.

### 6.2.5 Wound Rotor Induction Machine Block

Inputs	Outputs	Parameters	Initial Conditions
$v_{as}, v_{bs}, v_{cs}$	$i_{ar}, i_{br}, i_{cr}$	$V_{LL,rms}, f_s$	$\omega_m(0)$
$v_{ar}, v_{br}, v_{cr}$	$\omega_{mech}$	$P_p, J, TR$	$\lambda_{sd}(0), \lambda_{sq}(0)$
$\theta_g, \omega_g$	$i_{as}, i_{bs}, i_{cs}$	$R_s, R_r$	$\lambda_{rd}(0), \lambda_{rq}(0)$
$T_{mech}$	$T_{em}$	$L_s, L_r$	
	$\lambda_{sd}, \lambda_{sq}$	$L_m, \sigma$	
	$\lambda_{rd}, \lambda_{rq}$		

Table 6.7: Simulation Variables of the Wound Rotor Induction Machine

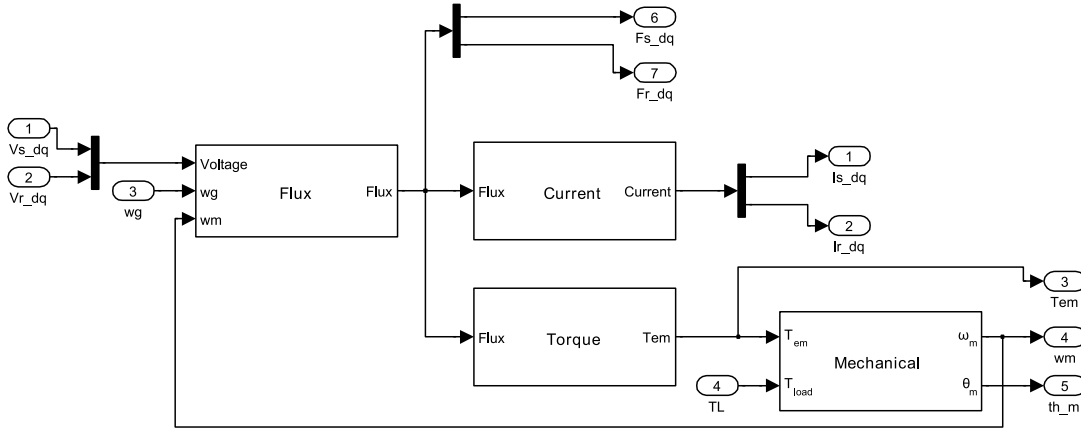


Figure 6.3: Simulink Block Diagram of Two-Axis Wound Rotor Induction Machine

This block models the actual wound rotor, machine dynamics. To the control blocks it is seen as a black box which accepts inputs and has measurable outputs. How the model calculates the outputs is of no concern to the rest of the model. The speed and position of the reference frame used in this block are completely independent of any other block. The two-axis representation of the machine is used because it is quick to calculate, but no particular alignment is necessary as it is in the control blocks. Note that its reference frame has been chosen to be the stator frame which is aligned to the reference axis at  $t = 0$ . The reason for this choice is that it is the simplest reference frame, defined by zero speed and a zero initial angle. Only real variables are exchanged through the input and output ports and fictitious two-axis variables remain inside the black box. Clarke transformations

and vector rotations are required on both the input and output to create the fictitious calculation environment. In between, the two-axis model of the wound rotor induction machine resides. Figure 6.3 shows the internal workings of this block. The flux subsystem implements Equation 3.34. The current subsystem implements Equations 3.25 and 3.26. These space vector equations were realized in matrix form for the simulation, similar to how the flux was in Equation 3.34. The torque subsystem calculates the torque using Equation 3.36. Finally, the mechanical subsystem implements the inertial mechanical model which relates electromagnetic torque to turbine torque using Equation 3.42.

### 6.2.6 Estimator Block

Inputs	Outputs	Parameters	Initial Conditions
$v_{as}, v_{bs}, v_{cs}$ $i_{ar}, i_{br}, i_{cr}$ $\omega_{mech}$	$\lambda_{sd}^{est}, \frac{d}{dt} \lambda_{sd}^{est}$ $\omega_{\lambda s}^{est}, \theta_{\lambda s}^{est}$ $\omega_m, \theta_m$	$R_s, L_m, L_s, P_p$	$\lambda_{sd}(0)$ $\theta_{\lambda s}(0)$

Table 6.8: Simulation Variables of the Estimator Block

The estimator block is responsible for calculating the position of the reference frame and all parameters that will be needed in the feed-forward control scheme. In reality, the inputs of this block would have to be measured with sensors. The initial conditions would also need to be calculated online, so when the control was turned on, the estimator could start working. Note that the initial position of the rotor is arbitrary and will not affect the operation of the estimator, so it is just initialized to zero. The estimator block realizes Equations 5.14 and 5.15, and is shown in Figure 6.4.

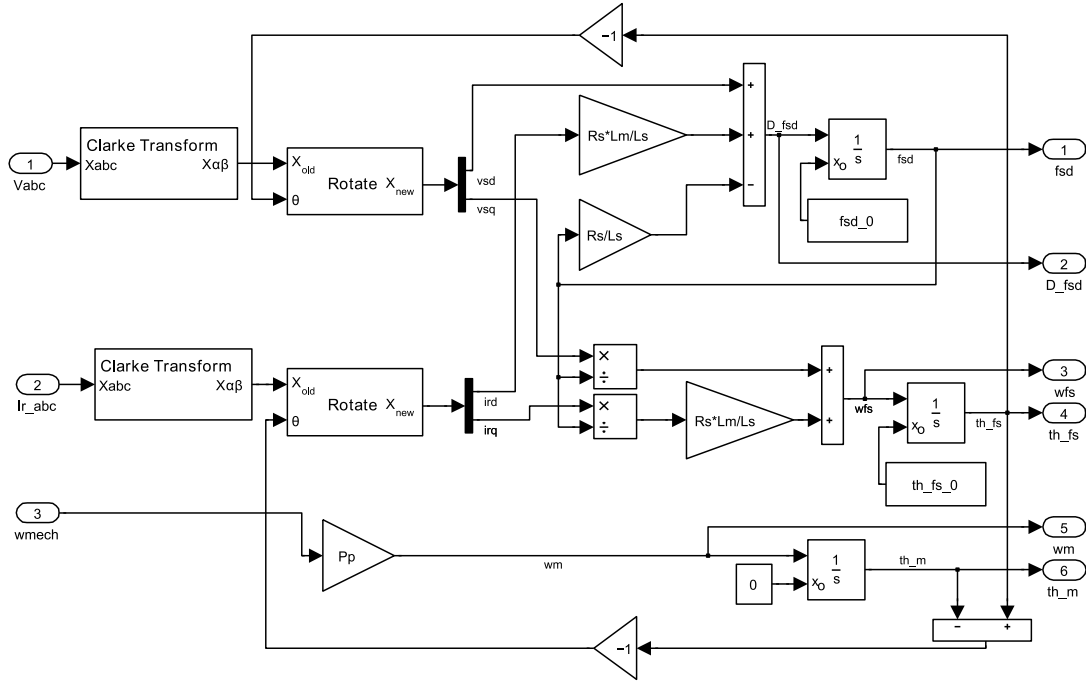


Figure 6.4: Simulink Block Diagram of Estimator



### 6.2.7 Feed Forward Cancellation Block

Inputs	Outputs	Parameters	Initial Conditions
$i_{rd}, i_{rq}$ $\omega_{\lambda_s}^{est}, \omega_m$ $\lambda_{sd}^{est}, \frac{d}{dt} \lambda_{sd}^{est}$ $v_{rd}^*, v_{rq}^*$	$v_{rd}^*, v_{rq}^*$	$L_s, L_r, L_m$ $\sigma$	none

Table 6.9: Simulation Variables of the Feed Forward Cancellation

The feed-forward block implements the compensation terms  $v_{rd,comp}$  and  $v_{rq,comp}$  found in Equations 5.8 and 5.9, and is shown in Figure 5.5.

### 6.2.8 PI Controller Blocks

	Inputs	Outputs	Parameters	Initial Conditions
Outer loop	$Q_s^{err}, Q_s$	$i_{rd}^*$	$K_{P2}, K_{I2}$	$i_{rd}^{KI}(0)$
	$P_s^{err}, P_s$	$i_{rq}^*$	$T_{s1}, T_{s2}, L_s, L_m,  \vec{v}_s $	$i_{rq}^{KI}(0)$
Inner Loop	$i_{rd}^{err}, i_{rd}$	$v_{rd}^*$	$K_{PI}, K_{I1}$	$v_{rd}^{KI}(0)$
	$i_{rq}^{err}, i_{rq}$	$v_{rq}^*$	$T_{s1}, \sigma, L_r, R_r$	$v_{rq}^{KI}(0)$

Table 6.10: Simulation Variables of the PI Controller Block

There are four separate PI controllers, one for each axis on the inner and outer loops. The structure of the PI controllers is shown for the inner loop in Figure 5.7 and for the outer loop in Figure 5.8. Unlike conventional PI controllers there are two inputs: the error signal and the measured value. The proportional and integral constants  $K_{P1}$ ,  $K_{I1}$ ,  $K_{P2}$ , and  $K_{I2}$  are calculated in Equations 5.24, 5.25, 5.37 and 5.38 respectively. Additionally, there are four integrators for the integral terms, so they must be initialized.

### 6.2.9 MPPT Block

Input	Output	Parameters	Initial Conditions
$\omega_{mech}$	$P_s^{ref}$	$GR, K_{opt}$	none

Table 6.11: Simulation Variables of the MPPT Block

Equation 5.39 is realized in this block. It is necessary to calculate the turbine shaft speed from the generator speed using the gear ratio  $GR$ . The value of  $K_{opt}$  is pre-calculated by curve fitting the MPPT characteristic as explained in Section 4.5. Also note that the power reference must be multiplied by  $-1$  so that the reference power is negative which implies generating.

## 6.3 Initialization of the Model

The methodology behind this model follows that of *Mohan et al.* in their work [8]. He describes in detail how to simulate a vector controlled, caged rotor machine. Here, his work is extended to a

wound rotor induction machine with a the wind turbine.

An important distinguishing feature of this type of modelling is that the simulation is not started from rest. In this way, the complicated start-up routines of the system and vector control can be avoided; the focus is on the transitions between usable operating points. This type of simulation is necessary in this work because, as mentioned in Section 4.2, only the MPPT region is studied. Starting from any steady-state operating point allows the system to start directly in Region 2, bypassing the start up routine of the turbine.

To perform the system initialization, first a steady-state operating point of the system needs to be calculated. Section 2.5 is used for this purpose. Next the dynamic model must be populated with the initial conditions corresponding to that operating point. Using the relationship in Section 3.3.3, the voltage phasors from the steady-state solution are related to space vectors at time  $t = 0$ , and the initial conditions are solved. This entails solving the value at  $t = 0$  for every variable which exits from an integrator in the model, including those in the control and those in the machine models. Furthermore, the turbine model needs to be initialized with its characteristics.

### 6.3.1 System Initialization

The turbine is the first system that must be initialized. This is because the wind is the first variable that sets the system in motion and all other initial conditions are derived from it. Before choosing a starting wind speed, the turbine characteristics must be loaded into the two-dimensional look-up table in the model. This procedure is described in Section 4.4.

The first step is to choose an initial wind speed  $v_{wind}(0)$ . It should be chosen between the cut in and rated speeds as this is the region for which the simulation is designed. This directly dictates the power that the turbine will produce and the speed of the whole system. Since the turbine is set to follow the MPPT curve, initial power of the turbine is computed as the maximum value for that particular wind speed and the corresponding turbine speed is found as well.

The next step is to load the parameters of the generator. Table 3.2 shows them for the sample generator chosen in this work. Since the initial turbine speed is known, it is related to the angular velocity of the generator  $\omega_m(0)$  through the gear ratio and pole pair relationships of Equations 4.8 and 2.2.

Next the initial power of the turbine is translated to a reference power by multiplying it by  $-1$ . This is because the generator model expects negative values for generating. At this point the reference value for reactive power must be chosen. It is selected at zero so that the stator operates at unity power factor.

With the real and reactive power and operating speed known from the turbine initialization, the rotor voltage injection required to achieve them can be deduced. Section 2.5 details the phasor solution of the steady state operating point, and these equations embody the next step in the initialization procedure.

Once the rotor and stator voltage phasors are known they are converted to their respective space

phasors at time  $t = 0$  using the information in Section 3.3.3 and the Clarke Transformation. The Clarke Transformation refers the space vectors to their own reference frames: the stator reference frame for the stator voltage and the rotor reference frame for the rotor voltage. To use these values in the same equation, they must be brought to the same frame. The rotor space vector should be rotated to the stator frame. At time  $t = 0$  the rotor's frame is aligned with the stator frame, that is  $\theta_r = 0$ . It was chosen this way because the rotor angle has no effect on the steady state behaviour of the machine, and it can be chosen arbitrarily.

Next, with the stator and voltages defined in the stator's reference frame, the flux linkages are directly computed by using Equation 3.34. Since it is a steady state operating point, the derivative vector can be set to zero and the flux components computed by inverting the matrix. Following that, the initial space vectors for the currents can be computed with Equations 3.25 and 3.26.

These variables would be sufficient to initialize the wound rotor induction machine block in the model; any consistent frame of reference will work for this block. However, the control blocks are computed in the stator flux oriented frame so all the space vectors need to be aligned to this vector at  $t = 0$ .

To do this, first the stator flux angle needs to be computed using Equation 5.2. Note that this result could also be obtained directly from the phasor solution of  $\lambda_s$  because the phase angle of a phasor is the same as the space angle of a space vector at  $t = 0$ , see Section 3.3.3.

Once this angle is known, using Equation 3.7 and Table 3.1 the space vectors are aligned to the stator flux. The last part of the initialization procedure calculates the PI gains as described in Sections 5.3.3.2 and 5.3.4.3. Lastly, the initialization script calculates the values necessary to initialize the controller integrators. This will be described in the next section.

## 6.3.2 Calculation of the Initial Conditions for System Integrators

The model is built from differential equations, represented in integral form. This means that each and every dynamic equation in the system contains an integrator. According to the method presented in [8], every integrator requires an initial condition. This is because the simulation is solved numerically with integrators that compute by adding to a previous value. Furthermore, the simulation is not started at rest, where most variables are zero, but at some steady state operating point while the machine is running. Thus the simulation can only be fully initialized once these integrators are fed with their initial conditions.

The model has fourteen integrators to initialize; fortunately, most of them can be supplied with values already computed by the initialization script for the system. The initial condition for a particular integrator is the value at time  $t = 0$  of the signal at its output.

### 6.3.2.1 Wound Rotor Induction Machine Initial Conditions

Seven of the integrators are related to the wound rotor induction machine block. The integrator responsible for computing the reference frame dictates the alignment of the block and the internal

integrator initial conditions are dependant on it. This is because although any reference frame can be used for the calculation of this block, once a particular one is chosen it must be consistent throughout the subsystem. The space vectors for the stationary and stator flux oriented synchronously rotating reference frame were computed in Section 6.3.1, so they are the best choice. The stator reference frame is chosen because it allows for the simpler initialization, with zero chosen for the reference frame integrator. This choice forces the use of stator reference frame oriented initial conditions for the four flux integrators. These were solved directly from Equation 3.34:  $v_{sD}(0)$ ,  $v_{sQ}(0)$ ,  $v_{rD}(0)$  and  $v_{rQ}(0)$ . Inside the wound rotor induction machine's mechanical subsystems are two more integrators, one for the speed and another for the rotor angle. As commented on before, the initial position of the rotor has no effect on any equation because the rotor is assumed to be uniform with no saliency. It is still imperative to keep track of the angle once the simulation starts; it is needed to convert rotor quantities to other frames. For the initial condition any value can be chosen, so zero is taken. The rotor speed is not zero, since it is a steady state operating point, so its integrator must be initialized with the rotor speed in electrical radians per second,  $\omega_m(0)$ , which was also computed in the initialization script. Notice that neither the rotor speed nor position initial conditions depend on the chosen reference frame as the flux did.

### 6.3.2.2 Estimator Initial Conditions

Since the estimator is derived from half of the machine model, it contains integrators as well. There are three integrators, however one is for rotor position, and as described in the previous section, this can safely be taken as zero. The estimator block also requires the  $d$ -axis stator flux linkage initial condition,  $\lambda_{sd}(0)$  as well. It must in the stator flux oriented frame, because the estimator was derived on that reference frame. Finally, the initial stator flux position,  $\theta_{\lambda_s}(0)$  must also be provided. Both of these initial conditions were calculated in the initialization script.

### 6.3.2.3 PI Controller Initial Conditions

The initial conditions for the PI controllers are not so apparent to solve. Technically, the simulation will work without these initial conditions; the controllers will respond to correct the system, but not without a large initial transient.

The initial condition for each of the four PI controllers is different. The signal to solve for can be seen on the block diagram as the signal exiting the integrator. Figure 5.7 explicitly shows the signal to be initialized as  $v_{rd}^{K_I}$ . From the diagram it can be seen that,

$$v_{rd}^{K_I}(0) - K_{P1}i_{rd}(0) = v'_{rd}(0), \quad (6.4)$$

and  $v'_{rd}(0)$  can be computed using Equation 5.8, therefore

$$v_{rd}^{K_I}(0) = K_{P1}i_{rd}(0) + v_{rd}(0) + \sigma L_r [\omega_{\lambda_s}(0) - \omega_m(0)] i_{rq}(0) - \frac{L_m}{L_s} \frac{d}{dt} \lambda_{sd}(0). \quad (6.5)$$

Similarly the  $q$ -axis inner loop PI signal to be initialized is  $v_{rq}^{K_I}$ ,

$$v_{rq}^{K_I}(0) - K_{P1}i_{rq}(0) = v'_{rq}(0). \quad (6.6)$$

Since the  $q$ -axis has different feed-forward terms, its initial condition will be different than the  $d$ -axis. Applying Equation 5.9 to solve for  $v'_{rq}(0)$ ,

$$v_{rq}^{K_I}(0) = K_{P1}i_{rq}(0) + v_{rq}(0) + \sigma L_r [\omega_{\lambda_s}(0) - \omega_m(0)] i_{rd}(0) - \frac{L_m}{L_s} (\omega_{\lambda_s}(0) - \omega_m(0)) \lambda_{sd}(0). \quad (6.7)$$

To solve Equation 6.5 and 6.7, the initial conditions  $\omega_{\lambda_s}(0)$  and  $\frac{d}{dt}\lambda_{sd}(0)$  are needed. These can be solved with the estimator using equations 5.14 and 5.15,

$$\omega_{\lambda_s}(0) = \frac{v_{sq}(0)}{\lambda_{sd}(0)} + R_s \frac{L_m}{L_s} \frac{i_{sq}(0)}{\lambda_{sd}(0)}, \quad (6.8)$$

$$\frac{d}{dt}\lambda_{sd}(0) = -\frac{R_s}{L_s}\lambda_{sd}(0) + v_{sd}(0) + \frac{L_m}{L_s}R_s i_{rd}(0). \quad (6.9)$$

Figure 5.8 shows the two signals that need to be solved for in the outer loops,  $i_{rd}^{K_I}$  and  $i_{rq}^{K_I}$ ,

$$i_{rd}^{K_I} = i_{rd}(0) - K_{P2}Q_s(0), \quad (6.10)$$

$$i_{rq}^{K_I} = i_{rq}(0) - K_{P2}P_s(0). \quad (6.11)$$

Applying Equations 5.31 and 5.32,

$$i_{rd}^{K_I}(0) = i_{rd}(0) \left(1 + \frac{3}{2} \frac{L_m}{L_s} |\vec{v}_s| K_{P2}\right) - \frac{3}{2} \frac{|\vec{v}_s|}{L_s} \lambda_{sd}(0) K_{P2}, \quad (6.12)$$

$$i_{rq}^{K_I}(0) = i_{rq}(0) \left(1 + \frac{3}{2} \frac{L_m}{L_s} |\vec{v}_s| K_{P2}\right). \quad (6.13)$$

It must be noted that the variable  $|\vec{v}_s|$  is evaluated by applying Equations 3.9 and 6.1 to yield,

$$|\vec{v}_s| = \frac{3}{2}V = \frac{3}{2} \frac{\sqrt{2}}{\sqrt{3}} V_{LLrms} = \frac{\sqrt{3}}{\sqrt{2}} V_{LLrms}. \quad (6.14)$$

Equations 6.7, 6.5, 6.12, 6.13, 6.8 and 6.9 must be included in the initialization script to finally complete the initialization procedure of the entire system.

## Chapter 7

# Model Validation, Testing and Discussion

This chapter puts the model to the test. First, the main components, the WRIM, the wind turbine and the vector control are validated to ensure they properly represent their respective systems. Once this point has been established the model is used in a case-study for its intended purpose, maximum power point tracking of a wind turbine. The results are presented and discussed with respect to experiments carried out by others in the field. Finally the model deficiencies are discussed, with suggestions for improvements and recommendations on how to extend the work towards a practical implementation.

### 7.1 Validation of System Components

To ensure that the major subsystems are working properly, several simulations will be employed whose results are compared to those published in literature.

#### 7.1.1 Validation of the Wound Rotor Induction Machine Model

Two tests will be conducted that will investigate the model's ability in dynamic and steady state conditions. It must be understood that the inputs to the model are stator and rotor voltages and the load torque, so the tests have to revolve around these types of inputs. For example, the voltage developed at the stator terminals due to a known rotor excitation and rotor speed cannot be simulated since that requires rotor speed as an input and stator voltage as an output.

### 7.1.1.1 Free Acceleration Test

In their well respected book, “*Analysis of Electric Machinery and Drive Systems,*”, *P.C. Krause et al.* develop a 5<sup>th</sup> order simulation model of an caged induction machine [20]. To demonstrate its operation they provide the free acceleration characteristics, which trace the speed, torque and other variables as the machine is started from rest. A properly working induction machine model should exhibit the same characteristics for the same inputs and parameters.

The free acceleration test is conducted as follows:

- The parameters of Krause’s 2250 hp induction machine are loaded into the model.

Parameter	Symbol	Value	Unit
rated power	$P_{rated}$	2250	hp
rated stator frequency	$f_s$	60	Hz
rated stator voltage (line-to-line, rms)	$V_{LLrms}$	2300	V
number of pole pairs	$P_p$	2	dimensionless
stator resistance	$R_s$	29	m $\Omega$
stator leakage inductance	$L_{ls}$	0.6	mH
rotor resistance (referred)	$R_r$	22	m $\Omega$
rotor leakage inductance (referred)	$L_{lr}$	0.6	mH
magnetizing inductance	$L_m$	34.6	mH
system inertia	$J$	63.87	Kg · m <sup>2</sup>

Table 7.1: Krause’s Parameters for a 2250 hp IM [20].

- The model is loaded with all initial conditions set to zero, the speed is at rest and there is no flux build up in the machine.

$$\omega_m(0) = 0; \lambda_{sD}(0), \lambda_{sQ}(0), \lambda_{rD}(0), \lambda_{rQ}(0) = 0$$

- The model is excited with the same inputs: the rotor voltages set to zero and the stator energized with line voltage.

$$\begin{aligned} v_{as} &= \sqrt{\frac{2}{3}} V_{LLrms} \cos(2\pi f_s t) & v_{ar} &= 0 \\ v_{bs} &= \sqrt{\frac{2}{3}} V_{LLrms} \cos\left(2\pi f_s t - \frac{2\pi}{3}\right) & v_{br} &= 0 \\ v_{cs} &= \sqrt{\frac{2}{3}} V_{LLrms} \cos\left(2\pi f_s t + \frac{2\pi}{3}\right) & v_{cr} &= 0 \end{aligned}$$

Figure 7.1 compares Krause’s calculations of torque vs speed with those from the model. The results match up as expected.

### 7.1.1.2 Initialization of the System to a Stable Doubly Fed Operating Point

The previous test treated the induction machine as a caged machine that is singly fed. To fully verify the model, it seems natural that it should be tested under double supply. Finding an appropriate doubly fed dynamic test to subject the machine model to for verification is not trivial. Since just

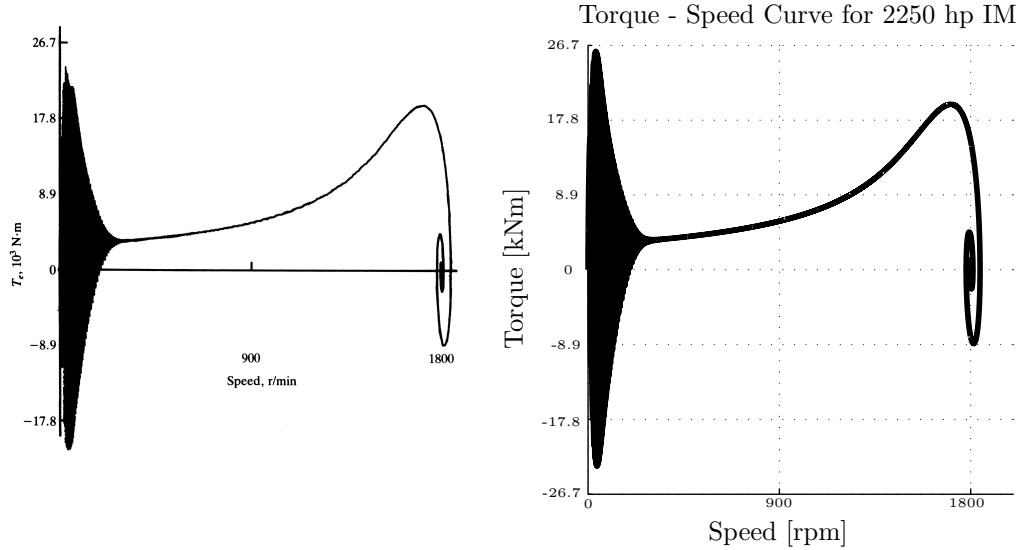


Figure 7.1: Left: Krause’s torque and speed for a 2250 hp IM published in “*Analysis of Electric Machinery and Drive Systems*” [20], Right: The same characteristic computed by the model.

the machine model itself is under test, it should not require any control, so it must be done in open loop. However the DFIG is never used without control; no practical system uses it in open loop. This point is made resoundingly clear in the work of *J.C. Prescott et al.* who showed how an induction machine under double supply is inherently unstable [30]. Some dynamic simulations of a DFIG model are presented in the work of *G. Abad et al.* [7], however even there a speed controller is used to stabilize the system.

Despite this issue, it is possible to verify the model under double supply in open loop. As discussed before, the methods of simulation in this dissertation follow those of *Mohan et al.* [8]. Therein, the model is proved to be working when it can be initialized to a steady state operating point, and then hold that position without deviation from it. With this strategy it is sufficient to find a well documented and stable steady state operating point for a DFIG in literature, and ensure the model can be initialized to it and hold the steady state indefinitely.

In open loop, like any induction machine, a DFIG is stable if the operating point falls in the stable region of the torque speed characteristic, between the breakdown and pullout torque [7]. This stable region is defined as the region that torque decreases almost linearly for an increase in speed [14].

In their recently published IEEE Press book “*Doubly Fed Induction Machine: Modeling and Control for Wind Energy Generation*”, *G. Abad et al.* explicitly calculate a stable operating point for a DFIG under open loop double supply [7]. Therefore this validation test checks if the model can be initialized to and hold this steady state operating point without deviation. It is conducted as follows:

- The machine model is loaded with the parameters of Abad’s machine, see Table 3.2.



- The model is initialized to the published operating point:

$$\begin{aligned}\bar{V}_s &= \frac{V_{LLrms}}{\sqrt{3}} \angle 0^\circ \\ \bar{V}_r &= 0.1 \frac{V_{LLrms}}{\sqrt{3}} \angle 1.5^\circ \\ \omega_m &= 0.93\omega_s\end{aligned}$$

- To verify these conditions will indeed constitute a stable point, the steady state solution is solved with the above inputs. To do this, Equations 2.14 through 2.19 and 2.43 are solved for the complete range of  $-1 < s < 1$ . The torque is then plotted versus the speed, refer to Figure 7.2. The operating point is indeed in the stable portion between breakdown and pullout indicated in blue. This computation is compared to the published torque speed characteristic. Note that the published work is displayed in per unit, so for the comparison, the computed torque speed characteristic was converted to per unit as well with base values:

$$\begin{aligned}\omega_{base} &= \omega_s = 2\pi 50 = 314.1593 \text{ [elec. rad/sec]} \\ T_{base} &= \frac{S_{base}}{\omega_{mech,base}} = \frac{3 \frac{V_{LLrms}}{\sqrt{3}} I_{s,rated}}{\frac{\omega_{base}}{P_p}} = \frac{3 \frac{690}{\sqrt{3}} 1760}{\frac{314.1593}{2}} = 13.4 \text{ [kN}\cdot\text{m]}\end{aligned}$$

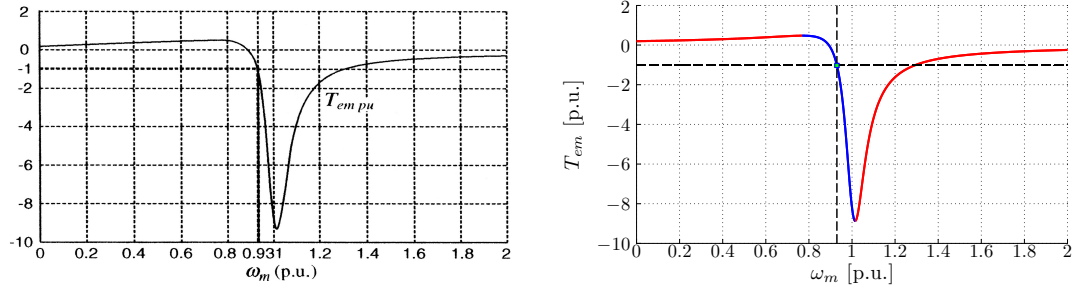


Figure 7.2: Left: Abad’s steady state torque speed curve for a 2 MW DFIG published in “*Doubly Fed Induction Machine: Modeling and Control for Wind Energy Generation*” [20], Right: The same characteristic computed by the initialization script for the model.

- Now that the steady state point has been proven stable, the initial conditions for the model are computed as described in Section 6.3.1. This results in:

$$\begin{aligned}\omega_m(0) &= 292.1681 \text{ [elec. rad/sec]} \\ \lambda_{sD}(0) &= -0.0160 \text{ [wb}\cdot\text{turns]} \\ \lambda_{sQ}(0) &= -1.8140 \text{ [wb}\cdot\text{turns]} \\ \lambda_{rD}(0) &= 0.4270 \text{ [wb}\cdot\text{turns]} \\ \lambda_{rQ}(0) &= -2.2199 \text{ [wb}\cdot\text{turns]}\end{aligned}$$

- These initial conditions are loaded into the model and it is ran for one second. Figure 7.3 shows

the torque and speed verses time. Both values are completely steady from time  $t = 0$  indicating that the model is properly initialized and is holding the operating point. Furthermore the value of torque computed by the dynamic model is  $-13.728[\text{kN}\cdot\text{m}]$  or  $-1.0252$  p.u. which matches up well with the published value.

Therefore the WRIM model has demonstrated its ability to compute dynamically under doubly fed conditions as well.

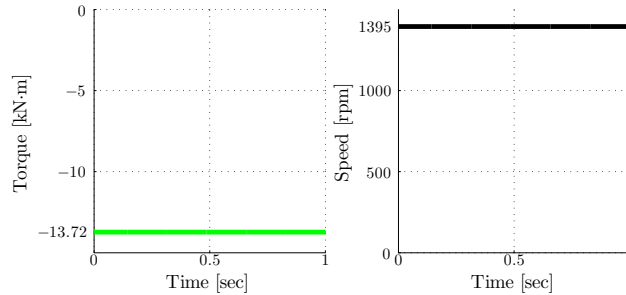


Figure 7.3: Both the torque and speed hold their steady state values with no fluctuations indicating that the dynamic model was initialized and is computing properly.

### 7.1.2 Validation of the Wind Turbine Model

The data for the wind turbine model was taken from manufacture data sheets for commercial wind turbines [27, 28]. To validate the model, its characteristics must be compared against those found in the data sheets. The most common characteristic provided by manufacturers is the output power verses wind speed. This curve corresponds to the maximum power curve. Until now, the wind turbine power curves have always been plotted against turbine shaft speed for several wind speeds. By plotting them against wind speed for several turbine shaft speeds, the results can be compared to the data sheet characteristic. Figure 7.4 plots the turbine output power curves against wind speed for several turbine shaft speeds. Superimposed on top is the maximum power curve vs wind speed in green, and the turbine output power stated in the data sheet in red. Note that the real power output is slightly less than the power computed by the model. This is because it is real data that has been measured by experiment and practical mechanical losses have occurred that the model does not take into account. Also note that the real turbine stops producing power at 2 MW, where as the model continues on its increasing trend. This is because at this wind speed the turbine has entered the third region, see Section 4.2 where it sheds power by pitching the blades. This region is out of the scope of the simulation, so this feature is not accounted for in the model. Despite these points, the model shows that it is able to adequately represent the turbines aerodynamic characteristics over the operating range of the simulation.

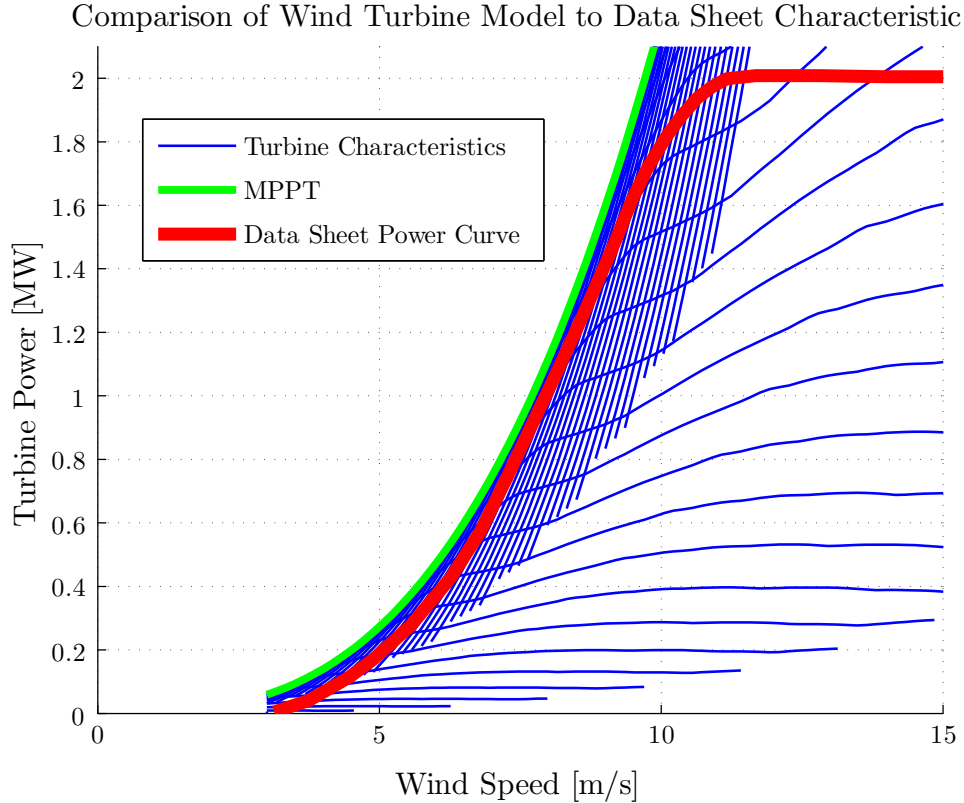


Figure 7.4: The output power of wind turbine according to manufacturer data sheet [27], is predicted well by the MPPT curve obtained from the model.

### 7.1.3 Validation of the Vector Control Subsystem

The vector control subsystem consists of the inner and outer loop PI controllers, and the feed-forward compensation. Validation of any control system can be done without comparison to other's work or data, the control system must be shown to achieve what it was designed to.

#### 7.1.3.1 Validation of the Inner Loop Vector Control

The goal of the inner control loop was to achieve decoupled control of the  $d$  and  $q$ -axis rotor current components. A properly working vector control scheme should be able to independently change one axis without effecting the other. Thus the acid test for vector control is to cause a step change in  $i_{rd}^*$  and  $i_{rq}^*$  at different times, and ensure that the dynamics are both decoupled and follow the designed criteria. Recall that the inner loop dynamics were designed to meet two requirements: a critically damped response and a settling time of 40 ms. The test of the inner loop is conducted as follows:

- The wind turbine and MPPT blocks are removed from the simulation, only the WRIM and the control is needed.
- The connections of the outer loop and inner loop are severed and step inputs are used to set the  $d$  and  $q$ -axis current references directly.

- The initialization script is modified to remove the wind turbine, an arbitrary power reference is chosen:

$$P_s^{ref} = -2 \text{ MW}$$

$$Q_s^{ref} = 1 \text{ MVAR}$$

The rotor currents needed to achieve this set point will be the references. they are calculated in the script by finding the rotor current in the stator flux oriented frame:

$$i_{rd}^* = i_{rd}(0) = -486.1 \text{ A}$$

$$i_{rq}^* = i_{rq}(0) = 2455.6 \text{ A}$$

- The PI controllers are directly fed with step inputs that start from the current references and jump to half of their respective value at  $t = 1.1$  sec for the  $d$ -axis and  $t = 1.2$  sec for the  $q$ -axis.
- The response is shown in Figure 7.5. Note that the two axis are completely decoupled, the step change on the  $d$ -axis has no effect on the  $q$ -axis and vice-versa. Furthermore the responses exhibit no overshoot indicating that they are critically damped. On both axes the currents settle within 50 ms, which is close to the designed value of 40ms.

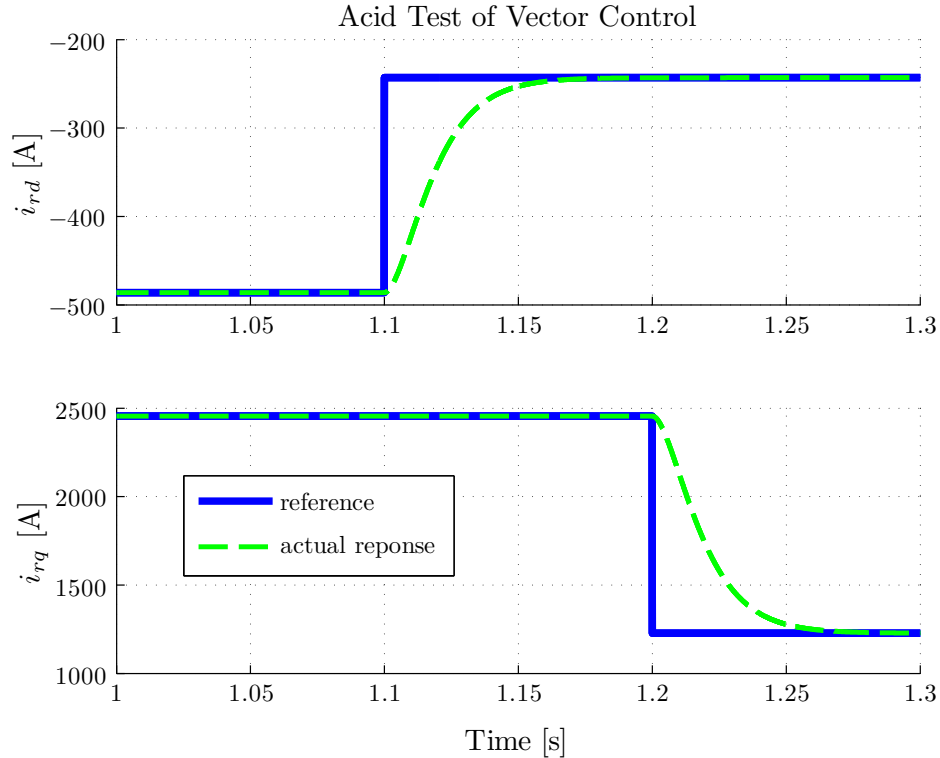


Figure 7.5: Top: the  $d$ -axis response, Bottom: the  $q$ -axis response

To check the effectiveness of the feed-forward block, it is bypassed and the same test is conducted. Figure 7.6 shows the response. Notice that it is degraded; there is coupling between the two axes,

overshoot is present and the responses even struggle to settle to the references. This simple test validates the feed-forward compensation block.

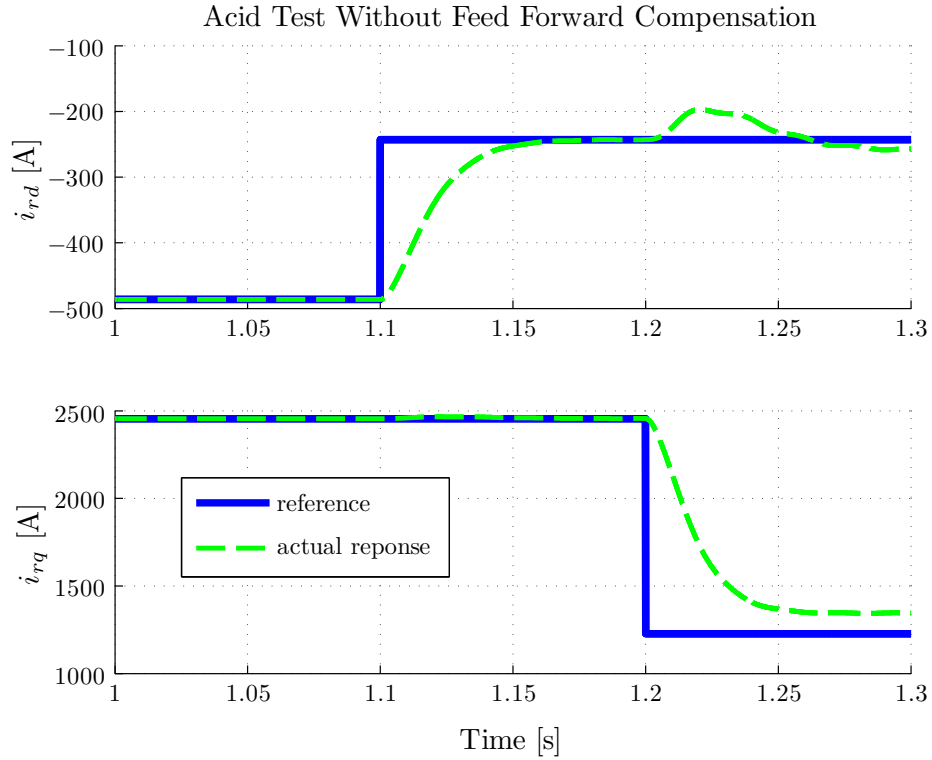


Figure 7.6: Top: the  $d$ -axis response, Bottom: the  $q$ -axis response

### 7.1.3.2 Validation of the Approximation of the Inner Loop Dynamics

To design the outer control loops, an important step in the method proposed by *Tapia et al.* [13] was to approximate the second order inner loop dynamics with a first order system. The accuracy of this approximation can be shown by plotting the step responses of the actual inner loop dynamics with its approximation. The second order transfer function is given in Equation 5.17, its first order approximation is given in Equation 5.33. Figure 7.7 compares the step responses. Notice that they are very similar thanks to the fact that the second order system was tuned to be critically damped with a specific settling time, and act like a first order system; hence the approximation is justified.

### 7.1.3.3 Validation of the Outer Loop Vector Control

The same procedure that was followed for the inner control loop is repeated for the outer control loop by forcing the real and reactive power to follow step responses. The test is conducted as follows:

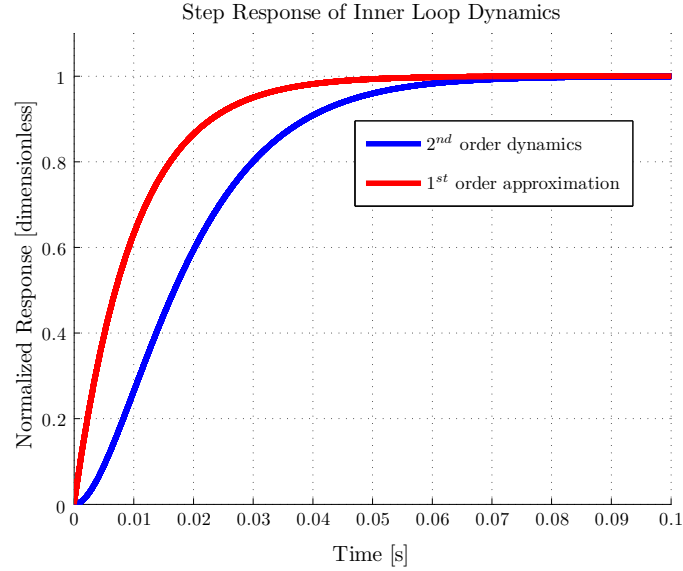


Figure 7.7: Since the second order dynamics were tuned to behave like a first order system, they can be accurately approximated by one.

- The references to the outer loop PI controllers are again arbitrarily chosen as:

$$P_s^{ref} = -2 \text{ MW}$$

$$Q_s^{ref} = 1 \text{ MVAR}$$

- Since only the outer loop is under test, but the inner loop is a necessary component, they are reconnected. The feed-forward system is employed so that the outer control loop sees the dynamics it was designed for.
- The PI controllers are directly fed with step inputs that start from the power references and jump to half of their respective value at  $t = 1.2$  sec for the  $d$ -axis and  $t = 1.4$  sec for the  $q$ -axis.
- The response is shown in Figure 7.8. Note that the two axes are completely decoupled, the step change on the  $d$ -axis has no effect on the  $q$ -axis and vice-versa. Furthermore the responses exhibit no overshoot indicating that they are critically damped. On both axes the currents settle within about 90ms, which is close to the designed value of 70ms.

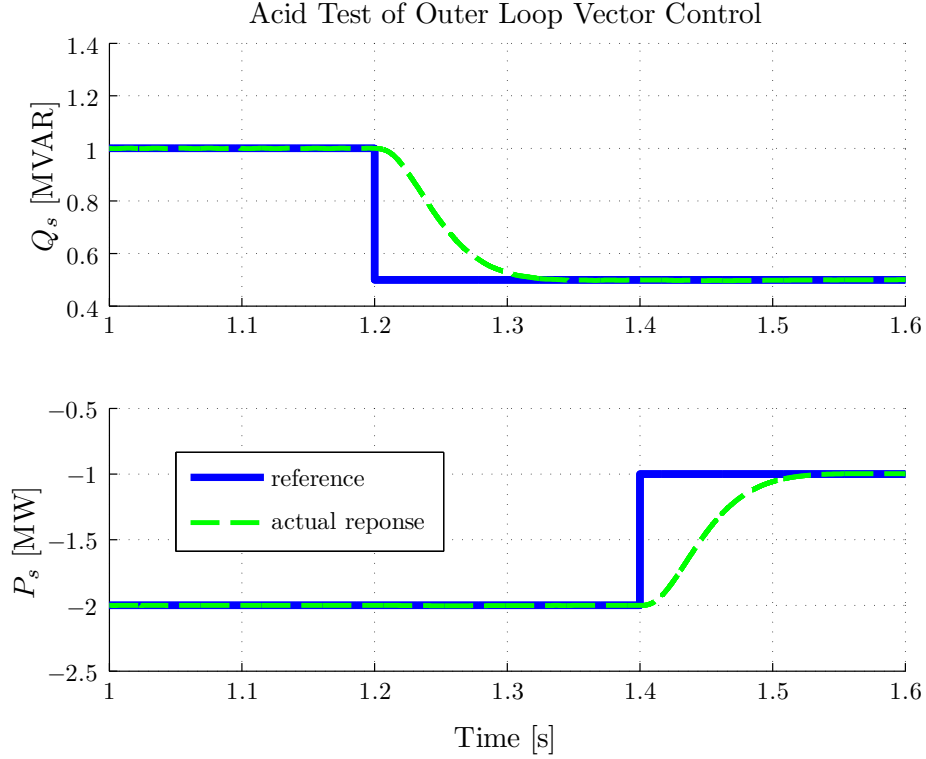


Figure 7.8: Top: the  $d$ -axis response, Bottom: the  $q$ -axis response

## 7.2 Case Study

In this case study the simulation model as a whole is put to the test. The main parameters used for the simulations in this section are given in Tables 3.2 and 4.1. The purpose of this set of tests is to show how the system accurately represents a wind turbine and doubly fed generator set.

First the system will be studied under steady wind conditions; during subsynchronous operation in low wind conditions and during supersynchronous operation in high winds. It will be shown that in its current configuration, the system is not ideally suited to handle the doubly-fed configuration, but is still operating as expected. A simple modification proposed by *Tapia et al.* is implemented and the improved performance is shown. Finally the dynamic system response to a step change in wind speed that causes the system to transition from the subsynchronous to supersynchronous operation is compared to the simulations of others in literature to demonstrate the ability of the model to describe the phenomena present in a DFIG coupled to a wind turbine.

### 7.2.1 Initialization to a Subsynchronous Operating Point

All the simulations in this section will focus on the real power flow in the machine, thus the reactive power reference is always set to zero,  $Q_s^{ref} = 0$ , for unity power factor operation for each test. To put the simulation into the subsynchronous mode, a wind speed must be chosen so that the maximum power at that wind speed corresponds to a shaft speed under synchronous. The turbine shaft speed

(in rpm) that corresponds to synchronous speed is:

$$\omega_{t, sync} = \frac{\omega_s}{GR} = \frac{1500}{103.2} \approx 14.5 \text{ [rpm]}$$

In Figure 4.5 it can be seen that wind speeds in the range of  $3 < v_{wind} < 6$  [m/s] will result in a shaft speed slower than  $\omega_{t, sync}$ . Therefore, the initial wind speed chosen is 5 [m/s]. The simulation is ran for 5 seconds and Figure 7.9 shows the system response. The plot shows the turbine power

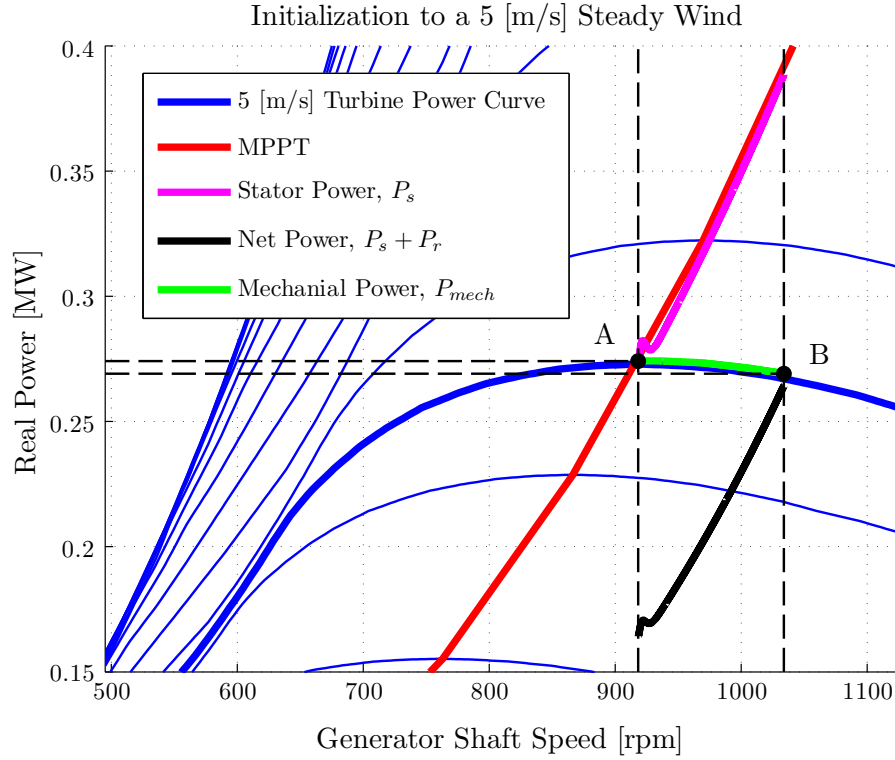


Figure 7.9: The system speeds up from its initialized operating point following the path from point A to B.

characteristics, the MPPT curve and the system response. The initial wind speed of 5 [m/s] is shown as a bold curve. The initial operating point is at A where the MPPT curve intersects the 5 [m/s] turbine power curve. It may be expected that the system would stay at this operating point since it was carefully initialized here, but nonetheless, the locus of the stator power moves up the MPPT curve to point B along the dynamic path shown in magenta. At first this may seem confusing; how can the system be generating more power than the turbine is extracting? The answer is simple: this behaviour is due to the natural power flow required for a DFIG to sustain generation at subsynchronous speeds. Refer to Figure 1.4, in the subsynchronous region the rotor must inject power from the grid to sustain the generation. The stator must also carry this additional power, so it actually has to carry both the mechanical power of the turbine and the injected power of the rotor,  $|P_s| \approx |P_{mech}| + |P_r|$ . At the initialized point the net power has not been taken into account. The MPPT algorithm forces the stator power along the curve of maximum power that the turbine can produce, without taking into account the rotor power that the stator must also carry. To satisfy the needs of the DFIG, the speed of the system increases until the point where the mechanical power



plus the required rotor power equal a stator power on the MPPT curve. It must be stressed that the turbine is not providing this extra power, it is being supplied by the grid, and actually since the speed has changed from the optimal value to extract maximum power, the power extracted from the wind is actually a bit lower at the new operating point. This can be seen by tracing along the 5 [m/s] power curve to the new speed (green curve). Notice at the new operating point, slightly less power is extracted. The net power is plotted in black and it can be seen that the turbine settles at the new operating point when the net power equals the turbine output power as expected from the physics of the power flow in the machine.

### 7.2.2 Initialization to a Supersynchronous Operating Point

The same test is conducted, this time with a wind speed that will drive the system into the supersynchronous generation mode, according to Figure 4.5,  $v_{wind} = 10$  [m/s] will suffice. Again the simulation is run for 5 seconds and Figure 7.10 shows the system response. This time the system

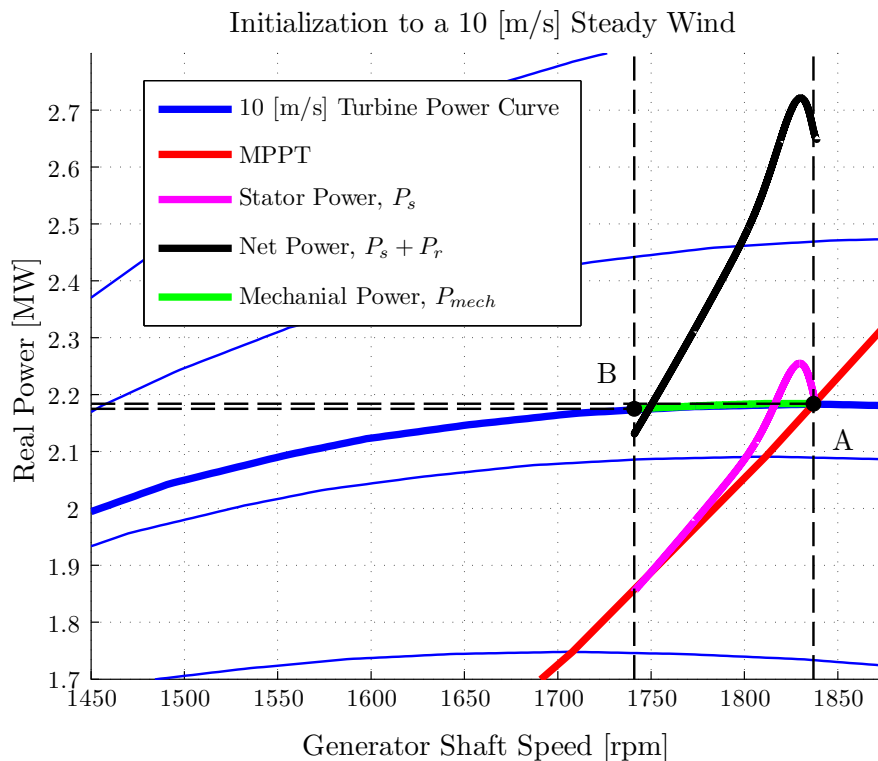


Figure 7.10: The system slows down from its initialized operating point following the path from point A to B.

slows and moves down the MPPT curve. The reason for this is the same as the subsynchronous case: the natural power flow in the DFIG. Again referring to Figure 1.4, it is seen that the stator actually handles a portion of the turbine power, less by about the same amount as the rotor power. Thus the MPPT algorithm forces the system to an operating point (point B) where the mechanical power of the turbine minus the rotor power equals the stator power. In the process it moves the

operating point away from the maximum power point for the 10 [m/s] wind and actually slightly reduces the amount of power being captured by the turbine.

### 7.2.3 Modification of the MPPT Reference to Improve Wind Power Capture for DFIG Power Flow

As it can be seen from Figures 7.9 and 7.10, the response for a steady wind does not completely maximize capture of wind power because the MPPT algorithm bases its reference on the stator power when the DFIG also utilizes the rotor for power flow. This drop in captured power is quite small as noted by *Tapia et al.* [31]:

“It should be noted that, once this outer control-loop has been correctly implemented, the amount of  $P_r$  active power interchanged between the grid and the DFIG through its rotor side, turns out to be only a short fraction of the wind turbine  $P_{net}$  active power. Consequently, the stator side active power does not differ significantly from  $P_{net}$ .”

The simulation results corroborate the fact that the drop in captured power ends up being very low but disagrees with the reasoning that it is because the rotor power is so low that it is negligible. Rather it is clear that the reason is that the machine changes speed to satisfy the power requirements of a DFIG and this balancing act only moves the operating point slightly up or down the turbine’s output power curve, even though the rotor power is quite significant. Regardless of the explanation for the phenomenon it is quite clear that making the MPPT algorithm actuate the net power  $P_{net}$  will rectify the situation. This is precisely the solution proposed by *Tapia et al.* [31]:

$$P_{net}^{ref} = P_s^{ref} - P_r. \quad (7.1)$$

Of course to implement this in practice the rotor power would need to be estimated, but this should not be an issue since rotor current is measured and rotor voltage is impressed for control. Figure 7.11 shows the slightly improved performance achieved by making this modification. The speed stays much closer to initialized value which results in the machine operating much closer to the intended maximum power point. Notice that in both cases at the new steady state operating point  $C$  that it is the net power  $P_{net}$  which is tracking the MPPT curve instead of the stator power.

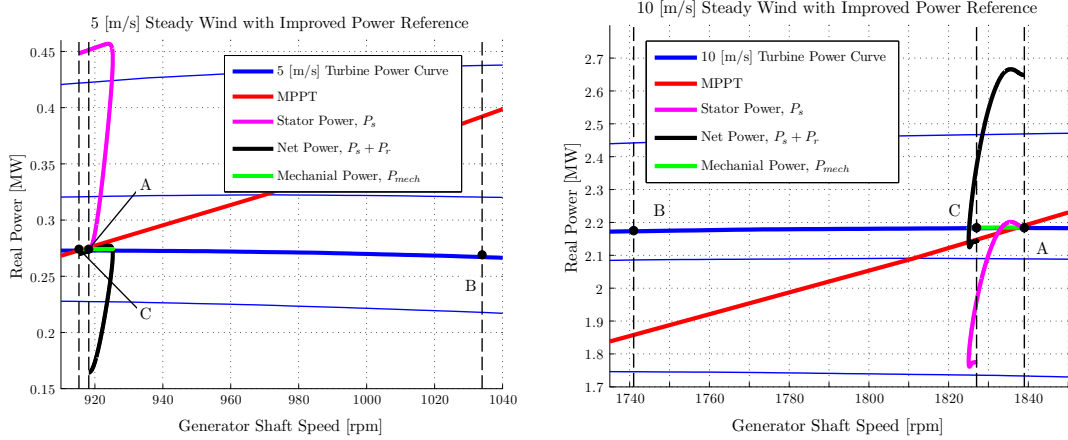


Figure 7.11: By forcing the net power  $P_{net}$  to track the MPPT curve instead of the stator power, the operating point  $C$  settles much closer to the maximum power point  $A$ , then it did before (point  $B$ ). Left: subsynchronous operation. Right: supersynchronous operation.

## 7.2.4 Dynamic Response Through Synchronous Speed

One of the most revealing experiments for a DFIG wind turbine system is to observe how it handles the transition from subsynchronous to supersynchronous generation. As mentioned in Section 3.7, a practical system will face the issue of loss of control as the rotor voltage becomes very low in magnitude and frequency. The simulation does not face these practical issues and can thus be compared to other researcher’s systems and simulations. The idea is to identify a few key characteristics which occur in all DFIG systems, as they transition from subsynchronous to supersynchronous operation, and inspect the waveforms to ensure the simulation models them. The following is a list of the expected characteristics:

- As noted by *Pena et al.*, [10] during one of the first experiments with DFIGs, the rotor currents should decrease in frequency around synchronous speed proportionally to the slip.
- Furthermore the phase sequence of rotor voltage and current should reverse on both sides of synchronous speed.
- The rotor power direction should switch from consuming in the subsynchronous mode to generating in the supersynchronous mode.
- Throughout the entire range the rotor power should be proportional to slip and stator power. At steady state the power in the machine should balance according to Equation 2.29.

The test is conducted as follows:

- The improved power reference of Section 7.2.3 is used so that the net power tracks the MPPT curve.
- The simulation is initialized to 5 m/s and is given 1 second to stabilize due to the new power reference.

- At  $t = 5$  seconds, the wind is increased to 10 /s in a step fashion to emulate a strong gust of wind applied to the turbine.

The ability of the system to track the maximum point is shown in Figure 7.12. Figures 7.13 through 7.18 plot the most relevant traces of the test for the 5 second time window  $4.5 < t < 9.5$  which contains the transition at  $t = 5.92$  seconds. On each diagram the time when the system passes synchronous speed is marked with a dashed line. In Figure 7.12 the effectiveness of the MPPT

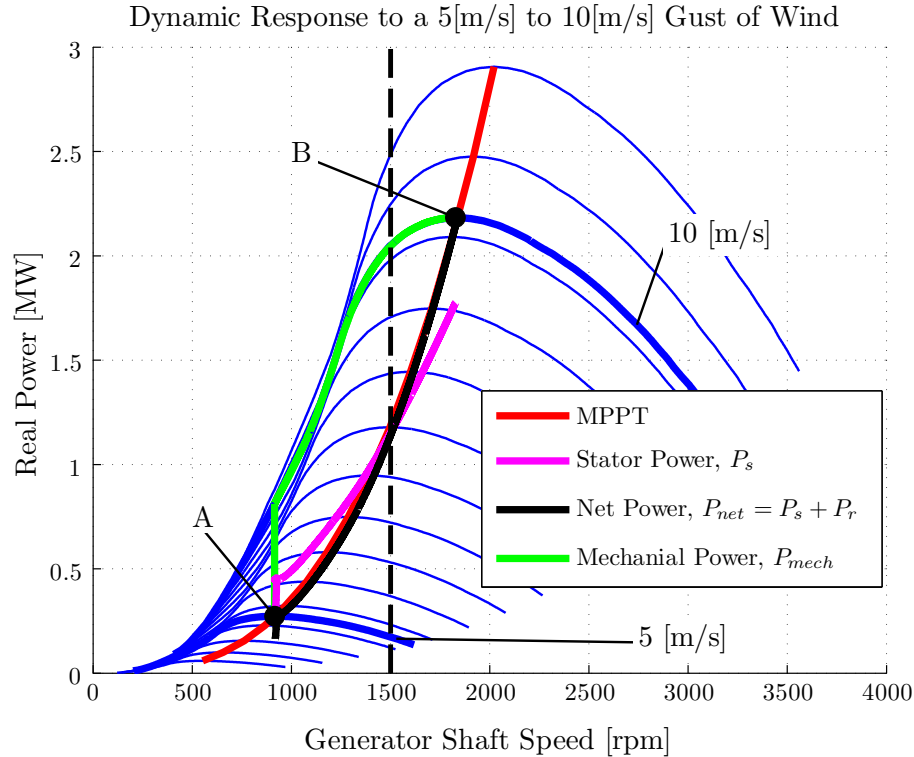


Figure 7.12: The net power tracks the MPPT curve from point A through synchronous speed and stabilizes when it matches power output of the turbine at point B.

algorithm is clearly demonstrated. At point A, the net power starts below the MPPT curve but immediately adjusts to track it. This means that the stator power must rise above the MPPT curve by the same amount since it needs to carry this rotor power. The gust of wind can be seen as a sharp increase in mechanical power jumping from the 5 m/s turbine power curve to the 10 m/s curve. The increased power and hence torque from the turbine causes the system to accelerate towards point B. Throughout the duration of the gust of wind the net power continues to track the MPPT curve. When the system crosses synchronous speed, the stator power falls below the net power, indicating that it is no longer carrying the rotor power, rather that the rotor power has reversed direction and is being supplied by the rotor itself.

Figure 7.13 traces the speed through the wind gust event. It smoothly transitions through synchronous speed and stabilizes at the new steady state within about 4 seconds. It is important to note that a response this fast would not be possible in an actual MW scale wind turbine. A reduced inertia is used so that the system can be simulated in a reasonable amount of time. The waveforms

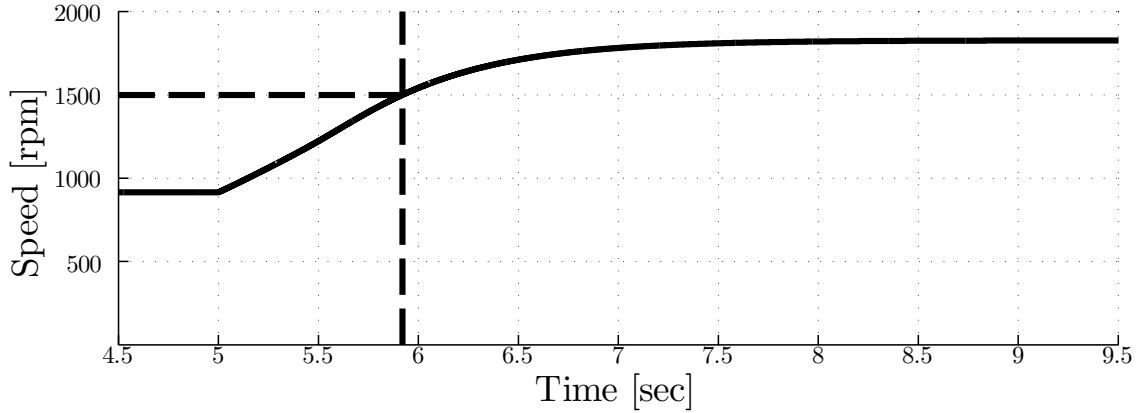


Figure 7.13: Generator Shaft Speed Response to a 5m/s Wind Gust

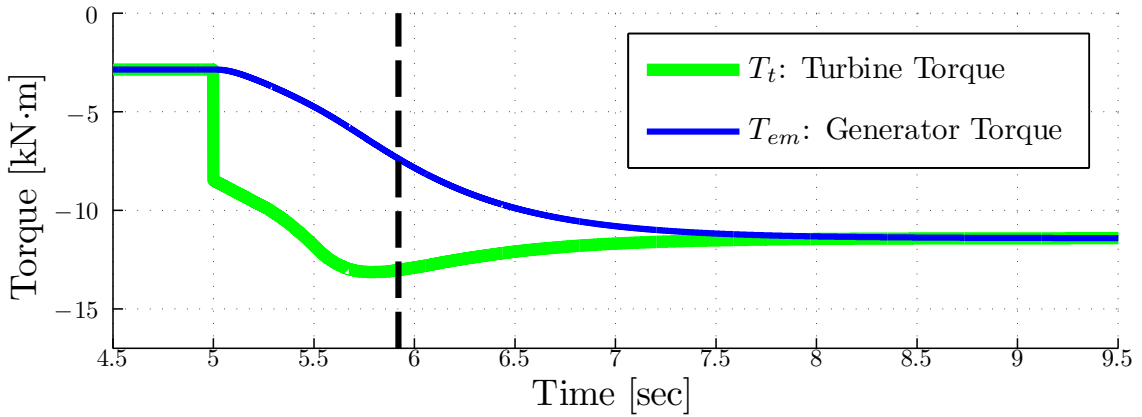


Figure 7.14: Generator and Turbine Torque Response to a 5m/s Wind Gust

would exhibit the same characteristics but over a longer time scale.

Figure 7.14 shows the torque imbalance between the turbine and generator during the wind gust that gives rise to the system acceleration. At  $t = 5$  seconds the turbine gives a step input in prime mover torque, the system responds with a smooth transition.

Figure 7.15 shows the power balance in the machine throughout the wind gust. The stator and rotor copper losses are not shown because they are negligible at the scale of the figure, combined they peak around 34 kW. First it is seen that the rotor power does switch direction through synchronous speed. In the subsynchronous mode it is positive, which means it is injected into the machine. As the speed crosses synchronous, the rotor power tends to zero and then becomes negative in the supersynchronous region, indicating that the rotor is indeed generating. The net power is equal to the mechanical power of the turbine in both steady state regions indicating that the generator is converting the full mechanical power of the wind. During the transition, the imbalance of power is used to accelerate the system. The stator clearly handles both the turbine and the rotor power in the subsynchronous region. In the supersynchronous region the stator handles less power than the turbine provides by the same amount of the rotor power, indicating that the system has split the

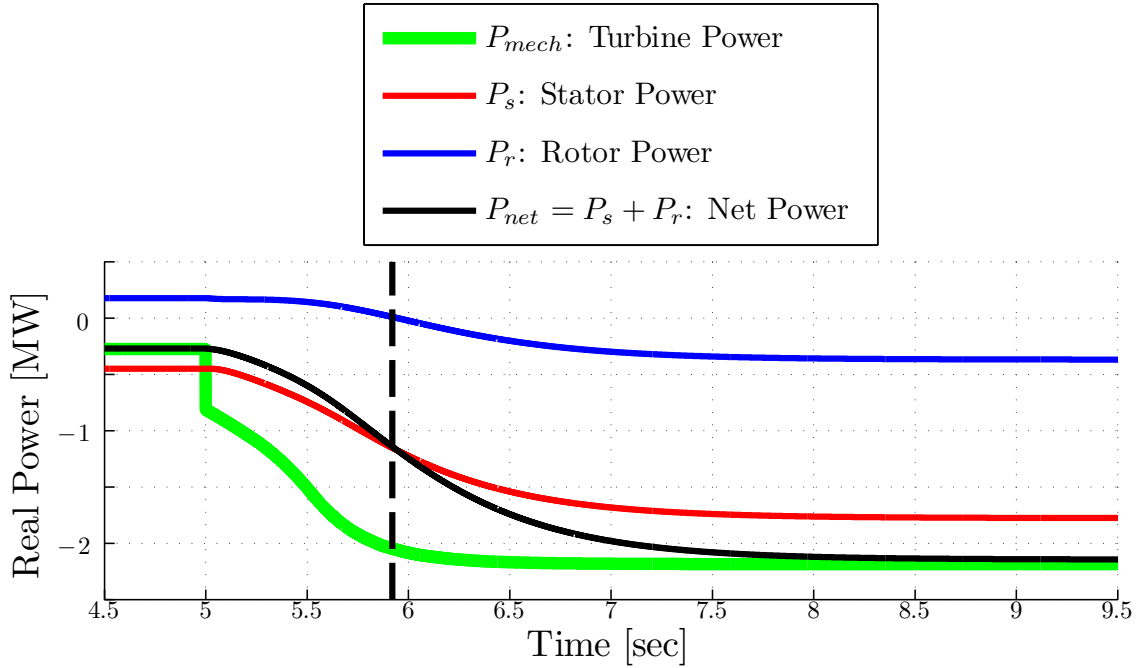


Figure 7.15: Power Balance Through a 5m/s Wind Gust

power between the two machine members. This allows the machine to produce on a whole over 2.5 MW while it is only rated for 2 MW without overloading any winding.

The increased power translates to an increase in stator current magnitude. Figure 7.16 shows that the current in the stator peaks out at 2.1 kA, or about 1485 A(rms). This is significantly less than the rated current of the stator,  $I_{s,rated} = 1760$  A(rms), showing again that the stator is not overloaded.

Figures 7.17 and 7.18 show the three phase rotor current and rotor voltage waveforms. It is important to note that these are the values directly applied to or produced from the simulation. Due to the turns

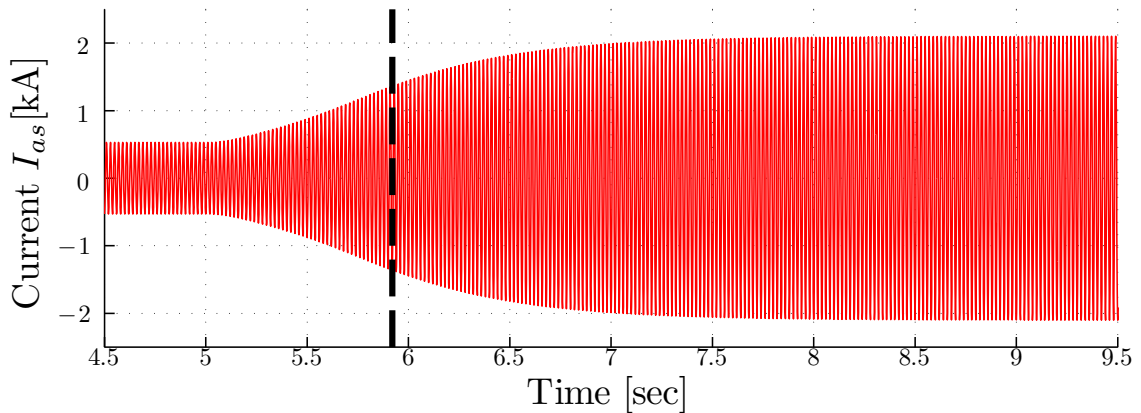


Figure 7.16: Stator Current Response to a 5m/s Wind Gust

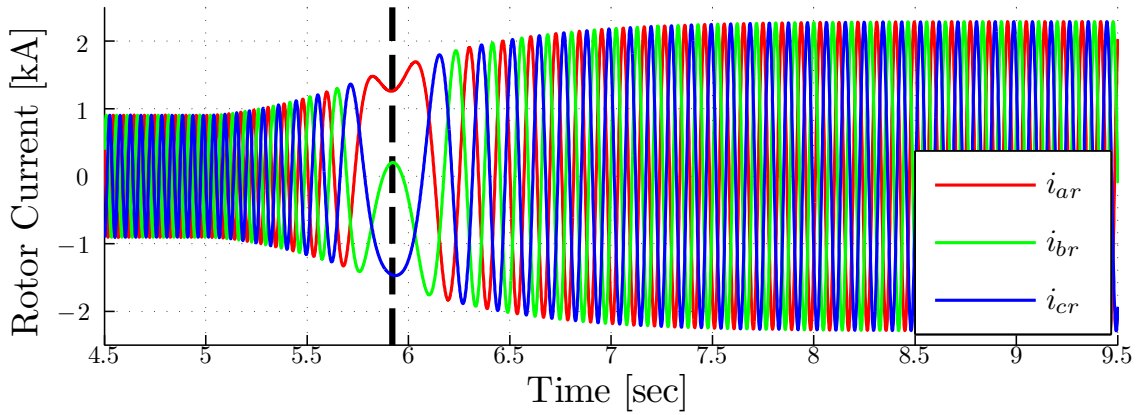


Figure 7.17: Rotor Current Response to a 5m/s Wind Gust

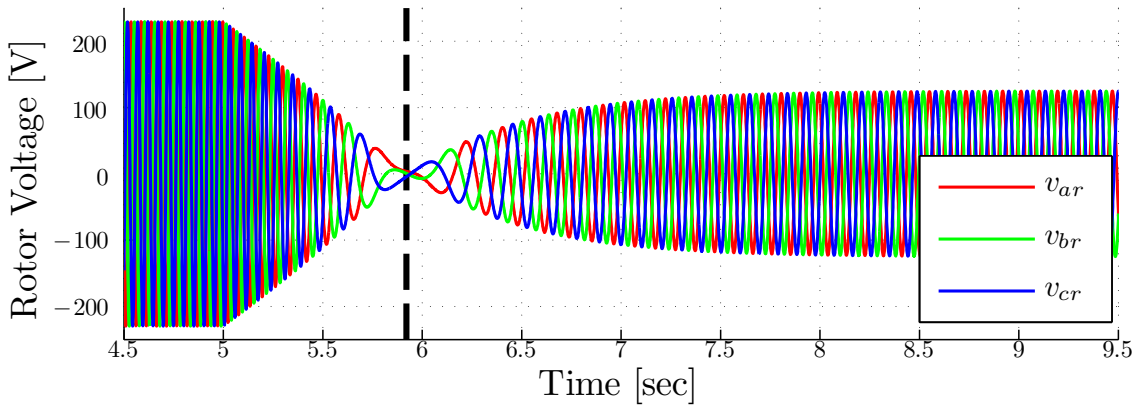


Figure 7.18: Rotor Voltage Response to a 5m/s Wind Gust

ratio of the machine, the actual rotor voltages would be about three times as high and the currents about three times as low. The frequency of both current and voltage reduce around synchronous speed. Furthermore the phase sequence reverses from a-b-c to a-c-b as expected. Finally note that the rotor voltage magnitude is also proportional to the slip, approaching zero as the machine passes synchronous speed.

This case study corroborates with the operating principals and phenomenon observed by researches who have experimented with actual DFIG systems [31, 10].

### 7.3 Future Work

The model presented is the simplest possible description of a DFIG and wind turbine that can reproduce the phenomena needed for dynamic control. There are however serious deficiencies in the model which can be improved upon.

### 7.3.1 Deficiencies in the Model

Loss in the generator model is treated lightly. Only the stator and rotor copper losses are considered. Modelling the mechanical, core and hysteresis losses taking into consideration saturation of the iron would not be difficult to add to the model. However it would greatly increase the complexity of the control equations, obscuring any gain. This path is not recommended, it would be far better to look into control schemes that are robust enough to handle these degrading effects.

The wind turbine model could be improved in two ways. First pitch control could be added by allowing the variable  $\beta$  to be included in the description, instead of just setting it to zero. This would result in a three dimensional lookup table for the turbine torque but would allow the system to operate over the entire wind speed spectrum, instead of just the MPPT region.

The biggest area of improvement for the model is the converter. Currently it is modelled as completely ideal, whatever rotor voltage it is commanded it reproduces exactly. A proper pulse width modulated scheme would greatly enhance the simulation of the harmonics present. The reader is referred to Chapter 2 of “*Doubly Fed Induction Machine: Modeling and Control for Wind Energy Generation*” [7] for an solid introduction to the subject. With the inclusion of the converter would come the necessity to add grid and rotor side filters to mitigate the harmonic content of the waveforms. Other axillary equipment such as the crowbar and breakers could be added to allow for study on the start up and synchronization process of the system.

### 7.3.2 Towards a Practical Implementation

The ultimate goal of future work should be a small scale prototype of the system. The amount of hurdles faced cannot be predicted but it can be quite certain that it will be a much more difficult task than a working simulation. The reader is referred to “*Vector Control of Three-Phase AC Machines: System Development in the Practice,*” as a starting point [32]. It contains a practical treatment of a DFIG system that could be of some aid.

## 7.4 Conclusion

With the deficiencies in the model clearly explained the end result of this dissertation is a working model of a doubly fed induction generator connected to a wind turbine which achieves maximum power point tracking by employing stator flux oriented vector control. Each component has been validated through comparison to published results in literature and the system as a whole conforms with experimental results of other researchers as well. To extend this work and complete the model of all practical wind turbine subsystems it will be necessary to obtain the parameters of a real system, most preferably through collaboration with a local wind farm.



# Appendix A

## Derivations

### A.1 Equations 2.42 and 2.43: Steady State Torque Equations

Starting with Equation 2.41 for mechanical torque,

$$T_{em} = \frac{P_{mech}}{\omega_{mech}}, \quad (2.41)$$

expressions for  $P_{mech}$  and  $\omega_{mech}$  are found that contain electrical variables only. First, the rotor voltage is expressed in terms of currents by substituting Equation 2.17 into Equation 2.15:

$$\bar{V}_r = R_r \bar{I}_r + j\omega_r (L_m \bar{I}_s + L_r \bar{I}_r).$$

This expression for voltage is substituted into the expression for  $P_{mech}$  found in Equation 2.24:

$$\begin{aligned} P_{mech} &= 3|\bar{I}_r|^2 R_r \left( \frac{1-s}{s} \right) - 3 \left( \frac{1-s}{s} \right) \text{Re}\{\bar{V}_r \bar{I}_r^*\} \\ &= 3|\bar{I}_r|^2 R_r \left( \frac{1-s}{s} \right) - 3 \left( \frac{1-s}{s} \right) \text{Re}\left\{ [R_r \bar{I}_r + j\omega_r (L_m \bar{I}_s + L_r \bar{I}_r)] \bar{I}_r^* \right\} \\ &= 3 \left( \frac{1-s}{s} \right) \left[ R_r |\bar{I}_r|^2 - \text{Re}\left\{ R_r |\bar{I}_r|^2 + j\omega_r L_m \bar{I}_s \bar{I}_r^* + j\omega_r L_r |\bar{I}_r|^2 \right\} \right] \\ &= 3 \left( \frac{1-s}{s} \right) \omega_r L_m \text{Im}\{\bar{I}_s \bar{I}_r^*\}. \end{aligned} \quad (2.24)$$

Note that the identity  $\text{Re}\{jz\} = \text{Im}\{z\}$ , where  $z \in \mathbb{C}$  was applied in the final step. Next the mechanical angular velocity is written in terms of the rotor's angular velocity in electrical radians per second using Equations 2.2, 2.7b and 2.7d:

$$\begin{aligned} \omega_{mech} &= \frac{\omega_m}{P_p} \\ &= \frac{(1-s)\omega_s}{P_p} = \left( \frac{1-s}{s} \right) \frac{\omega_r}{P_p}. \end{aligned} \quad (2.2)$$

Substituting the derived expressions for  $P_{mech}$  and  $\omega_{mech}$  into the expression for  $T_{em}$  yields:

$$\begin{aligned} T_{em} &= \frac{P_p}{\omega_r} \left( \frac{s}{1-s} \right) \cdot 3 \left( \frac{1-s}{s} \right) \omega_r L_m \text{Im}\{\overline{I_s} \overline{I_r}^*\} \\ &= 3P_p L_m \text{Im}\{\overline{I_s} \overline{I_r}^*\} \end{aligned}$$

To express this in terms of flux linkage to arrive at Equation 2.43,  $\overline{I_s}$  and  $\overline{I_r}$  are replaced with Equations 2.19 and 2.19:

$$\begin{aligned} T_{em} &= 3P_p L_m \text{Im}\{\overline{I_s} \overline{I_r}^*\} \\ &= 3P_p L_m \text{Im}\left\{ \left( \overline{\lambda_s} \frac{1}{\sigma L_s} - \overline{\lambda_r} \frac{L_m}{\sigma L_s L_r} \right) \left( \overline{\lambda_r} \frac{1}{\sigma L_r} - \overline{\lambda_s} \frac{L_m}{\sigma L_s L_r} \right)^* \right\} \\ &= 3P_p L_m \text{Im}\left\{ \frac{\overline{\lambda_s} \overline{\lambda_r}^*}{\sigma^2 L_s L_r} + \frac{L_m^2 \overline{\lambda_s}^* \overline{\lambda_r}}{\sigma^2 L_s^2 L_r^2} - \frac{L_m |\overline{\lambda_s}|^2}{\sigma^2 L_s^2 L_r} - \frac{L_m |\overline{\lambda_r}|^2}{\sigma^2 L_s L_r^2} \right\} \\ &= 3P_p L_m \text{Im}\left\{ \overline{\lambda_s} \overline{\lambda_r}^* \left( \frac{1}{\sigma^2 L_s L_r} - \frac{L_m^2}{\sigma^2 L_s^2 L_r^2} \right) \right\} \\ &= 3P_p L_m \text{Im}\left\{ \overline{\lambda_s} \overline{\lambda_r}^* \left( \frac{L_s L_r - L_m^2}{\sigma^2 L_s^2 L_r^2} \right) \right\} \\ &= 3P_p L_m \sigma \frac{1}{L_s L_r \sigma^2} \text{Im}\{\overline{\lambda_s} \overline{\lambda_r}^*\} \\ &= 3P_p \frac{L_m}{L_s L_r \sigma} \text{Im}\{\overline{\lambda_s} \overline{\lambda_r}^*\}. \end{aligned}$$

Note that the identity  $\text{Im}\{z^*\} = \text{Im}\{-z\}$  where  $z \in \mathbb{C}$  was applied to simplify the expression.

## A.2 Equation 3.4: Space Vector from Three Phase Components

Substituting equation 3.3 into 3.2:

$$\vec{v}_s^s = V \cos(\omega t + \phi) e^{j0} + V \cos(\omega t + \phi - \frac{2\pi}{3}) e^{j\frac{2\pi}{3}} + V \cos(\omega t + \phi - \frac{4\pi}{3}) e^{j\frac{4\pi}{3}}$$

Applying Euler's formula,  $e^{j\theta} = \cos \theta + j \sin \theta$ :

$$\begin{aligned} \vec{v}_s^s &= V [\cos(\omega t + \phi) + \cos(\omega t + \phi - \frac{2\pi}{3}) \cos(\frac{2\pi}{3}) + j \cos(\omega t + \phi - \frac{2\pi}{3}) \sin(\frac{2\pi}{3}) \\ &\quad + \cos(\omega t + \phi - \frac{4\pi}{3}) \cos(\frac{4\pi}{3}) + j \cos(\omega t + \phi - \frac{4\pi}{3}) \sin(\frac{4\pi}{3})] \end{aligned}$$

Applying the trigonometric equality,  $\cos(\alpha + \beta) = \cos \alpha \cos \beta \mp \sin \alpha \sin \beta$ :

$$\begin{aligned}\vec{v}_s^s &= V\{\cos(\omega t + \phi) + \cos(\frac{2\pi}{3})[\cos(\omega t + \phi) \cos(\frac{2\pi}{3}) + \sin(\omega t + \phi) \sin(\frac{2\pi}{3})] \\ &\quad + j \sin(\frac{2\pi}{3})[\cos(\omega t + \phi) \cos(\frac{2\pi}{3}) + \sin(\omega t + \phi) \sin(\frac{2\pi}{3})] \\ &\quad + \cos(\frac{4\pi}{3})[\cos(\omega t + \phi) \cos(\frac{4\pi}{3}) + \sin(\omega t + \phi) \sin(\frac{4\pi}{3})] \\ &\quad + j \sin(\frac{4\pi}{3})[\cos(\omega t + \phi) \cos(\frac{4\pi}{3}) + \sin(\omega t + \phi) \sin(\frac{4\pi}{3})]\} \\ \vec{v}_s^s &= V\{\cos(\omega t + \phi) - \frac{1}{2}[\cos(\omega t + \phi)(-\frac{1}{2}) + \sin(\omega t + \phi)(\frac{\sqrt{3}}{2})] \\ &\quad + j \frac{\sqrt{3}}{2}[\cos(\omega t + \phi)(-\frac{1}{2}) + \sin(\omega t + \phi)(\frac{\sqrt{3}}{2})] \\ &\quad - \frac{1}{2}[\cos(\omega t + \phi)(-\frac{1}{2}) + \sin(\omega t + \phi)(-\frac{\sqrt{3}}{2})] \\ &\quad - j \frac{\sqrt{3}}{2}[\cos(\omega t + \phi)(-\frac{1}{2}) + \sin(\omega t + \phi)(-\frac{\sqrt{3}}{2})]\}\end{aligned}$$

Simplifying:

$$\begin{aligned}\vec{v}_s^s &= \frac{3}{2}V[\cos(\omega t + \phi) + j \sin(\omega t + \phi)] \\ &= \frac{3}{2}V e^{j(\omega t + \phi)}\end{aligned}$$

### A.3 Equation 3.5: Choosing $c$

The inverse Clarke transform is given in Equation 3.6 with  $c = \frac{2}{3}$ . If  $c$  is left arbitrary the effect it has on equations will become apparent. To find the inverse Clarke transform the matrix in Equation 3.5 must be inverted. However it is not a square matrix and thus has no inverse. The reason it is not square is because of a simplifying assumption. The input waveforms were assumed to be completely balanced, and thus have no zero sequence components. If it is generalized so that there can be zero sequence components, another row is added to the bottom of Equation 3.5. When using  $c = \frac{2}{3}$  the values of the entries in the matrix for the zero sequence can be found to be  $\frac{1}{2}$  as seen in [20]. Factoring out the constant of  $\frac{2}{3}$  and replacing it with a general constant  $c$  leaves the entries for the zero sequence row to be  $\frac{1}{3c}$ . Now the Clarke transform becomes:

$$\begin{bmatrix} F_D \\ F_Q \\ F_0 \end{bmatrix} = c \begin{bmatrix} 1 & -\frac{1}{2} & -\frac{1}{2} \\ 0 & \frac{\sqrt{3}}{2} & -\frac{\sqrt{3}}{2} \\ \frac{1}{3c} & \frac{1}{3c} & \frac{1}{3c} \end{bmatrix} \begin{bmatrix} F_a \\ F_b \\ F_c \end{bmatrix}$$

Now the inverse is readily found to be:

$$\begin{bmatrix} F_a \\ F_b \\ F_c \end{bmatrix} = \frac{1}{c} \begin{bmatrix} \frac{2}{3} & 0 & c \\ -\frac{1}{3} & \frac{1}{\sqrt{3}} & c \\ -\frac{1}{3} & \frac{1}{\sqrt{3}} & c \end{bmatrix} \begin{bmatrix} F_D \\ F_Q \\ F_0 \end{bmatrix}$$

Discarding the last column (assuming everything is balanced) and explicitly writing out the abc quantities in terms of DQ components:

$$\begin{aligned} F_a &= \frac{1}{c} \frac{2}{3} F_D \\ F_b &= \frac{1}{c} \left( -\frac{1}{3} F_D + \frac{1}{\sqrt{3}} F_Q \right) \\ F_c &= \frac{1}{c} \left( -\frac{1}{3} F_D - \frac{1}{\sqrt{3}} F_Q \right) \end{aligned}$$

The power in the abc frame is given by:

$$P_{abc} = v_a i_a + v_b i_b + v_c i_c$$

In terms of two axis components:

$$\begin{aligned} P_{abc} &= \frac{1}{c} \frac{2}{3} v_D \frac{1}{c} \frac{2}{3} i_D + \frac{1}{c} \left( -\frac{1}{3} v_D + \frac{1}{\sqrt{3}} v_Q \right) \frac{1}{c} \left( -\frac{1}{3} i_D + \frac{1}{\sqrt{3}} i_Q \right) + \frac{1}{c} \left( -\frac{1}{3} v_D - \frac{1}{\sqrt{3}} v_Q \right) \frac{1}{c} \left( -\frac{1}{3} i_D - \frac{1}{\sqrt{3}} i_Q \right) \\ &= \frac{1}{c^2} \frac{2}{3} (v_D i_D + v_Q i_Q) \end{aligned}$$

Choosing  $c = \sqrt{\frac{2}{3}}$ :

$$P_{abc} = v_D i_D + v_Q i_Q = P_{DQ}$$

The power is now the same in both frames.

Choosing  $c = \frac{2}{3}$ :

$$P_{abc} = \frac{3}{2} (v_D i_D + v_Q i_Q) = \frac{3}{2} P_{DQ}$$

Power (and torque) equations must be multiplied by  $\frac{3}{2}$  for equivalence in three and two axis frames. This work uses  $c = \frac{2}{3}$  so this extra factor of  $\frac{3}{2}$  is seen in all power and torque relations.

## A.4 Equations 3.21, and 3.22: Solution to Derivatives

In equation 3.21 the derivative is solved with the product rule:

$$\begin{aligned} \frac{d}{dt} (\vec{\lambda}_s^g e^{j\theta_g}) &= \frac{d}{dt} \vec{\lambda}_s^g \cdot e^{j\theta_g} + \vec{\lambda}_s^g \cdot j e^{j\theta_g} \frac{d}{dt} \theta_g \\ &= \frac{d}{dt} \vec{\lambda}_s^g \cdot e^{j\theta_g} + \vec{\lambda}_s^g \cdot j \omega_g e^{j\theta_g} \end{aligned}$$

Where it is recognized that  $\frac{d}{dt} \theta_g = \omega_g$ . Also recognizing  $\frac{d}{dt} \theta_m = \omega_m$ , the derivative in 3.22 is solved in a similar manner:

$$\begin{aligned} \frac{d}{dt} (\vec{\lambda}_r^g e^{j(\theta_g - \theta_m)}) &= \frac{d}{dt} \vec{\lambda}_r^g \cdot e^{j(\theta_g - \theta_m)} + \vec{\lambda}_r^g \cdot j e^{j(\theta_g - \theta_m)} \frac{d}{dt} (\theta_g - \theta_m) \\ &= \frac{d}{dt} \vec{\lambda}_r^g \cdot e^{j(\theta_g - \theta_m)} + \vec{\lambda}_r^g \cdot j (\omega_g - \omega_m) e^{j(\theta_g - \theta_m)} \end{aligned}$$

## A.5 Equation 3.36: Cross Product of Space Vectors

Recall the cross product operation in general three space,  $\mathbb{R}^3$ :

Let:

$$\begin{aligned}\vec{A} &= A_x \hat{x} + A_y \hat{y} + A_z \hat{z} \\ \vec{B} &= B_x \hat{x} + B_y \hat{y} + B_z \hat{z}\end{aligned}$$

Then:

$$\begin{aligned}\vec{A} \times \vec{B} &= \begin{vmatrix} \hat{x} & \hat{y} & \hat{z} \\ A_x & A_y & A_z \\ B_x & B_y & B_z \end{vmatrix} = \begin{vmatrix} A_y & A_z \\ B_y & B_z \end{vmatrix} \hat{x} - \begin{vmatrix} A_x & A_z \\ B_x & B_z \end{vmatrix} \hat{y} + \begin{vmatrix} A_x & A_y \\ B_x & B_y \end{vmatrix} \hat{z} \\ &= (A_y B_z - B_y A_z) \hat{x} - (A_x B_z - B_x A_z) \hat{y} + (A_x B_y - B_x A_y) \hat{z}\end{aligned}$$

Note that space vectors are two dimensional, the information they contain can be described with just the x and y axis, and they have no z-axis components. It is clear that setting  $A_z$  and  $B_z$  in the previous equation reduces the cross product to:

$$\vec{A} \times \vec{B} = (A_x B_y - B_x A_y) \hat{z}$$

The direction  $\hat{z}$  becomes unimportant, since the space vectors are located in the same plane, the cross product is perpendicular and a scalar value fully describes the quantity:

$$\vec{A} \times \vec{B} = A_x B_y - B_x A_y$$

Applying the concept to space vectors, the x and y components are replaced with real and imaginary components. As long as both space vectors are in the same frame the general results for cross product apply. For example:

$$\begin{aligned}\vec{\lambda}_r^g &= \lambda_{rd} + j\lambda_{rq} \\ \vec{\lambda}_s^g &= \lambda_{sd} + j\lambda_{sq} \\ \vec{\lambda}_r^g \times \vec{\lambda}_s^g &= \lambda_{rd}\lambda_{sq} - \lambda_{sd}\lambda_{rq}\end{aligned}$$

## A.6 Equations 5.17: Transfer Functions the Modified Inner Loop Control Structure

Referring to Figure 5.7, three equations can be readily determined:

$$\begin{aligned}i_{rd}^{err}(s) &= i_{rd}^*(s) - i_{rd}(s) \\v'_{rd}(s) &= i_{rd}^{err}(s) \frac{K_{I1}}{s} - i_{rd}(s) K_{P1} \\i_{rd}(s) &= v'_{rd}(s) \frac{1}{R_r + \sigma L_r s}\end{aligned}$$

Substituting the first two expressions into the third one yields:

$$\begin{aligned}i_{rd}(s) &= \left[ i_{rd}^{err}(s) \frac{K_{I1}}{s} - i_{rd} K_{P1} \right] \frac{1}{R_r + \sigma L_r s} \\&= \left[ (i_{rd}^*(s) - i_{rd}(s)) \frac{K_{I1}}{s} - i_{rd} K_{P1} \right] \frac{1}{R_r + \sigma L_r s}\end{aligned}$$

Grouping like terms:

$$i_{rd}(s) \left[ 1 + \left( \frac{K_{I1}}{s} + K_{P1} \right) \frac{1}{R_r + \sigma L_r s} \right] = i_{rd}^*(s) \frac{K_{I1}}{s(R_r + \sigma L_r s)}$$

Dividing output by input:

$$\begin{aligned}\frac{i_{rd}(s)}{i_{rd}^*(s)} &= \frac{K_{I1}}{s(R_r + \sigma L_r s)} \frac{1}{1 + \frac{K_{P1}s + K_{I1}}{s(R_r + \sigma L_r s)}} \\&= \frac{K_{I1}}{s^2 \sigma L_r + s(R_r + K_{P1}) + K_{I1}} \\&= \frac{\frac{K_{I1}}{\sigma L_r}}{s^2 + s \frac{(R_r + K_{P1})}{\sigma L_r} + \frac{K_{I1}}{\sigma L_r}}\end{aligned}$$

## A.7 Ensuring a Negative Feedback Structure in the Presence of a Negative Static Loop Gain

If the open loop system has negative static gain, the closed loop system will exhibit positive feedback, if the standard control structure is applied. Figure A.1 shows the situation.

$$\frac{Y(s)}{X(s)} = \frac{-kG(s)}{1 + (-kG(s)H(s))} = \frac{-kG(s)}{1 - kG(s)H(s)}$$

To fix this, *Tapia et al.* [13] suggests subtracting the reference value from the actual value instead. Figure A.2 shows the modification, from which the following equations can be written:

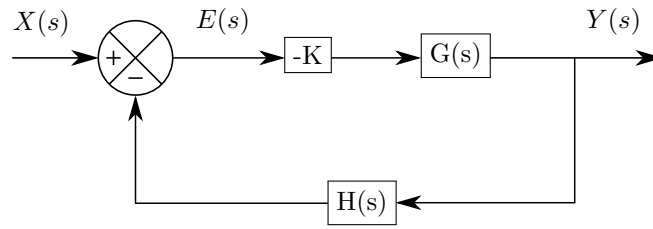


Figure A.1: Standard Feedback Control Structure

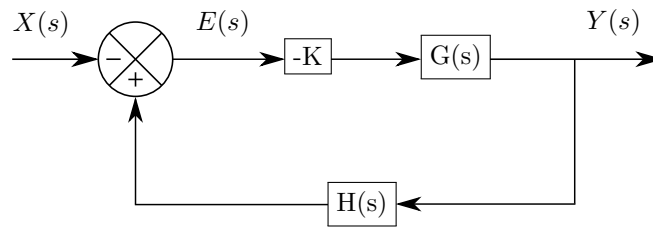


Figure A.2: Modified Feedback Control Structure

$$E(s) = H(s)Y(s) - X(s)$$

$$Y(s) = -kG(s)E(s)$$

Substituting the first expression into the second:

$$Y(s) = -kG(s)[H(s)Y(s) - X(s)]$$

Grouping like terms:

$$Y(s)[1 + kG(s)H(s)] = kG(s)H(s)X(s)$$

Dividing the output by the input:

$$\frac{Y(s)}{X(s)} = \frac{kG(s)H(s)}{1 + kG(s)H(s)}$$

The standard negative feedback system is obtained.

## A.8 Derivation of Equation 5.34: The Outer Loop Transfer Function

From Figure 5.8, the following equations are written:

$$\begin{aligned} i_{rq}(s) &= i_{rq}^*(s) \frac{1}{1 + \frac{T_{s1}}{4}s} \\ i_{rq}^*(s) &= P_s^{err}(s) \frac{K_{I2}}{s} + K_{P2} P_s(s) \\ P_s^{err}(s) &= P_s(s) - P_s^*(s) \\ P_s(s) &= -\frac{3}{2} \frac{L_m}{L_s} |\vec{v}_s^*| i_{rq}(s) \end{aligned}$$

Substituting the third equation into the second:

$$i_{rq}^*(s) = [P_s(s) - P_s^*(s)] \frac{K_{I2}}{s} + K_{P2} P_s(s)$$

Substituting in the first equation:

$$i_{rq}(s) \frac{1}{1 + \frac{T_{s1}}{4}s} = P_s(s) \left( K_{P2} + \frac{K_{I2}}{s} \right) - P_s^*(s) \frac{K_{I2}}{s}$$

Substituting in the fourth equation:

$$\frac{P_s(s)}{-\frac{3}{2} \frac{L_m}{L_s} |\vec{v}_s^*|} \cdot \frac{1}{1 + \frac{T_{s1}}{4}s} = P_s(s) \left( K_{P2} + \frac{K_{I2}}{s} \right) - P_s^*(s) \frac{K_{I2}}{s}$$

Collecting terms:

$$P_s(s) \left( K_{P2} + \frac{K_{I2}}{s} + \frac{\frac{1}{1 + \frac{T_{s1}}{4}s}}{\frac{3}{2} \frac{L_m}{L_s} |\vec{v}_s^*|} \right) = P_s^*(s) \frac{K_{I2}}{s}$$

Dividing output by input:

$$\begin{aligned} \frac{P_s(s)}{P_s^*(s)} &= \frac{\frac{K_{I2}}{s}}{\left( K_{P2} + \frac{K_{I2}}{s} + \frac{\frac{1}{1 + \frac{T_{s1}}{4}s}}{\frac{3}{2} \frac{L_m}{L_s} |\vec{v}_s^*|} \right)} \\ &= \frac{6 \frac{L_m}{L_s} \frac{|\vec{v}_s^*|}{T_{s1}} K_{I2}}{s^2 + \left( \frac{4}{T_{s1}} + 6 \frac{L_m}{L_s} \frac{|\vec{v}_s^*|}{T_{s1}} K_{P2} \right) s + 6 \frac{L_m}{L_s} \frac{|\vec{v}_s^*|}{T_{s1}} K_{I2}} \end{aligned}$$



## Appendix B

# Initialization Script

This section gives in hard copy form, the Matlab code necessary to run the model. All code is also provided on the accompanying CD-ROM in the file *Init\_System.m*.

```
% Initialize DFIM and Wind Turbine Simulation
% Author: Matthew Hurajt
% Last Modified: July 16th, 2013
close all
clear
clc
%% Turbine Model Initialization

% Load Turbine Characteristic into the model
% Turbine Parameters
GR = 103.2;          % gear box ratio
R = 48.63;          % turbine radius [m]
rho = 1.21;         % air density [kg/m^3]
A = pi*R^2;        % swept area in [m^2]

% tip speed ratio from manufacturer datasheet
TSR_vector = xlsread('CpVsTSR_D49.xlsx',1,'A2:A67');
Cp_vector = xlsread('CpVsTSR_D49.xlsx',1,'B2:B67');

% Turbine Performace Curves (used in look-up tables)
vwind_vector = linspace(3,11,15); % vector of wind speeds [m/s]
wt_vector = linspace(.1234,3.6192,1000); % vector of turbine shaft speeds
% [mech rad/sec]
[X,Y]=meshgrid(vwind_vector,wt_vector); % X stores v, Y stores w
% v increases RIGHT, w increases DOWN
L = R*Y./X; % tip speed ratio [dimensionless]
Cp = interp1(TSR_vector,Cp_vector,L); % performance factor [dimensionless]
Pt = (1/2)*rho*A*X.^3.*Cp; % Turbine power [W]
Tt_matrix = Pt./Y; % Turbine torque [Nm]
Tt_matrix(isnan(Tt_matrix)) = 0; % remove NaNs
Tmech = Tt_matrix/GR; % Torque available at shaft of
% generator [Nm]
```

```

% Maximum Power Point Tracking
MPPT = zeros(1,length(vwind_vector)); % vector of maximum power points [W]
MPPT_w = zeros(1,length(vwind_vector)); % vector of turbine shaft speeds
% that correspond to the maximum
% power point [mech rad/sec]

for i = 1:length(vwind_vector);
    [MPPT(i),IND_MAX] = max(Pt(:,i)); % find maximum power points
    MPPT_w(i) = wt_vector(IND_MAX);
end

% fitting the function MPPT = Kopt * (wt)^3 yields:
% Curve fitting done offline using Matlab Curve Fit Toolbox
Kopt = 3.364e5;

% Initialization Starts Here %
%%%%%%%%%%%%%%%%%%%%%%%%%%%%%%%%%%%%%%%%%%%%%%%%%%%%%%%%%%%%%%%%%%%%%%%%
% Choose Wind Speed
%%%%%%%%%%%%%%%%%%%%%%%%%%%%%%%%%%%%%%%%%%%%%%%%%%%%%%%%%%%%%%%%%%%%%%%%
vw_0 = 5; % initial wind speed [m/s]
%%%%%%%%%%%%%%%%%%%%%%%%%%%%%%%%%%%%%%%%%%%%%%%%%%%%%%%%%%%%%%%%%%%%%%%%

% Initial Turbine Parameters calculated from initial wind speed
L_0 = R*wt_vector/vw_0; % initial tip speed ratio
Cp_0 = interp1(TSR_vector,Cp_vector,L_0); % initial performance factor
Pt_0 = (1/2)*rho*A*vw_0^3.*Cp_0; % initial turbine power curve

%Initial values of MPPT
[MPPT_0,IND_MAX] = max(Pt_0);
MPPT_w_0 = wt_vector(IND_MAX);

% Initialization of turbine for a particular wind speed
Pt_init = MPPT_0;
wt_init = MPPT_w_0;

% Plot Wind Turbine Data
figure(1)
hold on
grid on
for i = 1:length(vwind_vector)
    plot(wt_vector*60/(2*pi)*GR,Pt(:,i),'b-','Linewidth',1)
end
plot(wt_vector*60/(2*pi)*GR,Pt_0,'b-','Linewidth',3)
plot(MPPT_w*60/(2*pi)*GR,MPPT,'r-','Linewidth',1)
hold off

%% Initialize Wound Rotor Machine

% Load Parameters of Generator
VLLrms = 690; % line to line, rms, stator voltage [V]
fs = 50; % line frequency [Hz]
Pp = 2; % number of poles pairs [dimensionless]
J = 98.26 ; % system inertia (reduced for short simulation) [kg m^2]
TR = 0.34; % equivalent turns ratio [dimensionless]

```

```

Rs = 2.6e-3*1; % stator resistance [ohms]
Rr = 2.9e-3*1; % referred rotor resistance [ohms]
Lls = 87e-6; % stator leakage inductance [H]
Llr = 87e-6; % referred rotor leakage inductance [H]
Lm = 2.5e-3; % magnetizing inductance
Ls = Lm+Lls; % stator inductance [H]
Lr = Lm+Llr; % rotor inductance [H]
sig = 1-Lm^2/(Ls*Lr); % leakage factor [dimensionless]

% Conversion Multipliers
D2R = pi/180; % degrees to radians [rad/deg]
R2D = 180/pi; % radians to degrees [deg/rad]

%% Starting Point
% Starting Speeds
ws = 2*pi*fs; % synchronous angular frequency in [electrical rad/sec]
w_mech = wt_init*GR; % rotor shaft angular frequency in [mechanical rad/sec]
wm_0 = Pp*w_mech; % rotor shaft angular frequency in [electrical rad/sec]
s = (ws - wm_0)/ws; % slip [dimensionless]
wr = s*ws; % rotor angular frequency in [electrical rad/sec]

% P and Q references
Ps_ref = -Pt_init; % real stator power reference, three phase, [W]
Qs_ref = 0; % reactive stator power reference, three phase, [VAR]

%% Solve for rotor voltage accounting for Rs, and Rr, aiming for P and Q ref
% Step 1: solve for stator current from P and Q power ref

% line to neutral rms stator voltage magnitude [V]
Vs_mag = VLLrms/sqrt(3);
% stator voltage taken as reference [rad]
Vs_ang = 0;
% stator voltage phasor, rms [V]
Vs_phasor = Vs_mag*exp(1i*Vs_ang);

% stator current phasor, rms [A]
Is_phasor = (Ps_ref/3 -1i*Qs_ref/3)/Vs_phasor;
Is_mag = abs(Is_phasor);
Is_ang = angle(Is_phasor);

% Step 2: solve for all other phasors
% stator flux linkage phasor, rms [wb-turns]
Fs_phasor = (Vs_phasor - Rs*Is_phasor)/(1i*ws);
Fs_mag = abs(Fs_phasor);
Fs_ang = angle(Fs_phasor);

% rotor current phasor, rms [A]
Ir_phasor = (Fs_phasor - Ls*Is_phasor)/Lm;
Ir_mag = abs(Ir_phasor);
Ir_ang = angle(Ir_phasor);

% rotor flux linkage phasor, rms [wb-turns]
Fr_phasor = Lm*Is_phasor + Lr*Ir_phasor;

```

```

Fr_mag = abs(Fr_phasor);
Fr_ang = angle(Fr_phasor);

% rotor voltage phasor, rms [V]
Vr_phasor = li*wr*Fr_phasor + Rr*Ir_phasor;
Vr_mag = abs(Vr_phasor);
Vr_ang = angle(Vr_phasor);

% Power (positive consuming)
Ps = 3*real(Vs_phasor*conj(Is_phasor)); % real stator power [W]
Pr = 3*real(Vr_phasor*conj(Ir_phasor)); % real rotor power [W]
Qs = 3*imag(Vs_phasor*conj(Is_phasor)); % reactive stator power [Var]
Qr = 3*imag(Vr_phasor*conj(Ir_phasor)); % reactive rotor power [Var]

Ps_cu = 3*Is_mag^2*Rr; % stator copper loss [W]
Pr_cu = 3*Ir_mag^2*Rr; % rotor copper loss [W]

% electromagnetic torque [Nm]
Tem = 3*Lm/(sig*Lr*Ls)*Pp*imag(conj(Fr_phasor)*Fs_phasor);
nm = w_mech*30/pi; % rotor speed [rpm]
P_mech = Tem*w_mech; % mechanical power [W]

disp('----- Initial Steady State Operating Point -----')
disp('----- Phasor Solution -----')
disp([' Vs | ',num2str(Vs_mag),' /-',num2str(Vs_ang*R2D),' V'])
disp([' Vr | ',num2str(Vr_mag),' /-',num2str(Vr_ang*R2D),' V'])
disp([' Is | ',num2str(Is_mag),' /-',num2str(Is_ang*R2D),' A'])
disp([' Ir | ',num2str(Ir_mag),' /-',num2str(Ir_ang*R2D),' A'])
disp([' Fs | ',num2str(Fs_mag),' /-',num2str(Fs_ang*R2D),' wb-turns'])
disp([' Fr | ',num2str(Fr_mag),' /-',num2str(Fr_ang*R2D),' wb-turns'])
disp('-----')
disp([' Ps | ',num2str(Ps),' W'])
disp([' Pr | ',num2str(Pr),' W'])
disp([' Qs | ',num2str(Qs),' VAR'])
disp([' Qr | ',num2str(Qr),' VAR'])
disp([' Ps_cu | ',num2str(Ps_cu),' W'])
disp([' Pr_cu | ',num2str(Pr_cu),' W'])
disp('-----POWER BALANCE-----')
disp([' Ps + Pr | ',num2str(Ps+Pr),' W'])
disp([' P_mech + P_cu | ',num2str(Ps_cu + Pr_cu + P_mech),' W'])
disp('-----')
disp([' Tem | ',num2str(Tem),' Nm'])
disp([' nm | ',num2str(nm),' rpm'])
disp([' P_mech | ',num2str(P_mech),' W'])
disp('-----')

%% Initialize Dynamic model from Phasor Solution (align to stator flux)

% Phasor of Stator and Rotor Voltages are related to their space vectors at
% t=0 using Equation 3.10 from Section 3.3.3

%Stator Voltage
vas_0 = sqrt(2)*Vs_mag*cos(Vs_ang); % a phase stator voltage at t=0
vbs_0 = sqrt(2)*Vs_mag*cos(Vs_ang-2*pi/3); % b phase stator voltage at t=0

```

```

vcs_0 = sqrt(2)*Vs_mag*cos(Vs_ang-4*pi/3); % c phase stator voltage at t=0

vsD_0 = (2/3)*(vas_0 - 0.5*vbs_0 - 0.5*vcs_0); % D-axis stator voltage
vsQ_0 = (2/3)*(sqrt(3)/2*vbs_0 - sqrt(3)/2*vcs_0); % Q-axis stator voltage

Vs_s_0 = vsD_0 + li*vsQ_0; % stator voltage space vector (stator frame)

%Rotor Voltage
var_0 = sqrt(2)*Vr_mag*cos(Vr_ang); % a phase rotor voltage at t=0
vbr_0 = sqrt(2)*Vr_mag*cos(Vr_ang-2*pi/3); % b phase rotor voltage at t=0
vcr_0 = sqrt(2)*Vr_mag*cos(Vr_ang-4*pi/3); % c phase rotor voltage at t=0

vaph_0 = (2/3)*(var_0 - 0.5*vbr_0 - 0.5*vcr_0); % alpha-axis rotor voltage
vbet_0 = (2/3)*(sqrt(3)/2*vbr_0 - sqrt(3)/2*vcr_0); % beta-axis rotor voltage

Vr_r_0 = vaph_0 + li*vbet_0; % rotor voltage space vector (rotor frame)
% Initial rotor angle taken as 0
Vr_s_0 = Vr_r_0*exp(-li*(0)); % rotor voltage space vector (stator frame)
vrD_0 = real(Vr_s_0); % D-axis rotor voltage
vrQ_0 = imag(Vr_s_0); % Q-axis stator voltage

% Using the voltage space vector aligned to the stator frame, the flux is
% calculated using Equation 3.34, with the derivative vector set to zero
FM = [ -Rs/(sig*Ls), ws, Lm*Rs/(Ls*Lr*sig), 0; ...
       -ws, -Rs/(sig*Ls), 0, Lm*Rs/(Ls*Lr*sig); ...
       Lm*Rr/(Ls*Lr*sig), 0, -Rr/(sig*Lr), wr; ...
       0, Lm*Rr/(Ls*Lr*sig), -wr, -Rr/(sig*Lr)];

Flux_0 = -inv(FM)*[vsD_0,vsQ_0,vrD_0,vrQ_0]';
fsD_0 = Flux_0(1);
fsQ_0 = Flux_0(2);
frD_0 = Flux_0(3);
frQ_0 = Flux_0(4);

Fs_s_0 = fsD_0 + fsQ_0*li; % stator flux space vector at (stator frame)
Fr_s_0 = frD_0 + frQ_0*li; % rotor flux space vector at (stator frame)

% Currents are calculated with Equations 3.25 and 3.26
Is_s_0 = Fs_s_0/(sig*Ls) - Fr_s_0*Lm/(Ls*Lr*sig);
Ir_s_0 = Fr_s_0/(sig*Lr) - Fs_s_0*Lm/(Ls*Lr*sig);
isD_0 = real(Is_s_0);
isQ_0 = imag(Ir_s_0);

irD_0 = real(Ir_s_0);
irQ_0 = imag(Ir_s_0);

% Stator Flux Alignment
th_fs_0 = angle(fsD_0+ li*fsQ_0); % stator flux angle

% voltage, flux and current in the stator flux oriented reference frame
Vs_fs_0 = Vs_s_0*exp(-li*(th_fs_0));
vsd_0 = real(Vs_fs_0);
vsq_0 = imag(Vs_fs_0);

```

```

Vr_fs_0 = Vr_s_0*exp(-li*th_fs_0);
vrd_0 = real(Vr_fs_0);
vrq_0 = imag(Vr_fs_0);

Fs_fs_0 = Fs_s_0*exp(-li*th_fs_0);
fsd_0 = real(Fs_fs_0);
fsq_0 = imag(Fs_fs_0);

Fr_fs_0 = Fr_s_0*exp(-li*th_fs_0);
frd_0 = real(Fr_fs_0);
frq_0 = imag(Fr_fs_0);

Is_fs_0 = Is_s_0*exp(-li*th_fs_0);
isd_0 = real(Is_fs_0);
isq_0 = imag(Is_fs_0);

Ir_fs_0 = Ir_s_0*exp(-li*th_fs_0);
ird_0 = real(Ir_fs_0);
irq_0 = imag(Ir_fs_0);

%% Controller Initialization

% controller gains
% using Tapia's Method
% critically damped with Tset = 40ms
T1 = 40e-3; % settling time for inner loop

KI1 = (4/T1)^2*sig*Lr;
KP1 = 2*(4/T1)*sig*Lr-Rr;

% initialize the PI contoller integrators
w_fs_0 = vsq_0/fsd_0+Rs*Lm/Ls*irq_0/fsd_0;
Dfsd_0 = -Rs/Ls*fsd_0 +Lm*Rs/Ls*ird_0+vsd_0;

% Inner loop PI controller initial condtions
vrd_tapia = vrd_0 + sig*Lr*(w_fs_0-wm_0)*irq_0 - Lm/Ls*Dfsd_0 + KP1*ird_0;
vrq_tapia = vrq_0 - sig*Lr*(w_fs_0-wm_0)*ird_0...
            - (w_fs_0-wm_0)*Lm/Ls*fsd_0 + KP1*irq_0;

% Tapia's outer loop
T2 = 70e-3; % settling time for outer loop
KI2 = 8/3*T1/(T2^2)*Ls/Lm/(VLLrms*sqrt(3/2));
KP2 = 2/3*(2*T1-T2)/T2*Ls/Lm/(VLLrms*sqrt(3/2));

% Outerloop PI controller initial condtions
ird_tapia_IC = ird_0*(1+KP2*3/2*Lm/Ls*VLLrms*sqrt(3/2))...
              - KP2*3/2/Ls*VLLrms*sqrt(3/2)*fsd_0;
irq_tapia_IC = irq_0*(1 + KP2*3/2*Lm/Ls*VLLrms*sqrt(3/2));

```

# Bibliography

- [1] IEA. (Accessed: 2013-07-09) 2012 key world energy statistics. [Online]. Available: <http://www.iea.org/publications/freepublications/publication/name,31287,en.html>
- [2] BP. (Accessed: 2013-07-09) Bp statistical review of world energy june 2012. [Online]. Available: [bp.com/statisticalreview](http://bp.com/statisticalreview)
- [3] GWEC. (Accessed: 2013-07-09) Global wind statistics 2012. [Online]. Available: [http://www.gwec.net/wp-content/uploads/2013/02/GWEC-PRstats-2012\\_english.pdf](http://www.gwec.net/wp-content/uploads/2013/02/GWEC-PRstats-2012_english.pdf)
- [4] M. Liserre, R. Cárdenas, M. Molinas, and J. Rodriguez, “Overview of multi-mw wind turbines and wind parks,” *Industrial Electronics, IEEE Transactions on*, vol. 58, no. 4, pp. 1081–1095, 2011.
- [5] “IEEE application guide for IEEE std 1547, IEEE standard for interconnecting distributed resources with electric power systems,” *IEEE Std 1547.2-2008*, pp. 1–207, 2009.
- [6] B. Wu, Y. Lang, N. Zargari, and S. Kouro, *Power conversion and control of wind energy systems*. Wiley-IEEE Press, 2011.
- [7] G. Abad, L. Marroyo, G. Iwanski *et al.*, *Doubly Fed Induction Machine: Modeling and Control for Wind Energy Generation*. Wiley-IEEE Press, 2011, vol. 86.
- [8] N. Mohan, *Advanced Electric Drives: Analysis, Control and Modeling using Simulink*. Minnesota Power Electronics Research & Education (MNPERE), 2001.
- [9] F. Bonnet, P.-E. Vidal, and M. Pietrzak-David, “Dual direct torque control of doubly fed induction machine,” *Industrial Electronics, IEEE Transactions on*, vol. 54, no. 5, pp. 2482–2490, 2007.
- [10] R. Pena, J. Clare, and G. Asher, “Doubly fed induction generator using back-to-back pwm converters and its application to variable-speed wind-energy generation,” *Electric Power Applications, IEE Proceedings -*, vol. 143, no. 3, pp. 231–241, 1996.
- [11] P. Vas, *Vector Control of AC machines*. Clarendon press Oxford, 1990.
- [12] H. Akagi and H. Sato, “Control and performance of a doubly-fed induction machine intended for a flywheel energy storage system,” *Power Electronics, IEEE Transactions on*, vol. 17, no. 1, pp. 109–116, 2002.

- [13] G. Tapia, A. Tapia, and J. Ostolaza, "Two alternative modeling approaches for the evaluation of wind farm active and reactive power performances," *Energy Conversion, IEEE Transactions on*, vol. 21, no. 4, pp. 909–920, 2006.
- [14] S. Chapman, *Electric Machinery Fundamentals*, ser. Power and Energy Series. McGraw-Hill, 2005.
- [15] I. Boldea and S. Nasar, *The induction machine handbook*. CRC, 2001.
- [16] A. Fitzgerald, C. Kingsley, and S. Umans, *Electric Machinery, 6/E*, ser. McGraw-Hill series in electrical and computer engineering. McGraw-Hill, 2002.
- [17] I. Boldea, *Variable speed generators*. CRC, 2005, vol. 2.
- [18] R. Krishnan, *Electric Motor Drives: Modeling, Analysis, and Control*. Prentice Hall Upper Saddle River, NJ, 2001, vol. 626.
- [19] T. Miller, "Theory of the doubly-fed induction machine in the steady state," in *Electrical Machines (ICEM), 2010 XIX International Conference on*, 2010, pp. 1–6.
- [20] P. Krause, *Analysis of Electric Machinery. 1986*. McGraw-Hill.
- [21] R. Park, "Two-reaction theory of synchronous machines generalized method of analysis-part i," *American Institute of Electrical Engineers, Transactions of the*, vol. 48, no. 3, pp. 716–727, 1929.
- [22] N. Mohan, *Electric Drives: an Integrative Approach*. Minnesota Power Electronics Research & Education (MNPERE), 2003.
- [23] W. C. Duesterhoeft, M. W. Schulz, and E. Clarke, "Determination of instantaneous currents and voltages by means of alpha, beta, and zero components," *American Institute of Electrical Engineers, Transactions of the*, vol. 70, no. 2, pp. 1248–1255, July 1951.
- [24] I. Cadirci and M. Ermiş, "Double-output induction generator operating at subsynchronous and supersynchronous speeds: steady-state performance optimisation and wind-energy recovery," in *IEE Proceedings B (Electric Power Applications)*, vol. 139, no. 5. IET, 1992, pp. 429–442.
- [25] G. L. Johnson, *Wind energy systems*. Prentice-Hall Englewood Cliffs (NJ), 1985.
- [26] S. Heier and R. Waddington, *Grid integration of wind energy conversion systems*. Wiley Chichester, UK, 1998.
- [27] AMSC. (Accessed: 2013-06-20) wt2000df product brochure. [Online]. Available: <http://www.amsc.com/library/index.html>
- [28] B. Dynamics. (Accessed: 2013-06-20) D49 2mw datasheet. [Online]. Available: [http://www.bladedynamics.com/Dynamic49\\_DataSheet.pdf](http://www.bladedynamics.com/Dynamic49_DataSheet.pdf)
- [29] R. C. Dorf, *Modern control systems*. Addison-Wesley Longman Publishing Co., Inc., 1991.
- [30] J. Prescott and B. Raju, "The inherent instability of induction motors under conditions of double supply," *Proceedings of the IEE-Part C: Monographs*, vol. 105, no. 7, pp. 319–329, 1958.



- [31] A. Tapia, G. Tapia, J. X. Ostolaza, and J. R. Saenz, "Modeling and control of a wind turbine driven doubly fed induction generator," *Energy Conversion, IEEE Transactions on*, vol. 18, no. 2, pp. 194–204, 2003.
- [32] N. P. Quang and J.-A. Dittrich, *Vector control of three-phase AC machines: system development in the practice*. Springer, 2008.

# Vita Auctoris

NAME: Matthew Hurajt

PLACE OF BIRTH: Windsor, Ontario

YEAR OF BIRTH: 1988

EDUCATION: W. F. Herman Secondary School, Windsor  
2001-2006  
University of Windsor, Windsor, Ontario  
2007-2010 BAsC  
University of Windsor, Windsor, Ontario  
2010-2013 MASc